UNIVERSITY OF CALIFORNIA SAN DIEGO

Mitochondria: Diseases and Therapeutics

A dissertation submitted in partial satisfaction of the requirements for the degree
Doctor of Philosophy

in

Chemistry

by

Bashayer Althufairi

Committee in charge:

Professor Emmanuel Theodorakis, Chair
Professor Mohit Jain, Co-Chair
Professor William Gerwick
Professor Tadeusz Molinski
Professor Thomas Hermann
Professor Arnold Rheingold

2020

The dissertation of Bashayer Althufairi is approved, and it is acceptable in quality and form for publication on microfilm and electronically:

_____

_____

_____

_____

_____
Co-Chair

_____
Chair

University of California San Diego

2020

Table of Contents

List of Abbreviations and Symbols

$\Delta\Psi_m$: mitochondrial membrane potential
°C: degree Celsius
3-OH FA: 3-hydroxy fatty acid
3,5-DiOH FA: 3,5-dihydroxy fatty acid
3,5-DiOH-C14: 3,5-dihydroxytetradecanoic acid
3,5-DiOH-C16: 3,5-dihydroxy palmitic acid
AA: acetic acid
Ac_2O: acetic anhydride
Acetyl-CoA: acetyl-coenzyme A
ACN: acetonitrile
ACP: acyl carrier protein
ADP: adenosine diphosphate
$AlCl_3$: ammonium trichloride
AMP: adenosine monophosphate
AMPK: adenosine monophosphate-activated protein kinase
ATP: adenosine triphosphate
Bn: Benzyl
CE-MS: capillary electrophoresis-mass spectrometry
CGX: caged *Garcinia* xanthones
CH_3SO_3H: methanesulfonic acid
CoA: coenzyme A
CoQ_{10}: Coenzyme Q_{10}
CoxI: Complex I
CoxII: Complex II
CoxIII: Complex III
CoxIV: Complex IV
CoxV: Complex V
CPEO: chronic progressive external ophthalmoplegia
csv: comma separated values
CTD: C-terminal domain
$CuCl_2$: copper chloride
CUDA: 12-[(cyclohexylcarbamoyl)amino]-dodecanoic acid
CuI: copper iodide
Cys-CdTe QDs: cysteamine- coated cadmium-tellurium quantum dots
Cyt c: cytochrome c
DCC: 1,3-dicyclohexylcarbodiimide
DCM: dichloromethane
DDA: data dependent acquisition
DHS: 3-dehydroshikimate
DIA: data independent acquisition
diHOME: dihydroxy-9Z-octadecenoic acid
DIPEA: N,N-Diisopropylethylamine
DMAP: 4-(N,N-dimethylamino)pyridine
DMF: N,N-dimethylformamide
DNA: deoxyribonucleic acid
Equiv.: equivalents

Et_2O: diethyl ether
ETC: electron transfer chain
ETE: 6E,8Z,11Z,14Z-eicosatetraenoic acid
EtOAc: ethyl acetate
FA: fatty acid
$FADH_2$: flavin adenine dinucleotide
FAO: fatty acid β-oxidation
FAS: fatty acid synthesis
Fe_3O_4: ferrosoferric oxide
GBA: gambogic acid
GC-MS: gas chromatography-mass spectrometry
GNPS: global natural product social
HCl: hydrochloride
HETE: hydroxy-5Z,8Z,11Z,13E-eicosatetraenoic acid
HIF: hypoxia inducible factors
HODE: hydroxy-10E,12Z-octadecadienoic acid
HRMS: high resolution mass spectra
hrs: hours
Hsp 90: heat shock protein 90
Hsp: heat shock proteins
HTD2: 3-hydroxyacyl-thioester dehydratase
IC_{50}: inhibition concentration 50%
IEM: inborn errors of metabolism
IEMM: inborn error of mitochondrial metabolism
IMM: inner mitochondrial membrane
IMS: intermembrane space
inHg: inch of mercury
IPA: isopropyl alcohol
K_2CO_3: potassium carbonate
K_d: affinity constant
KG: alpha-ketoglutarate
KOH: potassium hydroxide
KSS: Kearns-Sayre syndrome
kV: kilovolt
LC-MS: liquid chromatography-mass spectrometry
LC: liquid chromatography
LCHAD: long-chain 3-hydroxyacyl-CoA dehydrogenase
LHON: Leber's hereditary optic neuropathy
LTB_4-d_4: leukotriene-6,7,14,15-d_4
LV: latent variable
M: molar
m/z: mass to charge ratio
malonyl-CoA: malonate coenzyme A
MD: middle domain
MDR: multidrug resistance
MELAS: mitochondrial myopathy, encephalopathy, lactic acidosis and stroke like episodes
MERRF: myoclonic epilepsy with ragged red fibers

mg: milligram
$MgSO_4$: magnesium sulfate
min: minute
ml: milliliter
mm: millimeter
mM: millimolar
mmol: millimole
MMS: mitochondrial medical society
MNGIE: mitochondrial neuro-gastrointestinal encephalopathy
MnO_2: manganese dioxide
MNP: magnetic nanoparticles
mRNA: messenger RNA
MS: mass-spectrometry
MS1: full scan mass spectrum
mtDNA: mitochondrial DNA
mtFAS: mitochondrial de novo fatty acid synthesis pathway
mTOR: mammalian target of rapamycin
NAB: nano- particle albumin-bound
NADH: nicotinamide adenine dinucleotide
$NaHCO_3$: Sodium bicarbonate
nBuLi: n-butyllithium
nDNA: nuclear DNA
ng: nanogram
NMR: nuclear magnetic resonance
NTD: N-terminal domain
OMM: outer mitochondrial membrane
OxPhos: oxidative phosphorylation
P_2O_5: phosphorous pentoxide
$Pb(OAc)_4$: lead tetraacetate
PC: principal components
PCA: principle component analysis
Pd: palladium
$Pd(PPh_3)_4$: tetrakis(triphenylphosphine)palladium(0)
PEG: polyethylene glycol
PEP: phosphoenolpyruvate
PGD: prostaglandin
PI3K: phosphoinositide 3-kinase
PKU: phenylketonuria
PLS-DA: partial least squares-discriminant analysis
PMD: primary mitochondrial diseases
$POCl_3$: phosphoryl trichloride
POLG: polymerase gamma
QDs: quantum dots
ROS: Reactive oxygen species
rpm: revolutions per minute
rRNA: ribosomal ribonucleic acid
rt: retention time
SAR: structure-activity relationship
SMD: secondary mitochondrial diseases

SPE: solid phase extraction
TBAF: tetra-n-butylammonium fluoride
TBS: tert-butyldimethylsilyl
tBuOK: potassium tert-butoxide
TCA: tricarboxylic acid cycle
TFA: trifluoroacetic acid
TfR-1: transferrin receptor 1
THF: tetrahydrofuran
TLC: thin layer chromatography
tRNA: transfer ribonucleic acid
TXB_2: thromboxane B_2
um: micrometer
uM: micromolar
UPLC: ultra-performance liquid chromatography
$ZnCl_2$: zinc dichloride
µL: microliter

List of Figures

List of Schemes

List of Tables

Acknowledgments

I'd like to acknowledge everyone at University of California San Diego and Virginia Commonwealth University who has a great help and support during my graduate study in the USA. I also like to acknowledge my friend Mariam Salib for her great support and useful discussion. Special thanks to Dr. Rodolphe Jazzar for his help in trouble shooting, discussion in topics of organic chemistry and life in general. I would love to thank my committee members and co-advisors. I'd like to acknowledge graduate division at University of California San Diego as well. Also, I'd like to acknowledge Edward Kantz for the valuable discussion about computational aspects of metabolomics.

Special thanks for Dr. Anthony Mrse and Dr. Yongxuan Su from the NMR and molecular mass spectrometry facilities at the department of chemistry and biochemistry for setting up accounts and help collecting compounds characterizing spectra of chapter 3. Finally, I'd like to express my love and acknowledgement to my parents, and my family for their love and care.

Chapter 1, in part, was adapted from published chapter, Caged Garcinia Xanthones: Synthetic Studies and Pharmacophore Evaluation, *Studies in Natural Products Chemistry*, on which I was a co-author. Oraphin Chantarasriwong and Emmanuel Theodorakis contributed thoughts, expert ideas, and opinions to the chapter.

Chapter 2, in full, is currently being prepared for a publication, on which I'm a primary author. I discovered new dihydroxyl fatty acid family that is never been reported or published in any scientific journals or patent. Dr. Tao Long and Kysha Mercader contributed to the project biostatistics aspect. Khoi Dao, Rafael Moranchel,

and Mahan Najhawan participated in LC/MS experiments. Dr. Mohit Jain supervised the overall project.

Chapter 3, in full, is currently being prepared for a publication, on which I'm a primary author. I contributed to the project novelty and the entire chemical experiments. I generated for first time a new chemical derivatization, that could also be applied to other caged garcinia xanthones, to produce unique library of forbesione analogs. The compounds were sent to Dr. Mary Alphaugh to perform cytotoxicity assays on breast cancer cell lines. Emmanuel Theodorakis is the advisor.

Vita

2011 B Pharm, University of Kuwait, Kuwait

2011-2012 Pharmacist in Ministry of Health, Kuwait

2013-2016 Master of Pharmaceutical sciences, Virginia Commonwealth University

2016-2020 Doctor of Philosophy, University of California San Diego

PUBLICATIONS

Mosier, P. D; Chiang, M-J; Lin, Z; Gao, Y; Althufairi, B; Zhou, Q; Musayev, F; Safo, M. K; Xie, H; Desai, U. R. Broad Spectrum Anti-Influenza Agents by Inhibiting Self-Association of Matrix Protein 1. *Nat. Sci Rep.* 2016, *6*, 32340.

Chiang, M-J; Musayev, F.; Kosikova, M.; Lin, Z.; Gao, Y.; Mosier, P. D.; Althufairi, B.; Ye, Z.; Zhou, Q; Xie, H.; Desai, U.; Safo, M. K. Maintaining pH-dependent conformational flexibility of M1 is critical for efficient influenza A virus replication. *Emerg Microbes Infect*. 2017, *6*, e108.

Chantarasriwong, O.; Althufairi, B. D.; Checchia, N. J.; Theodorakis, E. A. Chapter 4 - Caged Garcinia Xanthones: Synthetic Studies and Pharmacophore Evaluation. In *Studies in Natural Products Chemistry*, Atta ur, R., Ed. Elsevier: 2018; Vol. 58, pp 93-131.

ABSTRACT OF THE DISSERTATION

Mitochondria: Diseases and Therapeutics

by

Bashayer Althufairi

Doctor of Philosophy in Chemistry

University of California San Diego, 2020

Professor Emmanuel A. Theodorakis, Chair

Professor Mohit Jain, Co-Chair

Nearly 20 years ago, mitochondria were mistakenly considered only as the home production of energy molecule, adenosine triphosphate. However, a large growing research body has uncovered numerous vital roles of the mitochondria in various biological processes, such as aging, signaling, immunity, calcium homeostasis, and diseases including diabetes, cancer, and Parkinson's disease.

Mitochondrial dysfunction could result from mutation of its genetic component. It's quite tricky to relate mitochondrial dysfunction with certain pathogenic phenotype. Thus, metabolomic study was conducted to reveal causal metabolites, and classify their association with various symptoms. The untargeted metabolomic study was

performed in favor of the detection of bioactive lipid in the plasma of approximately two thousand patients with genetic mitochondrial diseases. Bioactive lipids are major chemical class in the body, containing inflammatory meditated lipids. Our studies on this topic led to the discovery of new hydroxyl fatty acid family that has been associated with mitochondrial diseases.

Mitochondria, on the other hand, have involved in cancer, and they are considered a great potential therapeutic target for the initiation of death pathway, and hence, it leads to the apoptosis of cancerous cells. Caged *Garcinia* xanthones (CGXs), which are natural products, have been identified as potent antitumor agents targeting the mitochondria. On this topic, we synthesized forbesione, a member of the CGX family, and various synthetic analogs in order to potentially produce more potent analogs compared to the parent compound.

Chapter 1 : Literature overview

1.1 Introduction

Mitochondria are crucial organelles that play important roles in vital cellular processes, such as Kreb's cycle, fatty acid β-oxidation (FAO), and energy production. Mitochondrion is a very ancient organelle whose origin was theorized to be from bacterial phylum α-Proteobacteria (Alphaproteobacteria).[1] Consistent with this theory, compared to other cellular organelles the mitochondrion possesses unique features including double membranes, double stranded deoxyribonucleic acid (DNA), and a self-division that is independent of the cell division.[2] Many aspects of its biochemistry remain largely ambiguous over last century; until Dr. Peter Mitchell (Nobel Prize, 1978) showed the mechanism of adenosine triphosphate (ATP) synthesis in oxidative phosphorylation (OxPhos).[1] The initial view that the main function of mitochondria is the generation of ATP was further refined in the 1990s' by considering that mitochondria are not only bioenergetic and biosynthetic organelles but also crucial signaling organelles dictating cell fate by signaling metabolites, such as reactive oxygen species. Yet, more continuous research efforts are needed in order to unravel complexities of mitochondria related cellular functions in health and disease states.[3, 4]

With regard to the anatomy of mitochondria, mitochondrion consists of the outer mitochondrial membrane (OMM), the inner mitochondrial membrane (IMM), and the intermembrane space (IMS), which is localized between OMM and IMM, and matrix.[2] IMM is folded into so-called cristae on which electron transfer chain (ETC) proteins are localized to execute OxPhos process.[5] There are nearly 1500 mitochondrial proteins, which mostly encoded by nuclear DNA.

1.2 Mitochondrial genome

Mitochondria are maintained by dual control of mitochondrial DNA (mtDNA) and nuclear DNA (nDNA). mtDNA consists of 16,569 base pairs, double stranded, circular molecule that exists in certain number of copies depending on the bioenergetic state of the organ.[6] This genome comprises 37 genes, which encodes 13 proteins, two ribosomal ribonucleic acid (rRNA) molecules, and 22 transfer ribonucleic acid (tRNA) molecules. The mitochondrially synthesized proteins are merely associated with OxPhos process.[7] The genes coding for the 13 proteins include *ND1, ND2*, *ND3*, *ND4*, *Nd4L*, *ND5*, and *ND6*, which are associated with Complex I (CoxI) (figure **1.1**). Additionally, *Cyt b* is the only mtDNA-encoded subunit of Complex III (CoxIII). For complex IV (CoxIV), there are three genes, *COXI, COXII*, *COXIII*, while *ATP6* and *ATP8* are associated with Complex V (CoxV).[8, 9]

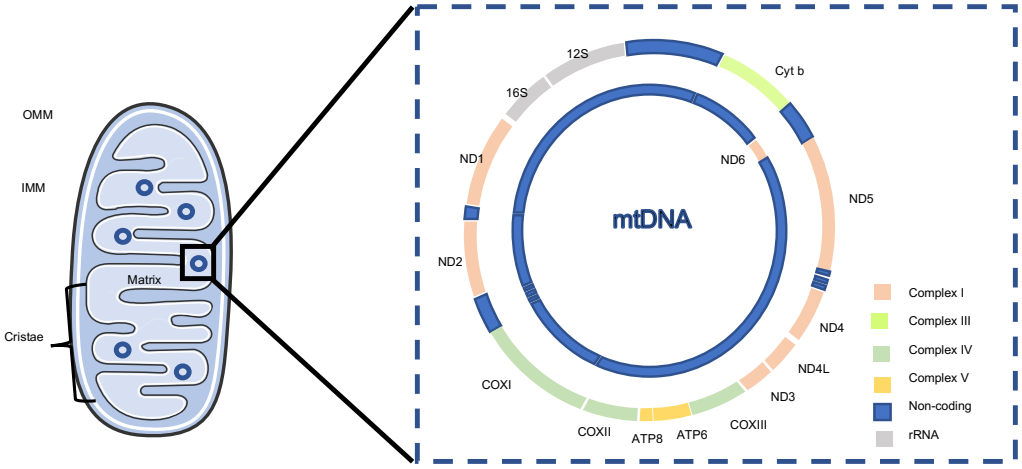

Figure 1.1. Mitochondria structure and its DNA. Cristae is the folding structure of IMM

1.3 Mitochondria as energy house

Mitochondria are known as the powerhouse because they generate cellular energy represented in the ATP molecules and electron transfer via OxPho process. This system comprises of five multimeric enzymes, supercomplexes I through V and two electron carriers, Coenzyme Q_{10} (CoQ_{10}) and cytochrome c (Cyt c).[10] This process is connected to other pathways such as Kreb's cycle and FAO. Reducing molecules such as nicotinamide adenine dinucleotide (NADH) and flavin adenine dinucleotide ($FADH_2$) produced from Kreb's cycle fed into ETC complexes.[11] NADH:ubiquinone oxidoreductase, known as CoxI, is the largest complex consisting of 45 subunit proteins. CoxI, which is located on the IMM, pumps four protons into the IMS mediated by NADH oxidation and reduction of CoQ_{10}. Complex II (CoxII), which is also called succinate-CoQ10 oxidoreductase, oxidizes succinate and reduces CoQ_{10} into ubiquinol. CoxII doesn't pump any proton into the IMS, and it's exclusively encoded by nDNA. Ubiquinol-cytochrome c oxidoreductase (CoxIII) utilizes ubiquinol to reduce Cyt c which is oxidized later by cytochrome c oxidase (CoxIV) to transfer the electrons to the molecular oxygen and pumps protons into the IMS. The pumped protons in the IMS generate electrochemical gradients.[6, 10] This gradient produces energy as protons move toward the matrix through CoxV that creates mechanical energy catalyzing chemical bond formation between adenosine diphosphate (ADP) and phosphate to yield ATP.

Tricarboxylic acid cycle (TCA) was discovered by Hans Krebs and William Johnson in 1937.[12] The one turn of Kreb's cycle yields three NADH and one $FADH_2$ molecules as result of the oxidation of acetyl-coenzyme A (acetyl-CoA) to two carbon dioxide molecules.[9] Acetyl-CoA obtained from different pathways, such as glycolysis and FAO, is a substrate of the first reaction in the cycle in which Acetyl-CoA is

conjugated with oxaloacetate to furnish citric acid. Then, multiple oxidation steps proceed till forming another oxaloacetate molecule, which enters into another turn of the TCA as shown in figure **1.2**.[9]

Furthermore, FAO is another major pathway for energy homeostasis. First, fatty acid chain is activated by incorporation with coenzyme A (CoA) molecule to form acyl-CoA which is subjected for repeated cycles of beta-oxidation to produce acetyl-CoA and acyl-CoA chain having two carbon less after each turn until the chain is thoroughly consumed. There are four major steps initiated first with dehydrogenation of acyl-CoA into trans-2-enoyl-CoA.[13] The latter is hydrated to generate 3-hydroxyacyl-CoA, which is then oxidized to produce keto derivative. Lastly, 3-ketoacyl-CoA derivative is cleaved at beta position producing acetyl-CoA which is fed into TCA, and the cleaved acyl-CoA re-enters FAO cycle to fully be degraded. Additionally, each turn produces one of each NADH and $FADH_2$ molecules, which are used in the ETC process.[12, 14]

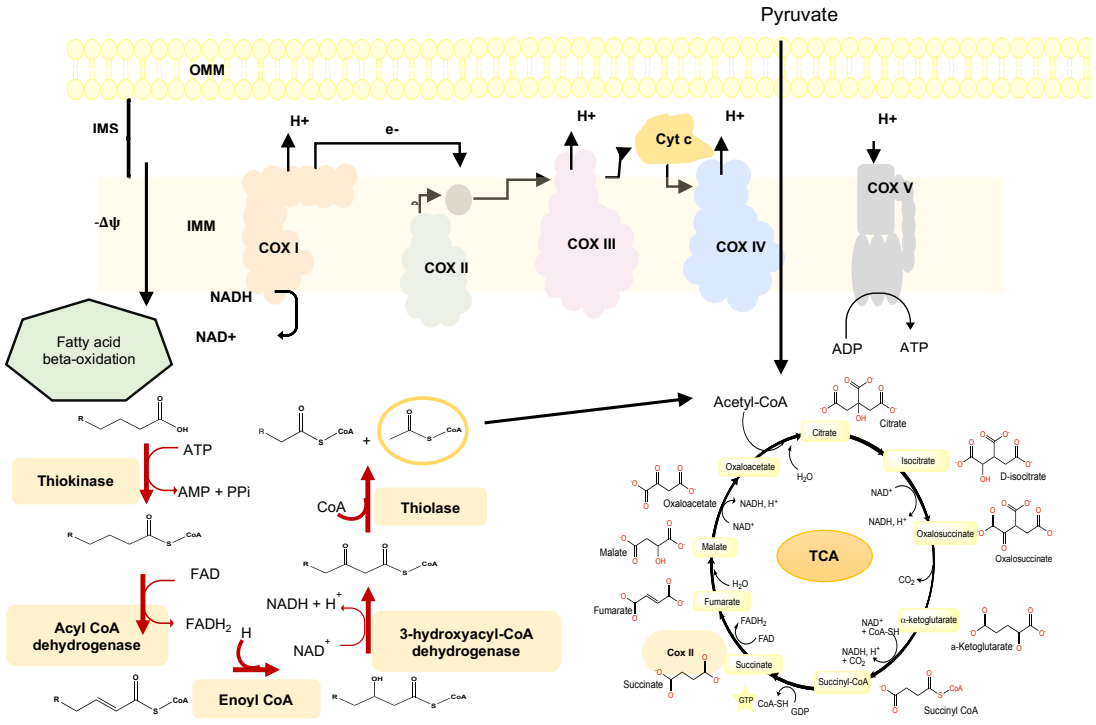

Figure 1.1. Mitochondrial ETC and ATP production in connection with TCA and FAO

1.4 Mitochondria as signaling organelle

Mitochondria are not isolated organelles from other cellular organelles but rather they mediate and communicate with various cellular pathways to adjust cellular needs according to any physiological changes. Mitochondrial TCA intermediates play vital roles other than the production of the reducing agents. For example, alpha-ketoglutarate (KG) has an epigenetic function since it's a substrate along with oxygen for KG-dependent dioxygenases that promote DNA and histone demethylation leading to pluripotency. Succinyl-CoA serves as a substrate in the rate-limiting step of heme synthesis, a condensation of succinyl-CoA and glycine to produce aminolevulinic acid via aminolevulinic acid synthase.[15] Moreover, citrate the first intermediate in TCA cycle is converted to aconitic acid via aconitase and then to isocitrate. Further, cis-aconitic can be decarboxylated to itaconitate via aconitate decarboxylase. Itaconitate is a potent inhibitor of isocitrate lyase, an important enzyme in the glyoxylate cycle which is a critical pathway for the survival of many parasites.[16] Thus, itaconitate acts as anti-inflammatory and antimicrobial activities in the macrophages.[17] When nutrients level is low, cells program their metabolism to increase catabolic pathways and diminish anabolic pathways. Under normal conditions, cells maintain ATP/ADP and ATP/ adenosine monophosphate (AMP) ratios to be 10:1 and 100/1, respectively. Under ATP deprivation, AMP level increases drastically which activates adenosine monophosphate-activated protein kinase (AMPK).[18] The latter kinase phosphorylates many anabolic proteins, such as mammalian target of rapamycin (mTOR).[19] Additionally, AMPK activates FAO pathway while suppress fatty acid synthesis.

1.5 Mitochondrial dysfunction

Mitochondrial diseases can be divided into primary and secondary mitochondrial diseases. Primary mitochondrial diseases (PMD) are inherited diseases

that affect directly or indirectly the ETC proteins as a result of either mtDNA or nDNA mutations.[20] On the other hand, secondary mitochondrial diseases (SMD) include wild range of pathogenic mitochondrial dysfunctions resulting from inherited diseases caused by mutations in non-ETC genes or environmental factor or ageing diseases such as Alzheimer's disease.[21] An estimate of ~ 15-20% of all inherited human mitochondrial disorders results from mtDNA mutations, while the remaining disorders are caused by nDNA.[22] As a matter of fact, nDNA mutations represent the large inherited mitochondrial abnormalities because the number of mitochondrial proteins encoded by mtDNA is only 13 proteins which are all respiratory protein subunits, whereas nDNA encodes ~ 77 of respiratory protein components along with all proteins required for the transcription, translation, modification, and assembly of the 13 mtDNA encoded proteins.[23]

Heteroplasmy is a special phenomenon of mtDNA biology. Heteroplasmy describes or annotates for the percentage of the mutant mtDNA to the wild mtDNA.[24] On the other hand, homoplasmy means there are identical copies of mtDNA across the cells, which might be either mutant or wild mtDNA.[24] Thus, heteroplasmy could be causal factor in mitochondrial diseases, and used as diagnostic measure. Depending on tissue bioenergetic status, certain threshold of heteroplasmy is required to develop pathogenic phenotype.[25]

Furthermore, mitochondrial diseases account for more than 50 conditions of inborn errors of metabolism (IEM) that are defined as genetic diseases of the intermediary metabolism resulting mostly from single gene defect, which could encode an enzyme, membrane transporter, or any other functional protein.[26] Some of these may present in neonates as acute sepsis-like illness, whereas others can present later in life with chronic progressive multisystem or specific organ involvement, e.g.

cardiomyopathy.[27] IEM has a diverse spectrum of genetic disorders involving lysosomal storage diseases, peroxisomal disorders, and mitochondrial disorders affecting many biochemical pathways. However, mitochondrial disorders are the most common form, having prevalence of 1:5000 of IEM birth conditions.[28]

Over the past decades, research of genetic diseases has been following the traditional biochemical research process of a mutated enzyme or protein, such as studying the effects of their deficiency within their own biochemical equation context omitting the effect of interactive metabolites from other pathways and/or overall the subsequent biochemical changes in the body.[29] As expected, this approach has failed in explaining sequences of a mutation from the clinical standpoint when patients present unrelated phenotypes of the particular genetic mutations.[30]

An example of a well-controlled inborn error of metabolism disease is phenylketonuria (PKU) that led to the discovery of more than 200 other inborn error of metabolism diseases.[31] Patients suffering PKU have mutation in gene encodes phenylalanine hydroxylase enzyme which catalyzes hydroxylation of phenylalanine to tyrosine, an important precursor for many neurotransmitter and hormones. Patients suffer from growth failure, global developmental delay, seizures, and intellectual impairments which were thought to be due to tyrosine deficiency.[32] In such a case, a supplement of tyrosine should take care and cure almost all neurological symptoms. However, this doesn't work as it was expected. The real reasons behind the development of these phenotypes were not due to tyrosine deficiency but rather the increase of toxic by-products or metabolites of phenylalanine metabolism, such as phenylpyruvate. These toxic metabolites are excreted in the urine and have a distinct smell leading to the discovery of PKU.[8, 33] Nowadays, PKU is managed by restricted diet of phenylalanine or proteins. Luckily, the neurological retardation is manageable

leading to the improvement in life quality of many PKU patients thanks to the accurate research investment in finding the root of metabolism error.[34]

Unfortunately, diseases of inborn error of mitochondrial metabolism (IEMM) are pointed as orphan diseases at both diagnostic and therapeutic levels.[35] Even though IEMM are not rare IEM diseases, neither diagnosis nor management is well established. As a result, mitochondrial medical society (MMS) in 2015 have reached consensus criteria based on Delph survey, which is a consensus method utilizing expert opinion to make knowledge-based decision when insufficient experimental-based information is available.[36] The next consensus was published in 2017, yet solidity of guidelines is still lacking evidence-based clinical protocols.[37] Sadly, an assessment accomplished by MMS showed 99% of 207 clinicians worldwide have seen those conditions but they lack firm resources for experimental-based guidelines to diagnose or manage the conditions. It's quite challenging to come up with correct and specific features of different mitochondrial diseases due to diverse overlapping phenotypes, and heterogenous nature of the IEM diseases.

Generally, IEM are diagnosed by newborn screening or clinical suspicion. Diagnostic tests include mitochondrial biomarkers in blood, urine, and spinal fluids, and enzyme testing.[38] However, these tests suffer from absence of sensitivity and specificity. For example, the blood lactate/pyruvate ratio is most reliable in differentiating ETC disease from disorders of pyruvate metabolism, but only when lactate levels are high, which is not necessary the case in some IEMM.[39] Often, invasive procedures are required, such as tissue, e.g. liver or muscular, biopsies. Collectively, the lack of evidence based clinical protocols, understanding of disease mechanism of metabolic abnormalities, and prediction of key toxic metabolites are the bottle neck of IEMM management.[27, 30]

1.6 Examples of mitochondrially-related IEM diseases

1.6.1 Diseases with neuro-ophthalmic manifestations

The neuro-ophthalmology of mitochondrial diseases are diseases of mtDNA defects that are characterized with dysfunction of the optic nerves, extraocular muscles, and retina.[40-43]

a) Leber's hereditary optic neuropathy (LHON)

In 1871, Leber's hereditary optic neuropathy (LHON) was first clinically diagnosed by the German ophthalmologist Theodore Leber. LHON was the first discovered primary mitochondrial disease with a point mutation in the mtDNA, which is transmitted maternally.[44] It usually affects patients between 15-35 years of old. Remarkably, LHON is more predominant in male patients than female.[45]

Furthermore, LHON is clinically represented as rapid and painless loss of central vision. It is developed mainly due to the degeneration of retinal ganglion cells. This degeneration occurs as a result of mtDNA mutations in CoxI.[44, 46] There are three primary LHON mutation which are located at nucleotide positions 11778 (~69% of LHON cases), 14484 (~14% of cases), and 3460 (13% of cases).[47] In some cases, LHON is accompanied with other neurological signs, such as multiple sclerosis like symptoms.

b) Chronic progressive external ophthalmoplegia (CPEO)

Another neuro-ophthalmological manifestation of mitochondrial diseases is chronic progressive external ophthalmoplegia (CPEO), which is a specific type of mitochondrial myopathy affecting ocular muscles.[48] This syndrome is also painless and progressive bilateral ptosis and ophthalmoparesis. This is serious as patient exhibits difficulty in reading and double vision. However, the vision acuity is not affected in this case. Additionally, other muscle weakness involves with CPEO like

neck and limb. CPEO usually occur in early adulthood, and it's devoid of gender bias.[49-53]

CPEO is quite different than LHON in that it can be caused by various genetic lesions of either mtDNA or nDNA, and frequently accompanied by various systematic symptoms, such as sensorineural hearing loss, myopathy, and optic neuropathy.[54] Usually, mtDNA genetic lesion is a partial deletion of a region in mtDNA molecule, while nDNA genetic lesion is associated with mitochondrial maintenance and replications, such as thymidine phosphorylase and polymerase gamma (POLG).[55, 56]

1.6.2 Systematic diseases

Systematic diseases are diseases characterized with different phenotypic variability, which means they can affect multiple organ system. Figure **1.2** represents some of the manifestations of systematic diseases.[57] These diseases are common with multiple mtDNA deletion or large scale delection; hence, the synthesis of many ETC proteins is affected.[49] In fact, CPEO has subclass known as CPEO plus which is simply ophthalmoplegia plus other symptoms from different organs. For instances, Kearns-Sayre syndrome (KSS) is a special disease with a combination of CPEO and one of the following abnormalities: cerebellar dysfunction or cardiac conduction abnormality.[4] It's quite challenging to categorize systematic diseases, however table **1.1** summarizes major mitochondrial diseases.

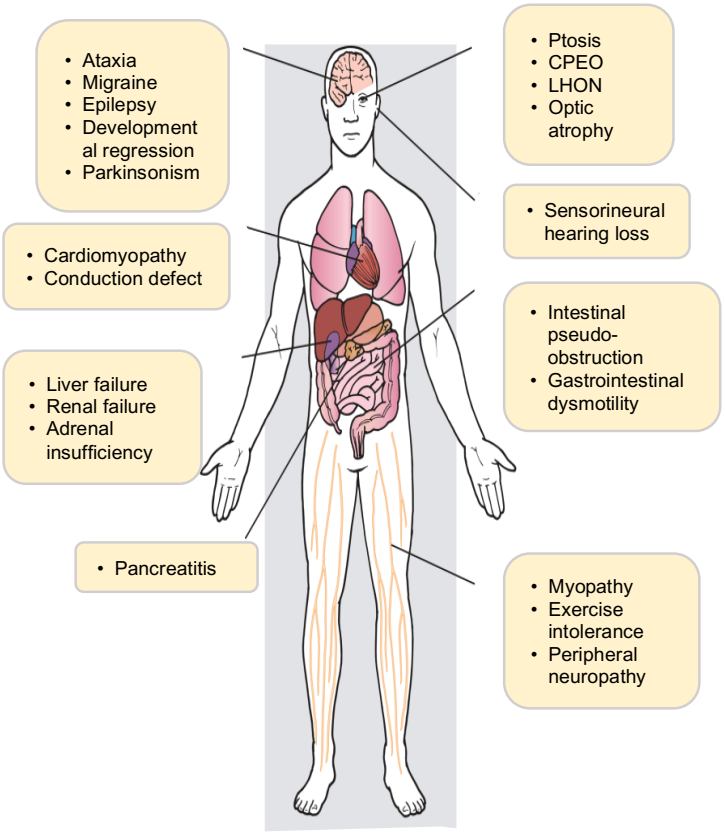

Figure 1.2. Clinical presentation of some mitochondrial diseases

Table 1.1. Clinical syndromes, gene defects, and phenotypic features of some mitochondrial diseases.

Syndrome	Genetic defect	Molecular defect	Clinical features
Kearns-Sayre syndrome (KSS)	Large scale mtDNA deletion	Multiple proteins in OxPhos, beta-oxidation and ...etc.	CPEO, deafness, diabetes, cerebellar ataxia
Myoclonic epilepsy with ragged red fibers (MERRF)	m.8344A>G, MT-TF, MT-TP	Mitochondrial tRNAs	Ataxia, epilepsy, weakness, sensorineural hearing loss, retinopathy
Mitochondrial myopathy, encephalopathy, lactic acidosis and stroke like episodes (MELAS) syndrome	m.3243A>G, MT-TQ, MT-TV	Mitochondrial tRNAs	Stroke-like episodes, cardiomyopathy, seizures, lactic acidosis
Mitochondrial neuro-gastrointestinal encephalopathy (MNGIE) syndrome	POLG	polymerase gamma that replicates mtDNA	Gastrointestinal dysmotility, muscle weakness, CPEO, neuropathy, retinopathy

1.7 Metabolomics

The biochemical and molecular information are expressed from DNA to messenger RNA (mRNA) transcripts, which are translated into proteins. The proteins produce metabolites, which mediates phenotypes. However, cellular communications nowadays are far from merely being a unidirectional flow as there are complex loops

of interactions between DNA, RNA, proteins and metabolites opening the door of various scenarios to describes at best the physiological events and phenotypic change.[58, 59]

Metabolome is defined as the downstream products of the genome and represents the complete collection of diverse metabolites in a cell, tissue, or organisms, which have biological function in normal and abnormal statuses.[60] Metabolites are those of low molecular weight (<1500 Da) measured in any biological sample, including but not limited to lipids, amino acids, short peptides, nucleic acids, sugars, alcohols and organic acids. Furthermore, they can be divided into two main types: endogenous, and xenobiotic metabolites.[61] The endogenous metabolites, which are called primary metabolites, are produced by encoding of host genome, and they are essential for key cellular functions.[62] Some essential metabolites can't be produced by host; however, they can be provided via, for example, gut microflora. Additionally, metabolites can be exogenous, which are called secondary metabolites and obtained from the diet or the environment, such as polyphenols, drugs, herbicides, and alkaloids.[63] The most variable metabolite type is the exogenous metabolites as the endogenous type is highly conserved. Despite of the difference, levels of the two metabolite types are affected by common factors, such as age, gender, diet, geographical site, and environment.[64]

Metabolomic is the study of metabolites and their concentrations within cell, tissue, and organism using analytical techniques in order to detect change of physiological stimulus or genetic alterations.[3] Furthermore, metabolomics as terminology was formulated for the first time by Oliver et al. and Nicholson et al. although the study of biochemical pathways and their corresponding metabolites were biologically characterized as far as 1950s.[65, 66]

1.8 Workflow of metabolomics

Many metabolomics studies have standardized workflow, but they can be customized sometimes by adding or editing additional step to fulfill experiment aims.[67, 68] In general, a biological sample is quenched or homogenized in case of tissue with a liquid, such as ethanol, in order to produce a liquid sample containing thousands of metabolites.[69] Then, extracted liquid can be examined using analytical chemistry techniques, such as integrated liquid chromatography-mass spectrometry (LC-MS), integrated gas chromatography-mass spectrometry (GC-MS), integrated capillary electrophoresis-mass spectrometry (CE-MS), and nuclear magnetic resonance (NMR). Figure **1.4** summarizes steps of metabolomics study.[58]

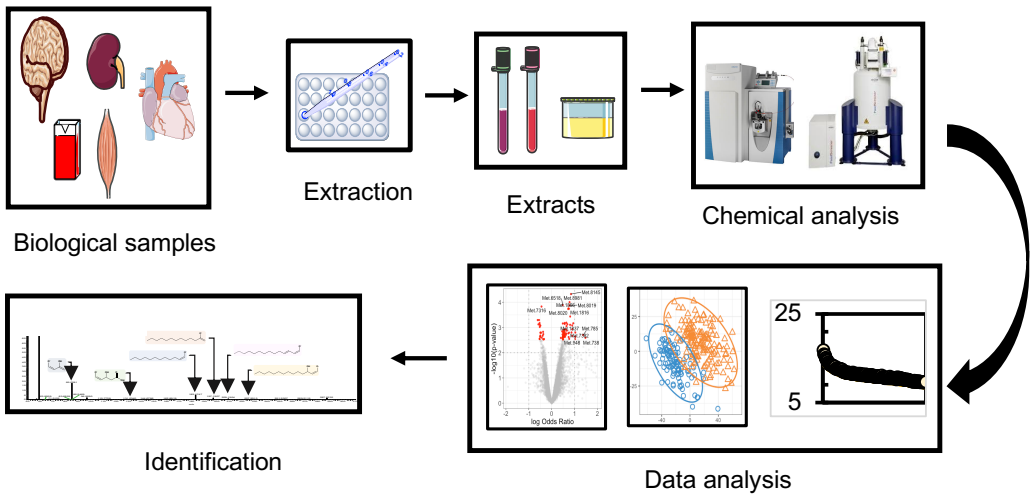

Figure 1.3. Experimental steps of metabolomics workflow

With respect to mass-spectrometry (MS) based techniques, the identification is based on the ionization of the target metabolites, which is highly dependent on chemical features and ionization modes, either positive or negative.[70] For analytical purposes, almost all metabolomics studies are performed with one of the chromatography techniques, such as liquid chromatography (LC).[67] The ion source of

choice used for MS metabolomics is the electrospray ionization. This method is extremely sensitive requiring microliter of sample; however, it is destructive, and sample can't be retrieved.[71] In MS technique, the measuring criteria are mass to charge ratio (m/z) of the parent molecule and its retention time (rt). These features are compared to referential MS scan of a standard compound for identification purposes along with fragments scans. Furthermore, each metabolite is assigned with both m/z and rt, and this label is called feature.[72]

On the other hand, NMR technique is nondestructive, and samples can be recovered, but NMR is not as sensitive as MS.[73] The experimental feature of NMR is the characteristic radio frequency absorption bands due to strong magnetic field effect on sample, which reorients nuclear spins of the atoms in the molecule. Each metabolite has a unique NMR spectrum of chemical shifts as each metabolite has its unique chemical structure.[71]

The most challenging step in the metabolomics workflow is the data pre-processing because of the identification of individual peak from thousands of collected peaks.[74] After acquiring data, LC-MS raw data are corrected and filtered by so-called data pre-processing, which is a series of computational modifications in order to prepare accurate data for the next step in the metabolomics workflow.[75] For example, noise filtering step removes noises and contaminants and enhances signals using methods such as, median filtering and Gaussian function. Moreover, the step of peak detection transforms raw continuous data into centroided discrete data, which reduces data dimension as it maintains true information and removes part of the noise.[76]

Normally, peak detection is performed based on m/z ratio because it is more precise than rt through extracted ion chromatograms, which is a 2-D intensity signal vs rt during a small m/z window. In the LC-MS technique, the time taking to run a single

sample in the LC is usually ranged from minutes to hours compared to the MS run which is instantly as the sample is eluted from LC.[74] Despite the efforts in optimizing the run time and elution gradient, there are several metabolites eluted at the same peak window or rt due to massive number of detected metabolites (~1000s) and similarity in their chemical features. Thus, spectral deconvolution, which is a step of decomposing overlapped peaks, is used to sort out individual peaks.[77]

In addition, retention time alignment is extremely useful to correct the drift in the rt of molecular ions because rt drift is noncontrollable and occurs spontaneously, especially in case of larger sample size. One way to solve rt drift is to add reference standard compounds within the samples during sample extraction and use them as landmark for peak alignments (figure **1.5**).[75] Many metabolites are diversely ionized into many ions as one metabolite can be identified as multiple ions which have different m/z values but very similar rt, such as isotopes, adducts, and neutral loss of fragments.

Therefore, ion annotation step is performed to explain m/z difference of ions eluted at same or similar rt with known isotopes, adducts, and neutral loss of fragments relationships. Another larger sample size variation beside rt drift is systematic variation of LC-MS data.[78] This can be easily resolved by calculating the ratio peaks intensities detected in the study to the internal standards, which are added in equal amount to all samples in the study. Finally, there are a good number of software tools available to computationally performed the abovementioned data pre-processing steps, such as MZmine, XCMS, and MetAlign.[79]

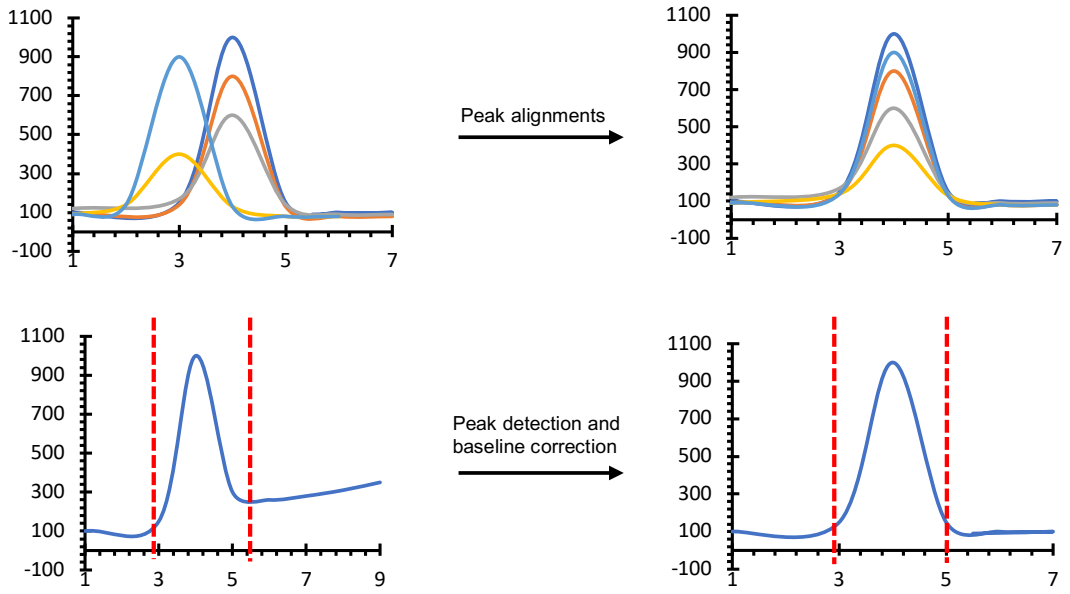

Figure 1.4. Examples of data pre-processing for peak detection and peak alignment. X-axis is the rt in min and Y-axis is the peak intensity

Afterward, a file of all metabolites peak intensities is generated for statistical analysis which highly relies on the nature of the study and what questions need to be answered. Furthermore, there are plenty of software packages for statistical analysis; however, the most sophisticated free software is R Studio, which uses C++ programming language to develop and perform functions for the production of statistical models.[3]

Generally, metabolomics studies can be classified into two approaches: targeted and untargeted.[3] Untargeted metabolomics studies are conducted for comprehensive analysis considering all measured metabolites in the study. Thus, this approach generates new hypothesis.[80] Furthermore, it focuses on acquiring data of larger samples than targeted metabolomics. Often, it is unbiased as it characterizes massive number of metabolites without confining a list of pre-determined metabolites; thus, it is very often used for the discovery of unknown metabolite. Untargeted metabolomics has two data acquisition modes: data independent acquisition (DIA) and

data dependent acquisition (DDA).[80] In the DIA, full MS1 scans are collected to generate full scan mass spectrum (MS1) of accurate mass measurements for each metabolite separated by LC. On the other hand, DDA produces fragmentation of metabolites with highest intensities. Contrary to untargeted metabolomics, targeted metabolomics studies focus on specific metabolites that are of interest, such as a substrate of an enzyme or a metabolite downstream a biochemical pathway. It is usually used for validation of a hypothesis or findings concluded from untargeted metabolomics or other biochemical studies.[58]

The procedure of metabolite identification will be mainly detected by MS/MS fragmentation of the key metabolite which would be compared with those reported in database searches including Human Metabolome Database (http://www.hmdb.ca), KEGG (http://www.kegg.com), METLIN (https://metlin.scripps.edu), MassBank (https://massbank.eu/MassBank/), and Chemspider (http://www.chemspider.com/). Some metabolite will be confirmed by comparison with available reference standards under the same LC-MS condition.[58]

Furthermore, the global natural product social (GNPS) infrastructure is a web-based mass spectrometry aiming to predict the structural identity and cover the chemical space of natural products and metabolites.[81] GNPS infrastructure comprises some spectral libraries, such as MassBank, ReSpect, and NIST along with GNPS house library. Molecular networking is another feature of GNPS in which groups of spectra can be correlated and visualized in a network. In the molecular networking, each node represents spectrum, and edges or connections are spectrum to spectrum alignment between nodes.[82]

1.9 Mitochondria in cancer

Disruption of mitochondrial functions has been linked to a wide range of pathologies, such as diabetes, Parkinson's disease, cancer, and many aging diseases. Cancer pathogenesis was mistakenly framed as merely genetic disease and having similar bioenergetic needs like normal cells.[83, 84] However, it has been shown that cancer cells have a different metabolic profile other than normal cells. The German physiologist Otto Warburg has suggested that cancerous cells rely on glycolysis as the major ATP generating pathway over OxPhos process.[85] That is why cancerous cells have large increase in lactate level. Therefore, cancer has a large defect in metabolism as a component of its pathogenesis. Mitochondrial metabolism contributes to different stages of cancer development.[86]

At malignant transformation, which is the transform of normal cell into a neoplastic precursor, three main mitochondrial activities enhance the proliferative capability: Reactive oxygen species (ROS), accumulation of toxic metabolites, such as fumarate and 2-hydroxyglutarate, and defect in mitochondrial permeability transition.[87] At a particular amount, ROS, such as H_2O_2, can serve as signaling molecule to facilitate tumorigenesis. H_2O_2 activates phosphoinositide 3-kinase (PI3K) pathway, which promotes proliferation and results in cancer cell survival.[88] In addition, H_2O_2 stabilizes the production of hypoxia inducible factors (HIF) by preventing their hydroxylation at proline residue because hydroxylation inhibits their crucial role in cancer; as they activate transcription of hypoxia response genes to allow cell survival under hypoxia.[89] Cancer cells adopt hypoxic environments due to incompatibility between the high proliferative rate of tumor cells and the ability of the blood supply to provide nutrients including oxygen.[90]

Therefore, there is a great interest in studying mitochondria as therapeutic target and discovering therapeutic agents that potentially modulate mitochondrial functions. Those agents are divided into two classes based on their site of action: mitochondria-targeted and non-mitochondria targeted agents.[88] The mitochondria-targeted agents act directly on a molecular target in the mitochondria, while the non-mitochondrial agents bind to a molecular entity which is located in the sub-cellular organelles other than the mitochondria, but this molecular target eventually modifies the activity of the mitochondria. Moreover, the molecule which has intrinsic affinity toward mitochondria is called "mitochondriotropic".[91, 92]

Mitochondriotropic agents are small molecules which accumulate at mitochondrial membrane or inside mitochondria without any structural modification using mitochondrially-targeted delivery system. For example, triphenylphosphonium cation was found to accumulate in mitochondria due to large mitochondrial membrane potential ($\Delta\Psi_m$).[93]

1.10 The family of caged *Garcinia* xanthones (CGX)

One of the chemical families that is considered mitochondriotropic is the caged *Garcinia* xanthones (CGX).[94-101] CGXs are isolated from the bark of *Garcinia* trees that are native to Indonesia, Brazil, India, and Africa.[102] The most common *Garcinia* tree is G. mangostana which is largely grown due to its production of valuable fruit, mangosteen. However, there are many other *Garcinia* species including G. forbesii, G. hanburyi, G. bracteat, G. gaudichaudii, G. lateriflora G. cantleyana, G. urophylla, and G. oligantha.[101, 103]

Various bioactive constituents are isolated from tree resins for many uses, such as colorants or therapeutic agents.[104] Among all extract components, gambogic acid

is the archetype of CGXs (**1.1**) whose chemical structure was reported in 1963.[105] The CGX family has distinct structural features. The general scaffold contains a xanthone of which the C-ring is a novel heterocyclic structure, 4-oxa-tricyclo[4.3.1.$0^{3,7}$]dec-8-en-2-one (figure **1.6**). Most structural differences among CGXs family arise from alkylation and/or oxidation on terminal prenyl group or A-ring.[106] The structure of forbesione (**1.2**), which is isolated from G. forbesii and G. hanburyi, is the main member upon which different chemical functional groups create various related CGXs agents as shown in figure **1.6**.[107] For instance, prenylation at C5 of **1.2** yields desoxygaudichaudione A (**1.3**). Further oxidation of the latter on methyl group (C30) to yield aldehyde and carboxylic acid counterparts, gaudichaudione A (**1.4**) and isogaudichaudiic acid (**1.5**), respectively. Likewise, geranylation at C5 generates desoxygambogenin **1.6**, and gambogin **1.7** is formed, when geranyl group forms pyran ring with hydroxyl group on C18. Further oxidation of C29 on **1.7** yields **1.1**.[108]

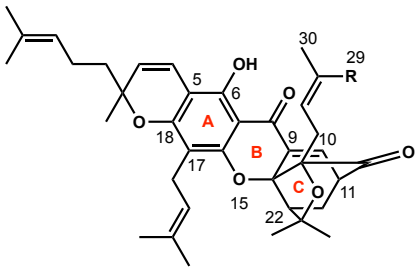

1.1: CO_2H, gambogic acid
1.7: CH_3, gambogin

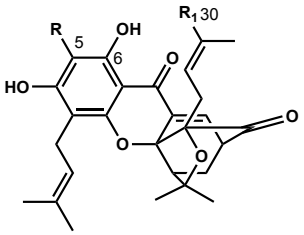

1.2: R=H, R_1= CH_3, forbesione
1.3: R=prenyl, R_1= CH_3, desoxygaudichaudione A
1.4: R=prenyl, R_1= CHO, gaudichaudione A
1.5: R=prenyl, R_1= CO_2H, isogaudichaudiic acid
1.6: R=geranyl, R_1=CH_3, desoxygambogenin

Figure 1.5. Some examples of caged Garcinia xanthone from Garcinia tree. Numbering of structures is depicted from the numbering of backbone of **1.1**

1.10.1 Biosynthesis of GCXs

CGXs are biosynthetically derive from xanthone scaffold, which is produced further from benzophenone products of mixed shikimate-acetate pathway.[109-114] This pathway starts with condensation of phosphoenolpyruvate (PEP) and D-erythrose 4-phosphate followed up with series of various reactions including oxidation, a β-elimination of inorganic phosphate, a reduction, a ring opening, and an intramolecular aldol condensation to produce 3-dehydroshikimate (DHS), which is reduced to shikimate (scheme **1.1**).[115] Also, DHS yields dihydroxybenzoic acid, protocatechuic acid, via dehydration. The latter reacts with CoA, then, the product undergoes sequential condensation of acetyl units obtained from three units of malonate coenzyme A (malonyl-CoA) to yield intermediate **1.8**, which is further transformed into benzophenone (**1.9**) intermediate by Dieckmann condensation and enolization.[116, 117] Lastly, xanthone, for example 1,3,5,6-tetrahydroxyxanthone, is produced by oxidative phenolic coupling of benzophenone counterpart.[118]

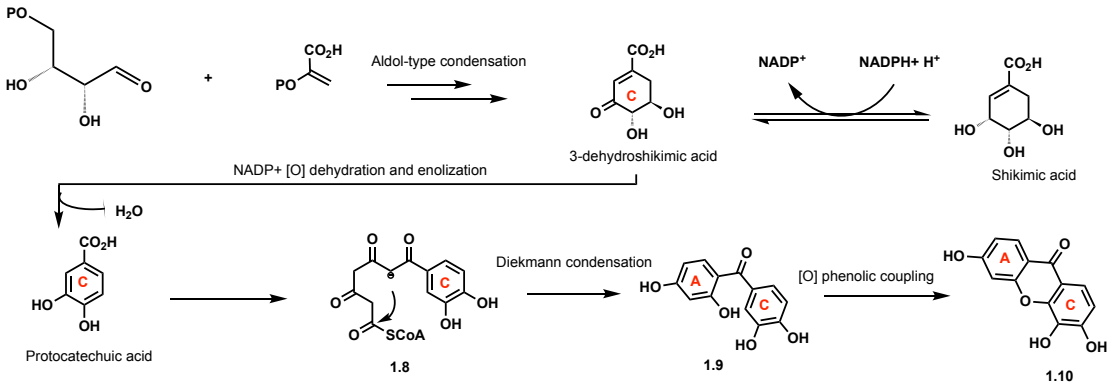

Scheme 1.1. Biosynthesis of xanthone and proposed mechanism of its formation

There are two possible proposals for the formation of caged structure. The first proposal was suggested by Kartha el al. and Ollis et al. which includes prenylation and oxidation of xanthone to yield **1.11** intermediate.[104] The attack of hydroxyl group

oxygen onto terminal alkene of prenyl group, and subsequently oxidation of C9 and C10 take place to produce caged nucleus **1.12** (Scheme **1.2**, A). The second proposal was proposed by Quillinan and Scheinmann which starts with allylation of vicinal hydroxyl of xanthone analog **1.13**.[119, 120] Afterward, Claisen rearrangement yields cyclohexane dienone **1.14** followed by intramolecular Diels-Alder reaction to produce caged nucleus **1.15**.[120] To approve the latter proposal, the authors approved experimentally that heating allylated tri-hydroxyxanthone in decalin at 190°C for 14h gave caged structure **1.15**. The result was suggestive of Claisen/Diels-Alder cascade in which C12 allyloxy unit had migrated onto the C13 center of 4, and allyloxy dienophile conjugated to form bridged cyclohexane with diene of C-ring (scheme **1.2**, B). The latter proposal has been approved experimentally when various natural CGXs products have been synthesized based on Claisen/Diels-alder cascade.

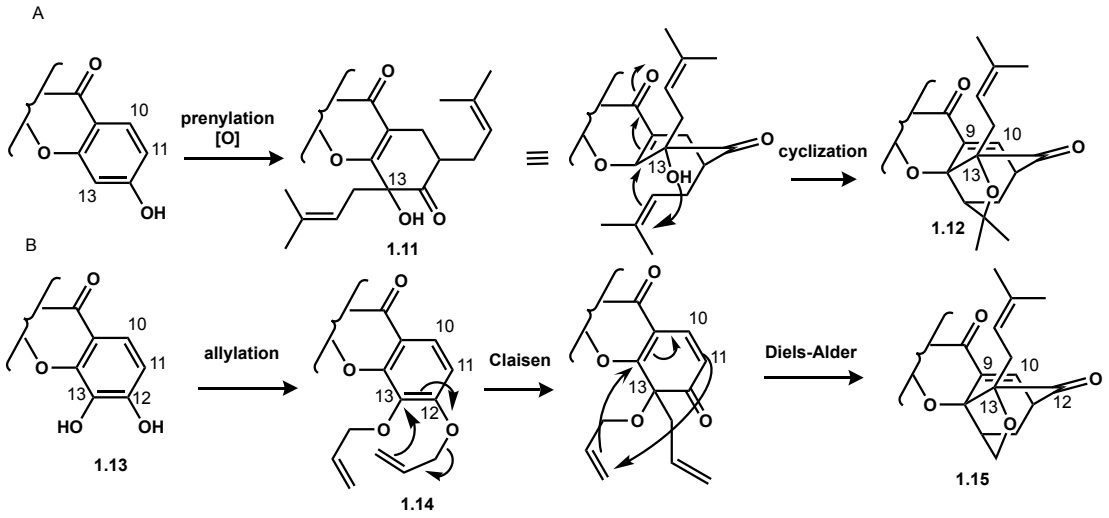

Scheme 1.2. Proposed mechanisms of biosynthesis of caged *Garcinia* xanthone. (A) nucleophilic cyclization cascade and (B) a Claisen/Diel-Alder reaction cascade

1.10.2 The route of CGXs synthesis.

Synthetic strategy of CGXs has been deduced from its biogenesis. There are three main steps: a) synthesis of the xanthone, b) installation of the reverse prenyl groups, and c) formation of the caged scaffold.

a) Synthesis of xanthone

Xanthone scaffold synthesis has been developed into different methods; however, there are two main approaches to construct xanthone. The more convenient method is a one pot reaction of salicylic acid and a phenol under higher temperature acidic conditions, such as $ZnCl_2/POCl_3$ or Eaton's reagent (P_2O_5 in CH_3SO_3H).[121, 122] Benzophenone intermediates has been formed in $ZnCl_2/POCl_3$ beside the desired xanthone product; however, by using Eaton's reagent, benzophenone intermediate is no longer or minimally formed, and xanthone is the major final product (scheme **1.3**, pathway I). The second approach utilizes Friedel-Crafts acylation of benzoyl chloride with phenol using strong Lewis acid, such as $AlCl_3$ to yield relative benzophenone intermediate.[99] Then, cyclization of benzophenone into xanthone is accomplished using basic condition (scheme **1.3**, pathway II).

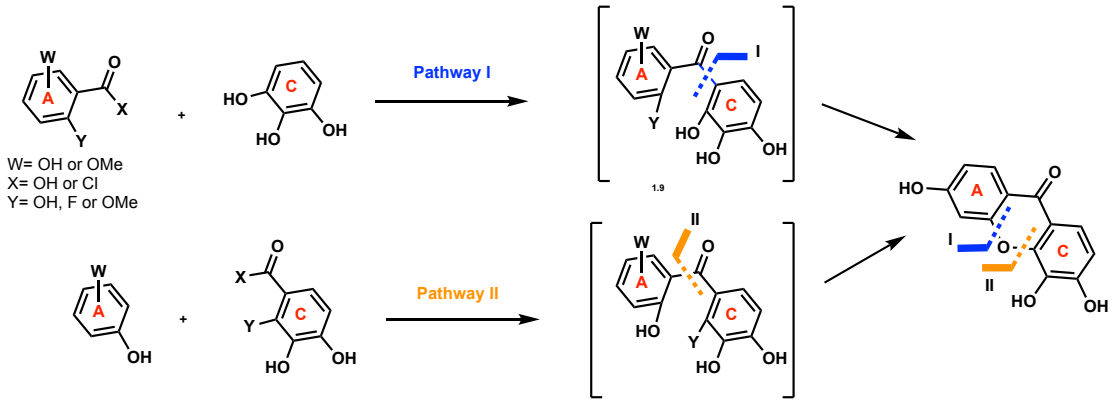

Scheme 1.3. The two synthetic approaches of xanthone formation

b) Installation of the reverse prenyl groups

There are three strategies for installation of the reverse prenyl groups on xanthone. This is a key step in the synthesis in all members of the CGXs family as the selective allylation of intended hydroxy groups is required from the other free hydroxy groups. The first method is the use of α-bromoisobutyraldehyde (**1.16**) and a strong base such as, tBuOK for the alkylation of intended hydroxy groups followed by Wittig olefination of the terminal aldehyde producing hydroxylated prenyl groups (scheme **1.4**, method I).[123] These two reactions are repeated multiple times until all intended hydroxyl groups are prenylated, thus, this strategy was not adopted due to its chemical waste and time consumption. The second method is also a two steps approach (scheme **1.4**, method II). The first step is cupper-catalyzed propargylation and of the hydroxyl groups using, CuI or $CuCl_2$, and the second step is hydrogenation of alkyne to alkene using Pd catalyst, such as Lindlar catalyst.[124] This approach is advantageous than the first one because a smaller number of steps is required to install reverse prenyl groups; however, hydrogenation step consumes time until it is optimized for intended alkene product.[96] The third method is based on Tsuji-Trost reaction which is palladium catalyzed allylation (scheme **1.4**, method III). This method requires preparation of prenylating reagent, but the installation of reverse prenyl groups takes place in a single step.[97]

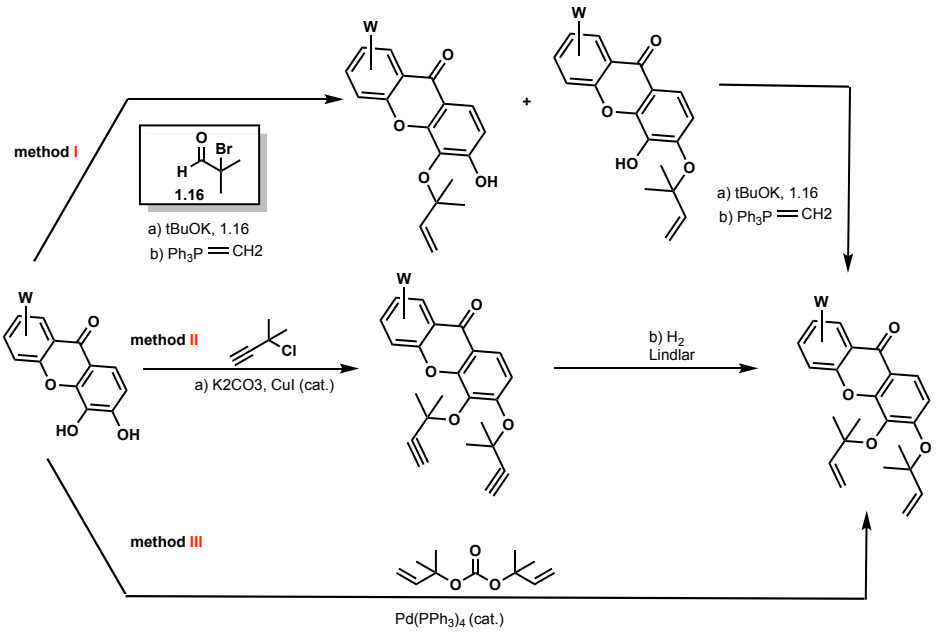

Scheme 1.4. The three methods for reverse prenylation

c) Formation of the caged scaffold

There are two reported methods for the construction of caged scaffold. The first method which is the least popular method is tandem Wessely oxidation/ Diels-Alder reactions.[106] Using $Pb(OAc)_4$, oxidation of phenol first occurs producing intermediate **1.17** followed by Diels-Alder reaction under thermal activation yielding final tricyclic lactone derivative (scheme **1.5**, method I). The overall yield of these two reactions is not great. Additionally, modification of lactone into tetrahydrofuran takes place to furnish the caged scaffold, which is another drawback for this approach. The other approach is biomimetic tandem Claisen/ Diels-Alder reaction cascade (scheme **1.5**, method II).[125] There are two different products due to two intermediates formed at Claisen rearrangement step. The two intermediates, **1.18a** and **1.18b**, are produced due to the migration of prenyl group on hydroxy groups of C12 or C13 to either C12 or C13. Afterward, Diels Alder reaction furnishes the corresponding caged final product of each intermediate. The intermediate **1.18a** yields regular caged nucleus by

cycloaddition of diene with the pendant C21-C22 dienophile (**1.19a**). Likewise, the intermediate **1.18b** undergoes cycloaddition of diene with the pendant C25-C26 dienophile to form the other caged isomer, neo caged nucleus (**1.19b**).[94, 95]

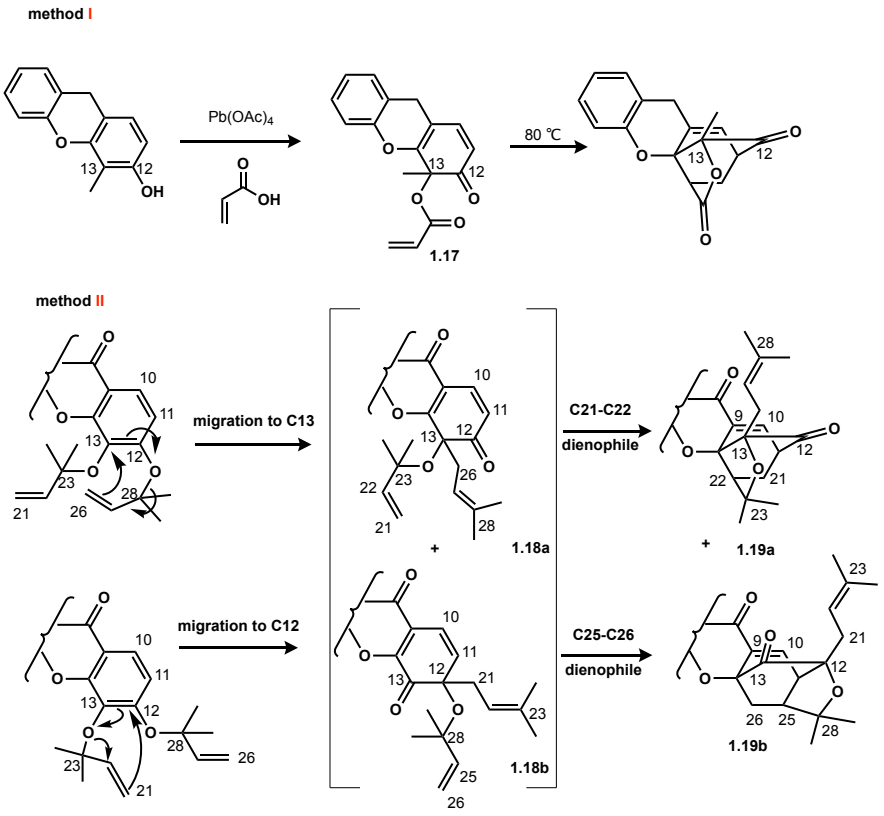

Scheme 1.5. The two approaches of C-ring (caged nucleus) of CGXs

1.10.3 Examples of the synthesis of CGXs molecules

Forbesione was first synthesized by Nicolaou and coworkers who were also first reported the use of Claisen/Diels-Alder reaction cascade.[125] The xanthone synthesis was performed over five steps of bromobenzene and benzaldehyde with protected hydroxyl groups (benzyl (Bn) and tert-butyldimethylsilyl (TBS)). Then, xanthone undergoes reiteration of two reactions, alkylation of α-bromoisobutyraldehyde and Wittig reaction, in order to furnish tri-prenylated xanthone

(**1.20**).[108] Finally, Claisen rearrangements and intramolecular Diels-Alder reaction took place under thermal activation in DMF at 120 °C to yield 6-O-methylforbesione (**1.21**) and 6-O-methylneoforbesione (**1.22**) (ca. 2.4:1 ratio). The yield of overall reactions in favor of 6-O-methylforbesione is 26% over ten steps.

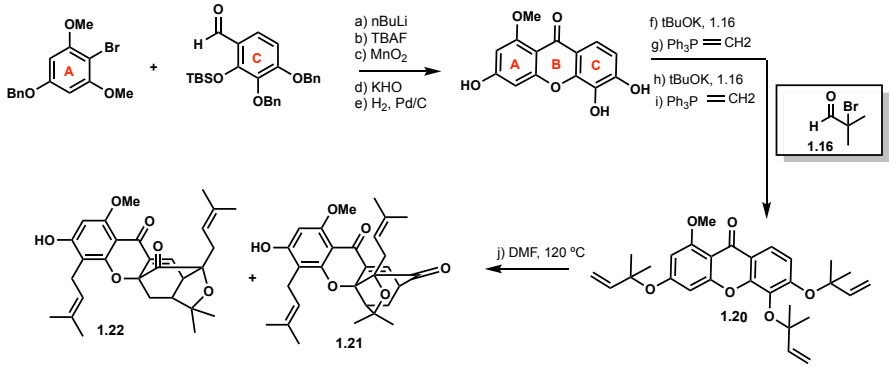

Scheme 1.6. Synthesis of 6-O-methylforbesione and corresponding neoforbesione. Bn, benzyl; nBuLi, n-butyllithium; MnO_2, manganese dioxide; KOH, potassium hydroxide; DMF, dimethylformamide; TBAF, tetra-n-butylammonium fluoride; TBS, tert-butyldimethylsilyl.

Similarly, Tisdale et al. has used Claisen rearrangement/ Diels-Alder reaction cascade to construct caged structure; however, the xanthone (**1.23**) formation occurred in one-pot reaction of 2,3,4-trihydroxybenzoic acid and phloroglucinol using $ZnCl_2/POCl_3$.[95] Afterward, two-step approach was implemented for prenyl group installation starting with cupper-catalyzed propargylation of xanthone using 2-chloro-2-methybutyne and K_2CO_3, then, reduction of alkyne into alkene using Lindlar reagent followed by acetylation of hydroxyl on C6 to furnish related tri-prenyl xanthone (**1.24**). By following Nicolaou's procedure, compound **1.24** was heated in DMF at 120 °C where Claisen rearrangement and Diels-Alder reactions had proceeded. The final products were **1.2** and isoforbesione (**1.25**) in ca. 1.4:1 ratio. It was interested to study which Claisen rearrangements occurring in A-ring or C-ring proceeds first. Using

spectroscopic studies, it was shown that C-ring Claisen rearrangement/ Diels-Alder reaction cascade proceeds first and A-ring Claisen rearrangement occurs afterward. Claisen rearrangement in A-ring is responsible for the production of forbesione and isoforbesione. In this study, the neo caged isomer of forbesione is not detected. Acetate group protecting hydroxyl group at C6 enhances the yield in favor of forbesione, which has overall yield of 6 % over five steps. The steric hindrance generated by acetate allows the migration of prenyl group in only to C17; thus, the regioselectivity of Claisen rearrangement products in A-ring can be tailored by steric hinderance on C6. It's interested that methoxyl group on C6 doesn't prevent isoforbesione formation as O-acetyl group.

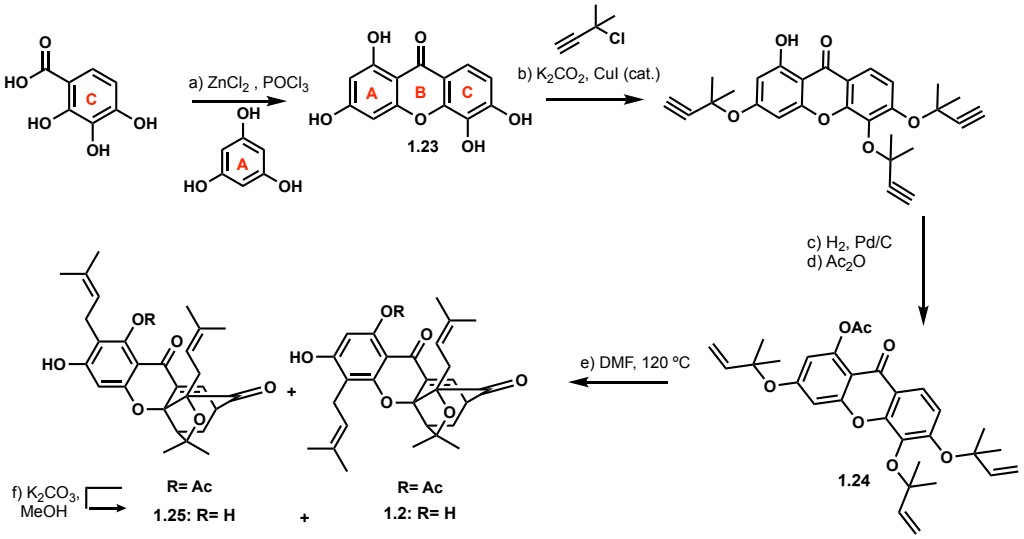

Scheme 1.7. Synthesis of forbesione and isoforbesione

1.10.4 Molecular Mechanism of Action of Gambogic Acid

Although the molecular mode underlying the biological activities of gambogic acid (GBA) is still under investigation, proteomic studies have established that it has multiple protein targets that are significant in various types of cancer. According to

Guo et al., gambogic acid affects the expression of 23 target proteins.[126] Moreover, the Xiao group has identified 80 and 116 GBA-targeted proteins in HeLa and K562 cells using activity-based proteome profiling.[127] The majority of these proteins are involved in various cellular functions such as regulation of redox state, metabolism, the ubiquitin-proteasome system, transcription, translation, as well as protein transport and modification. Selected examples include vimentin, Bax and Bcl-2, heat shock proteins (Hsp), steroid receptor coactivator-3, caspase-3, caspase-9, nuclear factor of k, and Fe-S cluster containing NEET proteins.[100, 128] Among these proteins, Bcl-2 and Hsp 90 have been intensively studied due to their cellular function. The Bcl-2 family of proteins includes proapoptotic and antiapoptotic members that play a vital role in the programmed cell death process (apoptosis).[129] When Bax protein, which is a proapoptotic protein, receives apoptotic stimuli, it undergoes conformational changes and polymerizes to generate pores at the mitochondrial outer membrane leading to its permeabilization. Subsequently, cytochrome c, which is an apoptogenic factor, is released from the mitochondria into the cytosol to activate the release of caspase-9 and ultimately caspase-3. Under cancerous conditions, Bcl-2, which is an antiapoptotic member of this family and overexpressed in tumor cells, binds to and inhibits Bax from initiating apoptosis. Gambogic acid alters the balance between Bcl-2 and Bax by decreasing mRNA expression of Bcl-2 and concurrently increasing mRNA expression of Bax. Definitely, GBA induces apoptosis in A375 cells at a rate that reached 41.87% in a dose-dependent manner.[130]

Heat shock protein 90 (Hsp 90), a well-validated anticancer target, was found to be prevented by GBA.[131] The Hsp 90 family supports cell viability by controlling protein folding (proteostasis).[132] Hsp 90 binds to about 200 client proteins to functionalize them, some of which are crucial for cell signaling and tumor

generation.[133] For example, pathways linked to cell apoptosis, growth, tissue invasion, and metastasis are functionally relied on Hsp 90. Due to its vital molecular contributions, Hsp 90 is considered as an indispensable target protein for cancer therapy. Recent competitive binding inhibition studies showed that GBA binds selectively to the b isoform of Hsp90 at a new site.[134]

Other studies have validated the proteasome, a large proteolytic complex that recognizes and degrades polyubiquitinated proteins into amino acids, as a target protein for GBA.[135] Mechanistically, GBA prevents chymotrypsin activity of the 20S proteasome, as well as deubiquitinating enzymes, which releases ubiquitin moieties for a new ubiquitination cycle. Both inhibitory effects lead to the accumulation of polyubiquitinated proteins leading to the death of cancerous cells.[135]

Maxim Pharmaceuticals identified transferrin receptor 1 (TfR-1) as a target of GBA.[136] This is a cell surface protein involved in iron transportation into the cell and is often overexpressed in various types of cancer.[137] The researchers proposed that the interaction of GBA with TfR-1 induces activation of caspase-8 resulting in initiation of apoptosis (figure **1.7**). More recent studies have suggested that GBA rapidly enters the cell and localizes in the mitochondria. This localization induces membrane depolarization and permeability leading to release of cytochrome c and induction of apoptosis.[98]

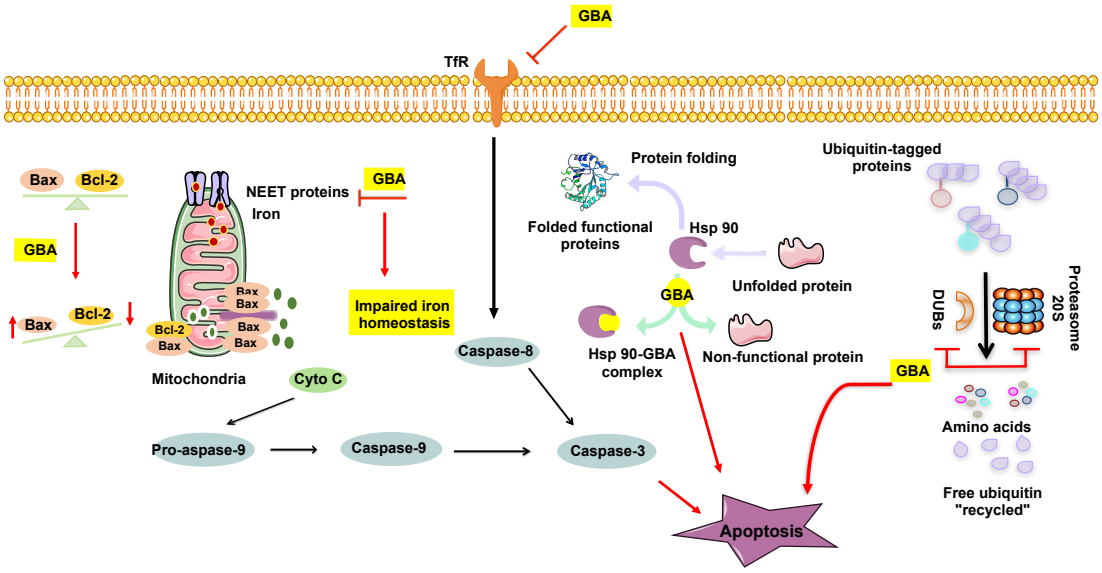

Figure 1.6. Proposed biological mode-of-action of gambogic acid based on selected protein targets. GBA, gambogic acid; TfR, transferrin receptor; Cyt c, cytochrome c; Hsp, heat shock

1.10.5 Gambogic Acid: Derivatives and structure-activity relationship (SAR) Studies

One distinct chemical feature of gambogic acid is the presence of a conjugated double bond at C9–C10. Its electrophilic property is increased due to an intramolecular hydrogen bond between the C6 hydroxyl group and the adjacent carbonyl oxygen.[138] It has been reported that storage of GBA in methanol led to the slow nucleophilic addition of a methoxy group at the C10 position (scheme **1.8**) to yield **1.26**.[139] This addition reaction also could also proceed via various heteroatom nucleophiles, such as thiols and amines, and is accelerated under basic conditions.[97] Based on these findings, it is recommended that GBA should not be stored for prolonged periods of time in alcoholic solvents.

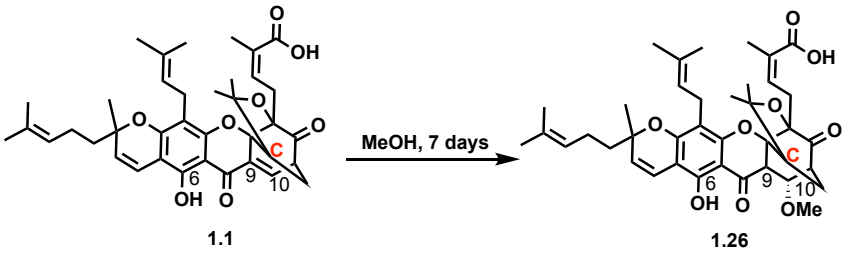

Scheme 1.8. The formation of gambogic acid analog (**1.26**) upon storage in methanol

Further chemical modifications at the C9–C10 enone have confirmed its biological influence. Reduced (**1.27**) or substituted (**1.28** and **1.29**) analogs (scheme **1.9**) at the C9–C10 site display significant loss of activity (more than 10-fold) when compared to GBA in T47D, ZR751, and DLD cell lines. This suggests that α, β-unsaturated ketone is critical to the biological activity of GBA, since it could be a site for nucleophilic attack from a target protein.[140] Michael-type addition reaction could produce stable adducts that, in turn, modulate the cytotoxicity of the parent molecule.[141]

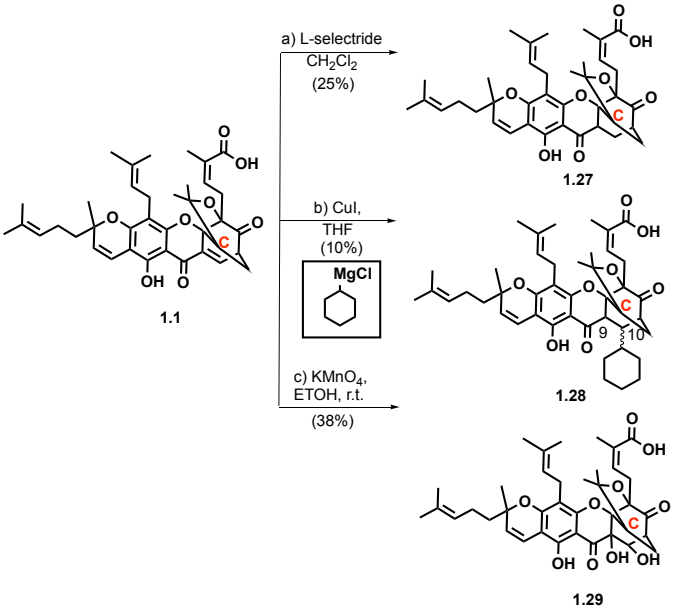

Scheme 1.9. Analogs of gambogic acid at α,β-unsaturated ketone

The C29 carboxylic acid functionality of GBA provides an interesting site for further structural modifications. Interestingly, the methyl ester of GBA has a similar IC_{50} and biological activity as the parent molecule in a caspase activation assay.[140] Typically, carbodiimide crosslinker chemistry has been employed to generate various GBA analogs at the carboxyl group.[142] The Cai group synthesized a series of amide-GBA analogs. Among them, analogs containing piperidine were found to be nearly twofold less active than GBA in induction of apoptosis using T47D cells.[140] Similarly, the Zhang group has synthesized a number of GBA analogs containing various hydrophilic alkanolamines in an attempt to improve water solubility and overall bioactivity. Furthermore, compound **1.30** (figure **1.8**), which encompasses a three-carbon alkanol spacer linked to a morpholine, exhibited the highest potency of any other analogs tested with an IC_{50} of 0.045 uM. In this assay, GBA was found to exhibit an IC_{50} of 0.75 uM. Compound **1.30** also showed selectivity toward hepatocellular carcinoma cells without affecting normal liver cells. However, similar analogs with a two-carbon alkanol linker and/or piperidine as cyclic amine exhibited considerably lower bioactivity. Furthermore, a furazan nitric oxide donor was incorporated via an ester bond at the carboxyl group of GBA due to its known antitumor activity. Unexpectedly, this analog **1.31** (figure **1.8**) displayed a dramatic decrease in cytotoxicity in a human lung carcinoma cell line (A549) compared to GBA.[143] Various thioesters were also synthesized but were found to be less active compared to GBA.[144]

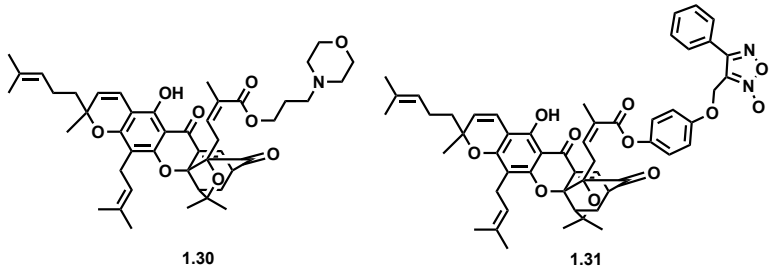

Figure 1.7. analogs of gambogic acid at carboxyl group.

Likewise, the carboxylic acid group can be utilized to produce GBA probes that can be used for target identification and kinetic assays.[100, 136] These probes, which are labeled with biotin, fluorescein, and agarose, are as active as the parent compound. Binding assays of biotinylated- GBA (**1.32**, Bio- GBA) (figure **1.9**) indicated that GBA is an apoptosis inducer and a substrate of TfR. This probe displayed a K_d of 2.2 uM and an IC_{50} of 1 uM using europium-labeled streptavidin in time-delayed fluorescence.[136] In a different study using streptavidin bead pulldowns from cell lysates, **1.32** revealed that GBA is an Hsp 90b-specific inhibitor. There are two major Hsp 90 isoforms: Hsp 90a and Hsp 90b. Hsp 90 consists of three main domains: N-terminal domain (NTD) with ATP binding pocket; the middle domain (MD), which is critical for client recognition and ATPase competence; and the C-terminal domain (CTD). Most anticancer drugs targeting Hsp90 have binding sites in the NTD and the CTD.[132, 145] Importantly, GBA binds selectively to Hsp90b at a novel pocket in the MD that is closer to the client binding site and distinctly different from any other identified pockets. Click chemistry between alkyne analog **1.33** (GBA-yne) (figure **1.9**) and tetramethylrhodamine-azide or biotin-azide has also been utilized to elucidate GBA molecular targets using quantitative mass spectrometry-based chemical proteomics.[127]

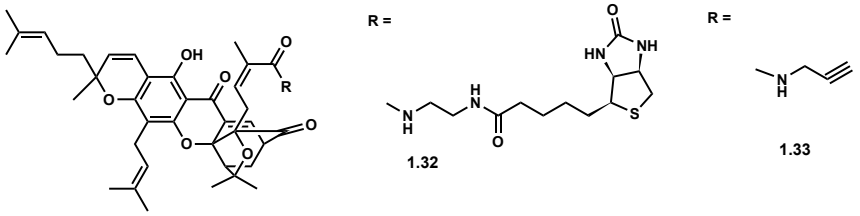

Figure 1.8. the synthetic probes of gambogic acid.

1.10.6 Gambogic Acid: Conjugation and Formulation Studies

Conjugation of GBA with various polymers has been explored in order to improve water solubility and oral drug delivery.[146] For example, a chain of polyethylene glycol (PEG) with L-leucine on each end connecting to two molecules of GBA improves water solubility by approximately sixfold.[147] In similar studies, a proline–proline GBA (PEG10kDa) conjugate showed a 36 times increased cytotoxicity than GBA alone.[148]

In addition, GBA was encapsulated into lactoferrin nanoparticles by nano-particle albumin-bound (NAB) technology to create an oral dosage form with similar antitumor activity as GBA -L-arginine injection. Lactoferrin, which is a cationic iron-binding glycoprotein, acts as a carrier of GBA to enable its absorption through lactoferrin receptors on intestinal cell surface.[149] Similarly, formation of GBA micelles with either N-octyl-O-sulfate chitosan or N-octyl-N-arginine chitosan provides a promising delivery system with better pharmacokinetic parameters.[150] GBA along with retinoic acid, which induces cancer cell apoptosis, was coloaded on glycol chitosan nanoparticles. This formula synergistically induces apoptosis and inhibits cancer cell proliferation. Another synergistic formula involves loading GBA on magnetic nanoparticles (MNP)-Fe_3O_4, which is more effective in inducing apoptosis than GBA alone.[151]

Quantum dots (QDs) are fluorescent semiconductor nanocrystals that have substantial applications in bioscience.[152] Due to electrostatic interactions, negatively charged GBA can be simply adsorbed on cationic cysteamine- coated cadmium-tellurium quantum dots (Cys-CdTe QDs) to yield a self- assembled GBA -Cys-CdTe QD nanocomplex.[153] With respect to cancer therapy, a number of advantages have been discovered when GBA is loaded on such QDs. For example, peripheral side effects of GBA can be minimized since the release of GBA from the QDs is highly dependent on pH. This implies that GBA is predominantly released in the microenvironment around tumor cells which usually have a lower pH than that of normal cells. Moreover, Cys-CdTe QD by itself has anticancer activity and can be used to overcome multidrug resistance (MDR). Most importantly, GBA-Cys-CdTe QDs can be utilized as a methodological fluorescence nanoprobe for real-time labeling to follow-up changes in the tumor cells. In another study, the GBA-Cys-CdTe QD nanocomplex was examined for the treatment of leukemia and was found to be potent against multiple resistant K562/A02 cell line.[154] In a related study, daunorubicin, a chemotherapy drug for Hodgkin's lymphoma, was added to GBA-Cys-CdTe QDs. This unique complex effectively bypassed P-glycoprotein, an efflux pump excreting xenobiotic out of the cell as mechanism of protection. As such, it considerably minimized MDR and increased sensitivity of tumor cells toward daunorubicin in vitro and in vivo.[155] The above studies imply that the carboxylic group of GBA is not essential for its bioactivity. However, it acts as a site for chemical modifications in order to enhance its biological and pharmacological profile.

Chapter 1, in part, was adapted from published chapter, Caged Garcinia Xanthones: Synthetic Studies and Pharmacophore Evaluation, *Studies in Natural Products Chemistry*, on which I was a co-author. Oraphin Chantarasriwong and

Emmanuel Theodorakis contributed thoughts, expert ideas, and opinions to the chapter.[101]

Chapter 2 : Metabolomics study of mitochondrial diseases

2.1 Introduction

Mitochondria are multifunctional organelles that have been involved in almost all interactive metabolic pathways affecting most of the vital cellular activities. Disturbance in their functionalities either directly or indirectly results in extremely complex pathogenesis that is difficult to understand.[4, 21, 41, 43, 58, 62, 148, 156, 157] It is very complicated to find out the main defective pathway because its connected pathways sequentially are affected as well, even though affected pathways themselves have normal activities.[14] On the other hand, some defective pathways are benign; however, accumulated substrate could activate other pathways leading to the production of toxic metabolites that is hard for the body to detoxify.[20, 21, 157]

Mitochondrion is unique cellular compartment as it has its own DNA. Also, nuclear DNA mediates mitochondrial replication and protein encoding.[50] Currently, many aspects and concepts of mitochondrial functions and/or performance being re-evaluated broadly. For example, resilient growing research effort has suggested that protein complexes of the electron chain transfer are farther from being merely a cascade for ATP production but also regulate vital processes such as fatty acid synthesis and can indicate for mitochondrial dysfunction.[57, 158] Furthermore, mitochondria have associated with many aging related diseases lacking precise explanation for the mechanism of its involvement.[61] In this study, we answered and determined unbiasedly the major metabolites and pathways presented the basis of mitochondrial dysfunction with certain phenotypes.

In collaboration with Dr. Holger Prokisch in Germany, we have conducted untargeted metabolomics study on plasma sample from patients with rare mitochondrial mutations and diseases, so-called MitoNet cohort.[159] Previous studies on the cohort have emphasized the overlap of various mitochondrial diseases despite the fact that they result from different genetic lesions. Moreover, one mutation can be presented with inter- and intra-familial clinical variabilities that occur in other mutation leading to challenging diagnosis and treatment regimes.[159-161]

This metabolomic study is, therefore, unique as it reflects the real biological events of mitochondrial dysfunctions taking place in the human body and the interaction with all counted and uncounted biochemical events. We aim to clarify some of ambiguous clinical observation and find out relationship between phenotype and metabolites level by metabolomic study. Not only that, but also this study could reveal some of mysterious mitochondrial mechanisms in ageing related diseases, such as diabetes. Figure **2.1** displays meta data of the MitoNet cohort. The majority of mitochondrial diseases in this cohort are mitochondrial diseases either with neuro-ophthalmic manifestations, such as LHON, or systematic diseases, such as KSS and MELAS.

A.

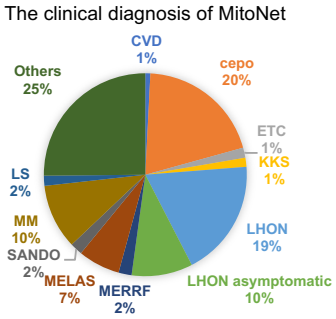

B.

Status	Gender	
	Female	Male
Mitochondrial disease	688	858
Control	287	190

C.

LHON classes	Gender		Mutation					
	Female	Male	11778 G>A	3460 G>A	14484 T>C	Multiple deletion	3243 A>G	NA
LHON symptomatic	28	124	82	22	14	4	1	29
LHON asymptomatic	84	26	61	14	10	4	0	24

Figure 2.1. Meta-analysis of MitoNet cohort. A) Clinical diagnosis of MitoNet patients with their proportions; B) Number and gender of MitoNet patients and control; C) Number and gender of LHON cohort with genetic lesions.

2.2 Materials

MitoNet samples were run according to untargeted LC/MS method of bioactive lipids developed by Jain's lab.[162] Approximately, two thousand of plasma samples were stored using polypropylene storage cryotubes with socketed screw caps like Thermo Scientific Matrix screw-top storage tubes distributed among 96-well tube racks. In order to run samples, mobile phase should be prepared with LC/MS grade solvents including organic solvents, acetonitrile (ACN) and isopropyl alcohol (IPA), and water. Furthermore, deuterated and non-deuterated internal standards were purchased from Cayman chemicals and used to prepare two mixture. The internal standard mixture (1) is a mixture docosahexaenoic acid-d_5, and some analogs of prostaglandin (PGD), hydroxy-5Z,8Z,11Z,13E-eicosatetraenoic acid (HETE), hydroxy-10E,12Z-octadecadienoic acid (HODE), dihydroxy-9Z-octadecenoic acid

(diHOME), 6E,8Z,11Z,14Z-eicosatetraenoic acid (ETE), and thromboxane B_2 (TXB_2), including 13,14-dihydro-15-keto-PGD_2-d_4, 13,14-dihydro-15-keto-$PGF_{2\alpha}$-d_4, PGD_2-d_4, $PGF_{2\alpha}$-d_4, PGE_2-d_4, 15-deoxy-$\Delta^{12,14}$-PGJ_2-d_4, 6 k-$PGF_{1\alpha}$-d_4, 5S-HETE-d_8, 12S-HETE-d_8, 15S-HETE-d_8, 20-HETE-d_6, 13S-HODE-d_4, 9S-HODE-d_4, 9,10-diHOME-d_4 and 12,13 diHOME-d_4, 5-Oxo-ETE-d_7, and TXB_2-d_4. While, the internal standard mixture (2) includes Resolvin D_1-d_5, 12-[(cyclohexylcarbamoyl)amino]dodecanoic acid (CUDA), and leukotriene-6,7,14,15-d_4(LTB_4-d_4). Stock internal standards were also prepared for the entire study at a final concentration of 1 ng/μL using LCMS grade ethanol in an amber glass container.

Additionally, some types of 96-well plates are needed for this method, such as 450 μL V-bottom, Axygen 600 μL V-bottom and Greiner 1.2 mL deep well. Solid phase extraction (SPE) was performed using Phenomenex Strata-X 33 μm polymeric 96-well (10 mg/well) solid phase extraction plates. For ultra-performance liquid chromatography (UPLC) separation, Phenomenex Kinetex C18-1.8 μm (100 × 2.1 mm) UPLC column coupled to a guard column, e.g. Waters UPLC BEH RP-18. With respect to instrumentations, we used Thermo vanquish UPLC for chromatography, Thermo QExactive Orbitrap mass spectrometer for mass spectrometry.

2.3 Methods

MitoNet plasma samples were distributed in 96-tube plate, and a one or two plates were run per a day. Each single run has 93 plasma samples from the study and three samples of pooled plasma as a control. Before the run, samples are allowed to thaw at 4 °C, then sample rack was shaken at 4 °C at 700 rpm for 15 min using Fisherbrand microplate vortex mixer. After that, 20 μL of each MitoNet plasma sample was added to the corresponding well in a 450 μL Thermo V-bottom 96-well

plate. In the empty wells A1, D12, and H12 of the same plate, another 20 µL of the pooled plasma was added. A solution of 100 µL of Internal standard mix (1) was added in 8.4 ml of −20 °C ethanol into a glass scintillation vial and mixed very well by vortexing; then an amount of 81 µL of this solution was added to each well containing the plasma samples. With no mixing, residual liquid drops on the lips of the wells were removed with Kimwipe; then, the plate immediately was sealed with an EZ-Pierce zone-free seal. The plate was gently shaken at 4 °C at 550 rpm for 15 min in order to allow mixing and quenching the sample removing protein and non-polar lipids. After 15 min, the plate was centrifuged at 4,000 × *g* at 4 °C for 10 min.

For extraction, a 96-well Strata-X SPE plate was placed on the top of the 96-well extraction plate vacuum manifold followed by a series of sequential washes of 600 µL ethanol, 600 µL methanol, and lastly 900 µL water. Vaccum was applied to pull through the solvent at 2.5 inHg until no liquid can be seen in the wells. In 96-well Axygen V-bottom plate, each well was filled with 350 µL water; then, 65 µL of supernatant of plasma/ethanol mixture from the quenching step was added. Another 65 µL of −20 °C ethanol (containing no standards) was added to protein precipitant in the 450 µL Thermo V-bottom 96-well plate, gently shaken and transferred to Axygen V-bottom 96-well plate. The total volume of 480 µL was transferred to SPE plate and liquid allowed to elute by gravity. Next, 600 µL solution of 10% aqueous methanol was added on SPE wells under 2.5 inHg vacuum. Once all liquid pulled through, a new 600 µL Axygen V-bottom plate was placed into the bottom of the vacuum manifold, and each well was washed with 450 µL ethanol to elute targeted bound metabolites under gravity in the first few minutes followed by vacuum of 10 inHg. Lastly, the eluent was dried using a vacuum concentrator operated at 40 °C.

For resuspension of extracted plate, 10 ml resuspension solvent (80:20 ethanol:water with 0.1% acetic acid (AA)) was transferred into 20 ml scintillation vial with 8.33 µL of the internal standard mix (2) followed by vortexing it for a minute. Resuspension solvent of 50 µL was added into each well of dried samples and sealed with an EZ-Pierce zone-free seal. Then, the sample plate was shaken at 4 °C at 650 rpm for 10 min. The content in the sample plate was transferred into glass inserts placed into corresponding wells of LC/MS sample plate, and the latter plate was sealed using 20 µm pierceable foil seal. To remove air bubbles from liquid, the LC/MS sample plate was centrifuge 500 rpm at 4 °C for 10 min; lastly, the plate stored in the 4 °C fridge while LC/MS experiment was arranged.

Before LC/MS analysis, two mobile phases (A) and (B) were prepared as following: mobile phase (A), 30% ACN in water and 0.1% of AA, and mobile phase (B), 50:50 mixture of IPA and ACN with 0.02% of AA. Both mobile phase bottles were mixed well and degassed via sonication

For LC/MS analysis, 20 µL of each sample in the prepared plate was injected in a column, heated at 50 °C for at least 10 min prior to running. The sample was separated using the following gradient: 1% B from 0 to 0.25 min, 1% to 55% B from 0.25 to 5.00 min, 55% to 99% B from 5.00 to 5.50 min, and 99% B from 5.50 to 7.50 min. A 1.0 min re-equilibration at 1%B should be applied after every injection. The flow rate was set at 0.375 mL/min. With regard the geometry of the heated electrospray ionization probe, the setting are as follows: negative ion mode profile data, sheath gas flow of 40 units, auxiliary gas flow of 15 units, sweep gas flow of 2 units, spray voltage of −3.5 kV, capillary temperature of 265 °C, aux gas temp of 350 °C, S-lens radio frequency at 45. For the MS1 scan settings, the scan range was of m/z 225–650, mass resolution of 17.5 k, automatic gain control of 1e6, and inject

time of 50 MS. In order to get diagnostic fragment peaks across the possible range of metabolites, MS/MS of DIA was acquired using mass windows at m/z 240.7-320.7, m/z 320.7-400.7, m/z 400.7-480.7, and m/z 480.7-560.7 with a normalized collision energy of 35 arbitrary units.

With regard to data pre-processing, raw data files suffer from many issues including rt drift leading to misaligned peaks, and bad peaks.[72, 163] First, raw files were acquired using Xcalibur software, and converted to mzXML (eXtensible Markup Language) data format using MSconvert software. Then, all data files were loaded into the open source program Mzmine 2.36. The alignment of rt was computed by using the retention times for all deuterated internal standards and nearly 90 endogenous landmark peaks to create a model for correcting all detected peaks. Then, rt corrected data file were loaded into Mzmine 2.36 for full data extraction. The parameters including mass detection, chromatogram builder, chromatogram deconvolution, and join aligner, are summarized in table **2.1**.

Table 2.1. Mzmine 2.36 settings

Parameters	**Values**
Mass detection	
scans	MS level: 1
Mass detector	Centroid
Chromatogram builder	
Scans	MS level: 1
Minimum time span (min)	0.05
Minimum height	2.00E+05
m/z tolerance	0.0 m/z or 10.0 ppm
Chromatogram deconvolution	
Algorithm	Local minimum search
Chromatographic threshold	0.00%
Search minimum in rt range (min)	0.03
Minimum relative height	2.00%
Minimum absolute height	4.00E+05
Minimum ratio of peak top/edge	1.5
Peak duration range (min)	0.04-4.00
Join Aligner	
m/z tolerance	0.00 m/z or 5 ppm
Weight for m/z	1
Retention time tolerance	0.001 min
Weight for rt	1
Peak list rows filter	
Minimum peaks in a row	70
Keep or remove rows	Keep rows that match all criteria

Afterward, bad peaks were removed by peak quality filtering step in which peak windows for each putative feature were generated with ranges of m/z minimum and m/z maximum and rt start and end. This step is based on image-based deep neural network model, which generates images of stacked peaks of a window

reflecting the peak intensity values. Then, classification of peaks as good or bad peak was determined through a machine learning model, neural network model of produced images, that has been developed in Jain's lab. As a result, acceptable peaks with good spectral features as positive signals were selected. Afterward, data were normalized by batch median correction across all batches. Additionally, machine learning pipeline produces a final comma separated values (csv) sheet containing all metabolites features with adduct and isotope information, peak intensities of all samples, and mass and rt error. The final csv sheet can now be utilized for statistical analysis in order to answer study's questions and find out relationships between metabolites and biological events.

There are a variety of statistical tests can be applied on different types of data set. In MitoNet cohort, we would like to study the association of metabolites with diseases, phenotypes and many more criteria by comparing case vs control samples. Binary logistic regression is a predictive regression model, used to classify independent variables into two classes of dependent variable, such as case vs control.[164] Another important feature of logistic regression is odd ratio, which measure the degree of association or the likelihood of the dependent variable with the independent. Furthermore, clustering methods are useful to reduce dimensionality of data, such as principle component analysis (PCA) and partial least squares-discriminant analysis (PLS-DA). In PCA, principal components (PC) are artificial variables that assemble in a linear manner the original variables and allow metabolites spanned into smaller space. Calculating the variance-covariance matrix of eigenvalues, which explain variance of each PC, and PCs with the highest variance are selected to unbiasedly visualize difference in the data.[165] On the other hand, PLS-DA is the supervised version of PCA, and it allows metabolites projection

into space according to categorical variable. In PLS-DA, latent variable (LV) is analogous to the PC of the PCA but measure covariance instead of variance. All statistic tests were carried out in RStudio (Version 1.1.463), an open source for direct code execution to run tremendous computational functions.

2.3 Results and discussion

2.3.1 Gender bias in mitochondrial diseases

The meta data has been filtered in a way that the replicate samples were removed, and single sample of each patient was included in the analysis. Depending on the phenotypes available in MitoNet cohort, we divided samples into LHON and non-LHON cohort, which contains all other genetic mitochondrial diseases. Data processing yields final csv sheet of 14690 metabolites to proceed with for statistical analysis. Multivariate logistic regression of each cohort was calculated using RStudio. For LHON, logistic regression was calculated to estimate odd ratio of the metabolites (149 of case samples and 109 of the control). The regression was repeated twice for two settings: age and gender corrected and age only corrected settings. For each metabolite, p-value and log odd ratio were calculated. For each setting, the top 300 significant metabolites with lower p-value were chosen to visualize the influence of gender bias. Likewise, logistic regression was calculated for non-LHON cohort with 445 case samples and 126 of the control. The two settings of logistic regression were applied, and top 300 metabolites were selected for comparison.

Gender bias is a common phenomenon in medical settings. In LHON, gender bias is a common clinical feature affecting male fivefold more than female patients.[166] Of interest, metabolomic approach was utilized to decipher gender preference in LHON at molecular level. Next, comparison of LHON metabolic profile to non-LHON

profile was performed to further examine metabolic trends of gender bias and find out a metabolic pattern describing the difference of the single or multiple organs involvement. In this study, we've noticed a great gender influence on LHON disease. The p-values of key metabolites in non-LHON subset were more significant than those of LHON subset by 12 order of magnitude. This could be due to sample size and metabolic nature of both cohorts since LHON diseases has lesser systematic metabolic involvement than non-LHON diseases. In LHON cohort, gender effect is allowed in one logistic regression model (figure **2.2**, A), and the key metabolites in that model have dropped considerably into nonsignificant p-value range when additional gender adjustment was applied. For non-LHON cohort, on contrary, key metabolites stays significant even after correcting for gender covariate (figure **2.2**, B). Thus, we continued to visualize this difference by PCA (figure **2.3**), but there is minor clustering of metabolites based on gender when they are projected between PCs on x and y axes (PC1 explained variation is 5%, and PC2 explained variation is 2%, respectively).[167]

PLS-DA was used to recognize whether metabolites could be clustered better based on patients' gender. The model reveals segregation of metabolites based on gender, explaining 7% of the variance in total (5% of variance explained by LV1 and 2% of variance explained by LV 2) (figure **2.4**). Hence, PLS-DA analysis displays better evidence for gender bias exhibited by patient with LHON. Furthermore, the result of the two logistic models of LHON, particularly metabolites p-value and odd ratio were plotted as volcano plot, which is scatter plot statistical significance e.g. -log p-values vs magnitude of change e.g. log odd ratio, which divides plotting points into left and right regions (figures **2.5** and **2.6**). Moreover, p-values of the key metabolites in age only adjusted logistic regression model (figures **2.6**) are five order of magnitude significant

of that with both age and gender adjusted logistic regression (figures **2.5**). Most likely these metabolites have hormonal component.[168] This result is supported by case reported for a female patient who had vision loss upon menopause, but her vision was recovered as she followed hormonal replacement therapy.[168] Furthermore, LHON cybrid cells carrying m.11778G>A mutation were treated with analog of estrogen, which binds to estrogen receptors.[169] As sequences, mitochondrial defect was diminished via reducing apoptosis, enhancing mitochondrial biogenesis, and a reducing ROS. Collectively, these data have supported that the gender bias is an important part in LHON pathogenesis as well as therapeutic management.[170] There are not many common significant metabolites between LHON and non-LHON cohorts, suggesting that metabolic profiles of LHON is distinct disease with great hormonal influence when compared to other genetic mitochondrial diseases. Furthermore, metabolic profiles obtained via metabolomic studies differentiate between phenotypic trends of mitochondrial diseases associated with defects in single or multiple organs. This finding recognizes metabolomics as the key analytical field to answer the questions related to clinical manifestations that are failed to be explained via other omics families, such as genomics and proteomics.

A.

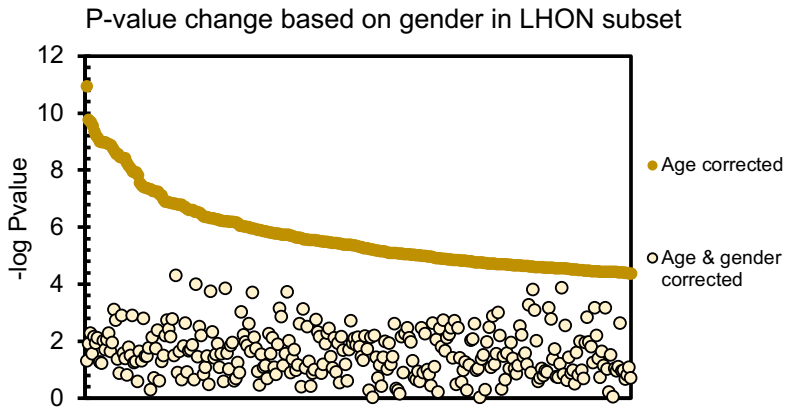

B.

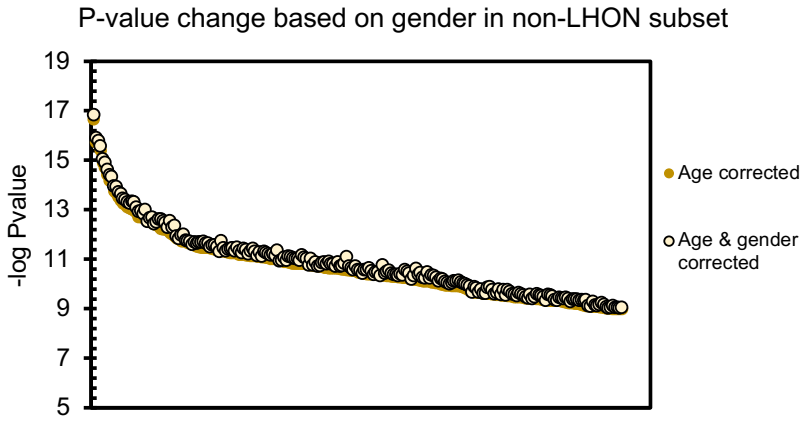

Figure 2.2. The plot (A) and (B) represent -log p-values of top 300 significant metabolites in LHON and non-LHON subset, respectively, under two settings, age corrected only, and age and gender corrected logistic regression

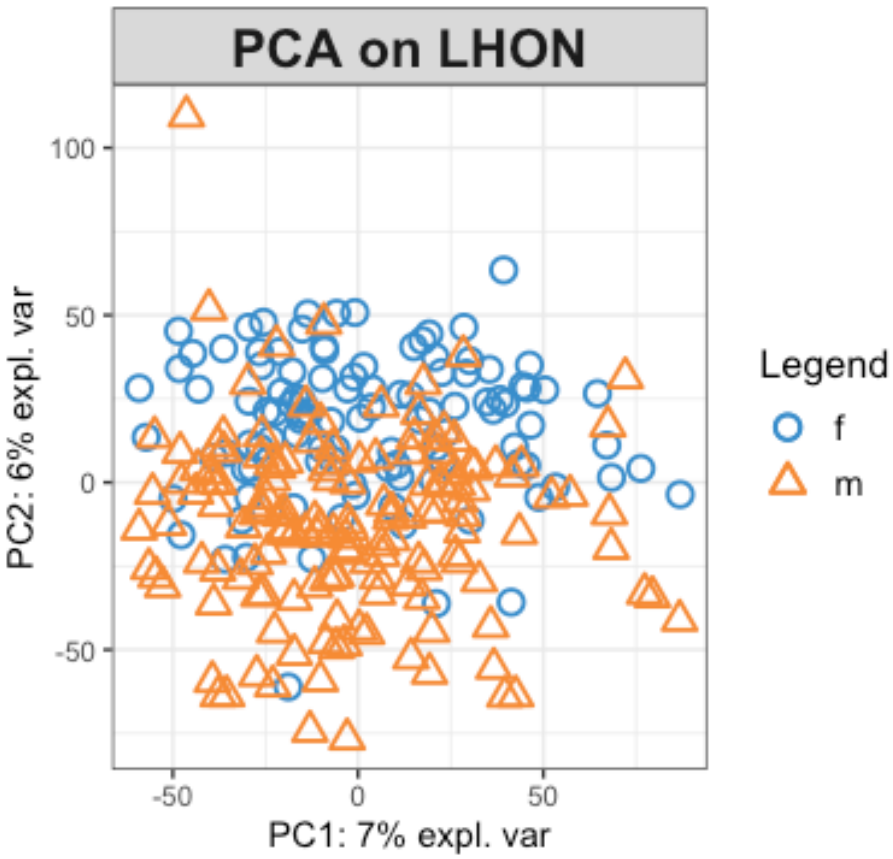

Figure 2.3. PCA plot of metabolites in LHON subset as they are labeled according to gender. Each point represents metabolites. Legend: m= male, f= female, exp. var= the amount of variation explained per component

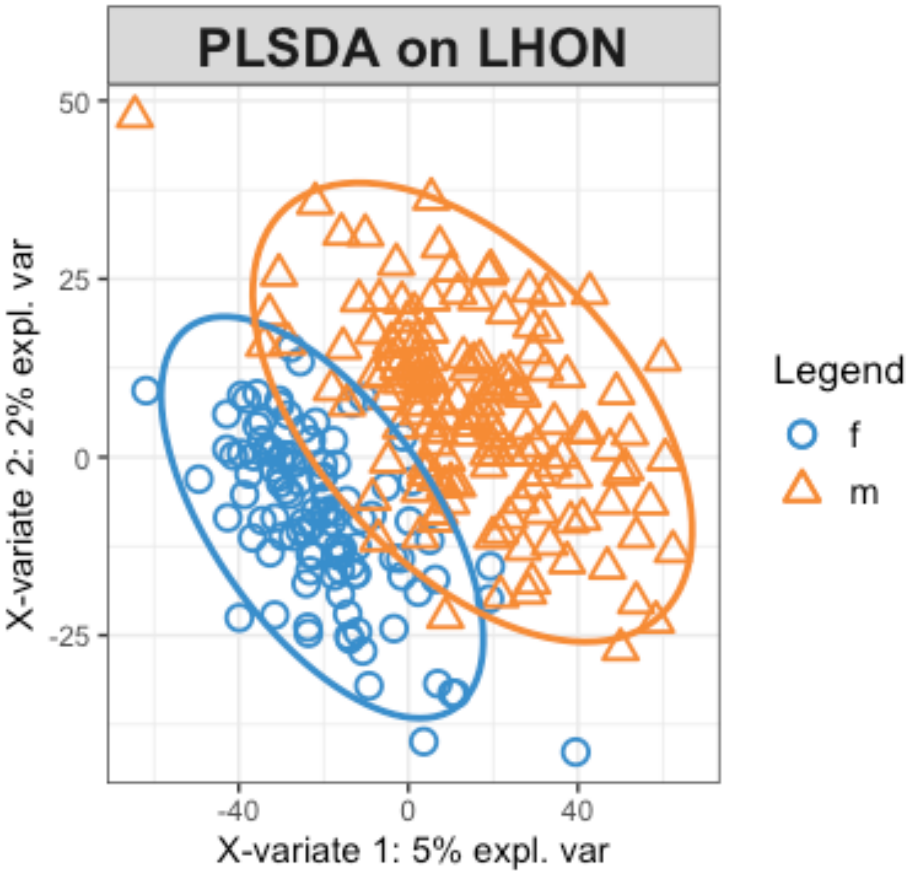

Figure 2.4. PLSDA plot of metabolites in LHON subset as they are labeled according to gender. Each point represents metabolites, the confidence level is set to 95% for ellipses, and the separation is based on latent variables (X-variate 1 and X-variate-2) Legend: m= male, f= female, exp. var= the amount of variation explained per component.

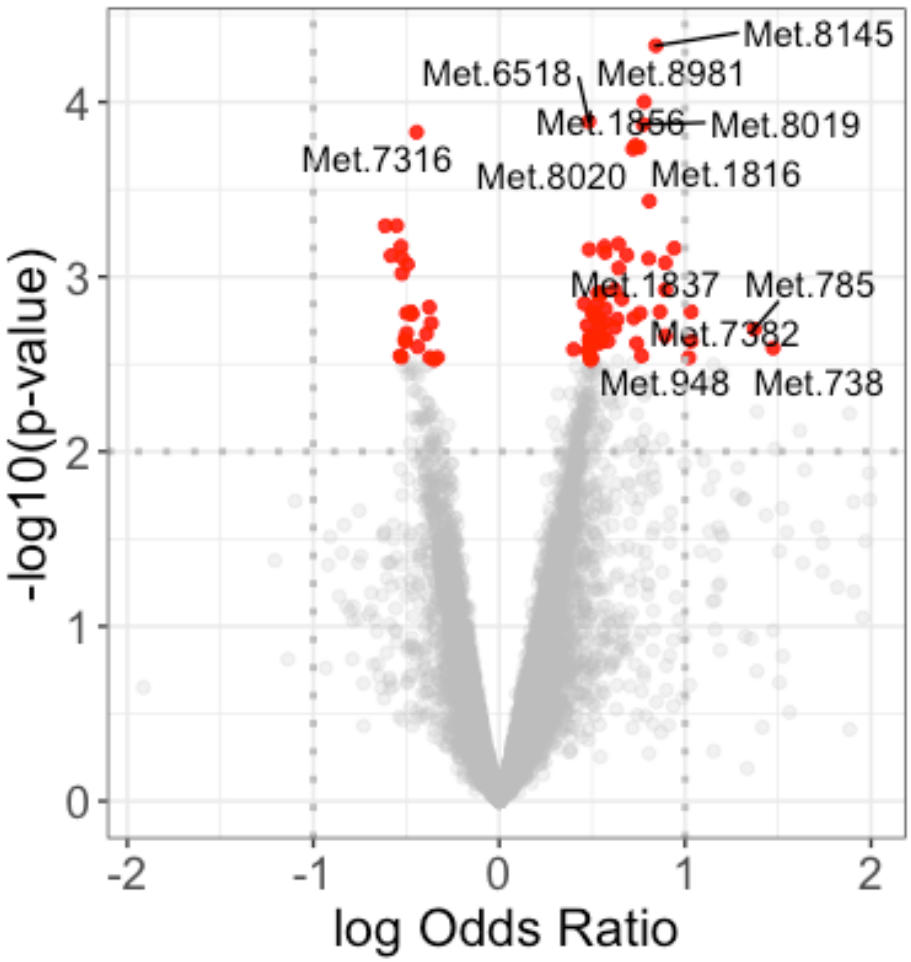

Figure 2.5. Volcano plot of p-values resulting from age and gender adjusted logistic regression model of LHON cohort. Negative log of p-value is y axis and log odd ratio is x axis. Some key metabolites are labeled with increased likelihood of associating with LHON than control. Met. = metabolite

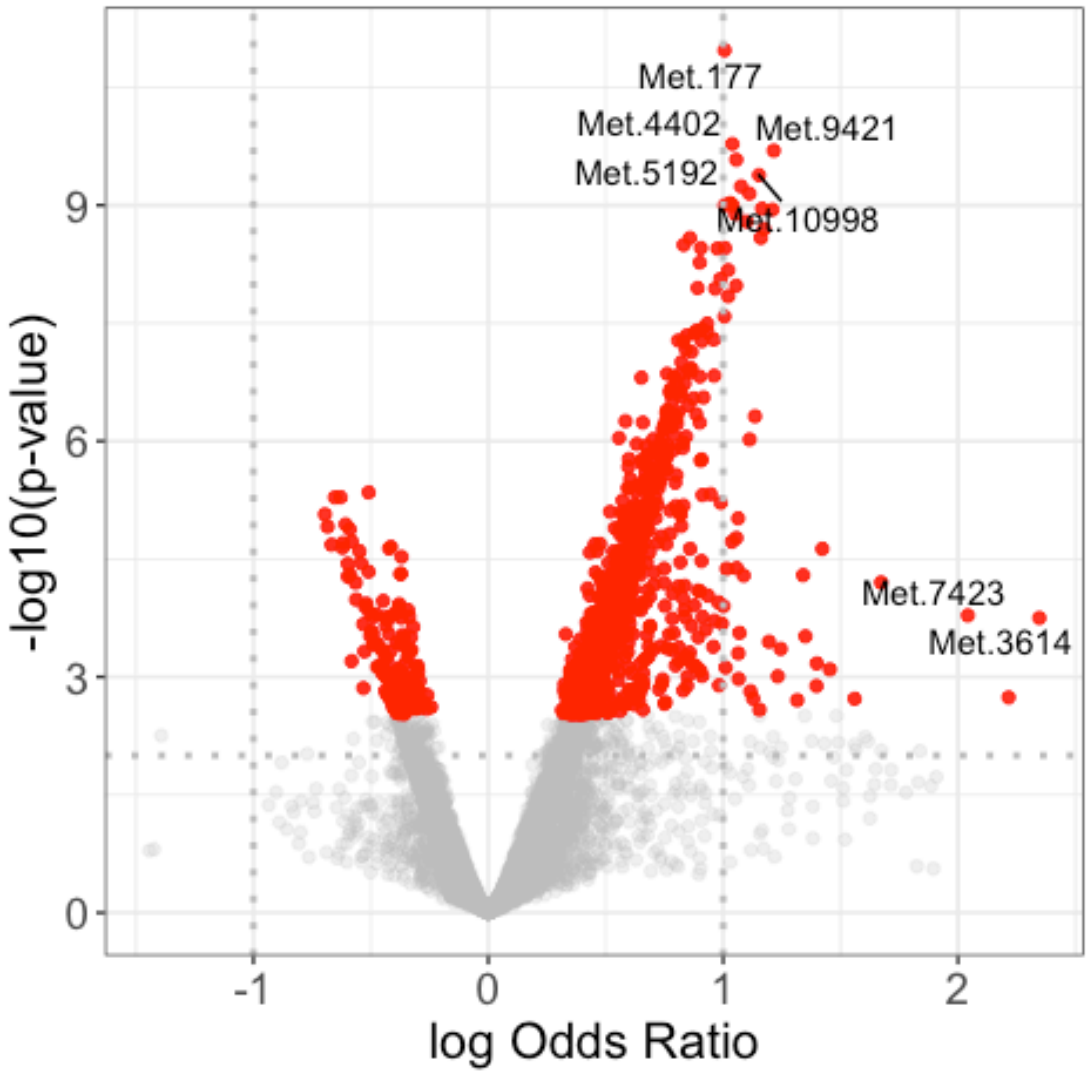

Figure 2.6. Volcano plot of p-values resulting from age only adjusted logistic regression model of LHON cohort. Negative log of p-value is y axis and log odd ratio is x axis. Some key metabolites are labeled with increased likelihood of associating with LHON than control. Met. = metabolite

2.3.2 Prediction of toxic putative metabolites in mitochondrial diseases

Over the past decades, the research in genetic mitochondrial diseases has been following the traditional biochemistry research process. This approach has failed in explaining sequences of a mutation from the clinical standpoint when patients have unrelated phenotypes of genetic mutations. We want to find out the causal metabolites that might discriminate the connections between phenotype, and genotype of diseases. The non-LHON cohort is a great data set to carry on MitoNet metabolomic study due to great statistical significance and sample size. Multivariate logistic regression yielded a long list of metabolites, whose p-values and odd ratios were plotted with volcano plot (figure **2.7**). The top significant 200 metabolites were considered for further analysis. The following stage was to elucidate the chemical identity of these significant metabolites. Individual LC/MS experiments were performed to collect MS/MS fragment scan of 200 top metabolites. There was a certain fragment having m/z of 85.0280 that appears in a group of metabolites.[171] With regard to their statistical significance, these metabolites appear to have the highest likelihood of association with mitochondrial disease than the control when compared to other significant metabolites as shown in red points in figure **2.7**. Furthermore, the fragment (85.028 m/z) is a signature for the functional group, 1,3-diol. One of the metabolites, mtb.1098294, with m/z value of 287.223 and predicted chemical formula of $C_{16}H_{32}O_4$ was chosen to be the representative example of the newly discovered fatty acid (FA) family since it has the highest odd ratio of mitochondrial disease association among other family members. It was examined carefully by collecting its fragments ions, and overall putative structure was predicted as shown in figure **2.8** (A). The fragment 59.0125 m/z is a common fragment for carboxyl group. To this point, mtb.1098294 was known to be dihydroxyl saturated FA, and the dihydroxy group is 1,3-diol. To

further determining its chemical identity, the other fragments were examined via their potential cleavage with respect to carboxyl group having position one in the fatty acid chain. The mechanism of fragmentation pattern is mainly due to alpha cleavage of hydroxyl groups along with loss of water molecule. As a result of applying the fragmentation mechanisms, the potential chemical structure of metabolite, mtb.1098294, is 3,5-dihydroxy palmitic acid (3,5-DiOH-C16). Similarly, other metabolites of the same family 3,5-dihydroxy fatty acid (3,5-DiOH FA) were discovered based on this analysis. The detected metabolites of the same family are two carbon difference in chain length. Members of this family seem to cluster together in the volcano plot sharing similar significance as shown in figure **2.7**.

Furthermore, another FA family was detected, 3-hydroxy fatty acid (3-OH FA) as shown in green points in figure **2.7**. They are more significant as they have lower p-values when compared to 3,5-DiOH FA. Two members of this family were found in patients of non-LHON cohort. Table **2.2** summarizes the two FA families. Additionally, the 200 top metabolites were subjected to clustering by GNPS molecular networking. The MS/MS spectra files were submitted to GNPS and displayed via Cytoscape 3.7.2.[172] The GNPS analysis revealed 78 nodes and six clusters. The largest cluster was for 3,5-DiOH FA of 14, 16, 18, and 20 carbons length chains designated as 3,5-DiOH-C14, 3,5-DiOH-C16, 3,5-DiOH-C18, and 3,5-DiOH-C20, respectively, as depicted in figure **2.9**.

Table 2.2. Metabolites of the two FA families listed with their detected molecular ions and chain length of each FA.

3,5-DiOH FA

Chain length	$[M-H]^-$
12	231.1599
14	259.1916
16	287.223
18	315.2542
20	343.2839

3-OH FA

Chain length	$[M-H]^-$
14	243.1965
16	271.228

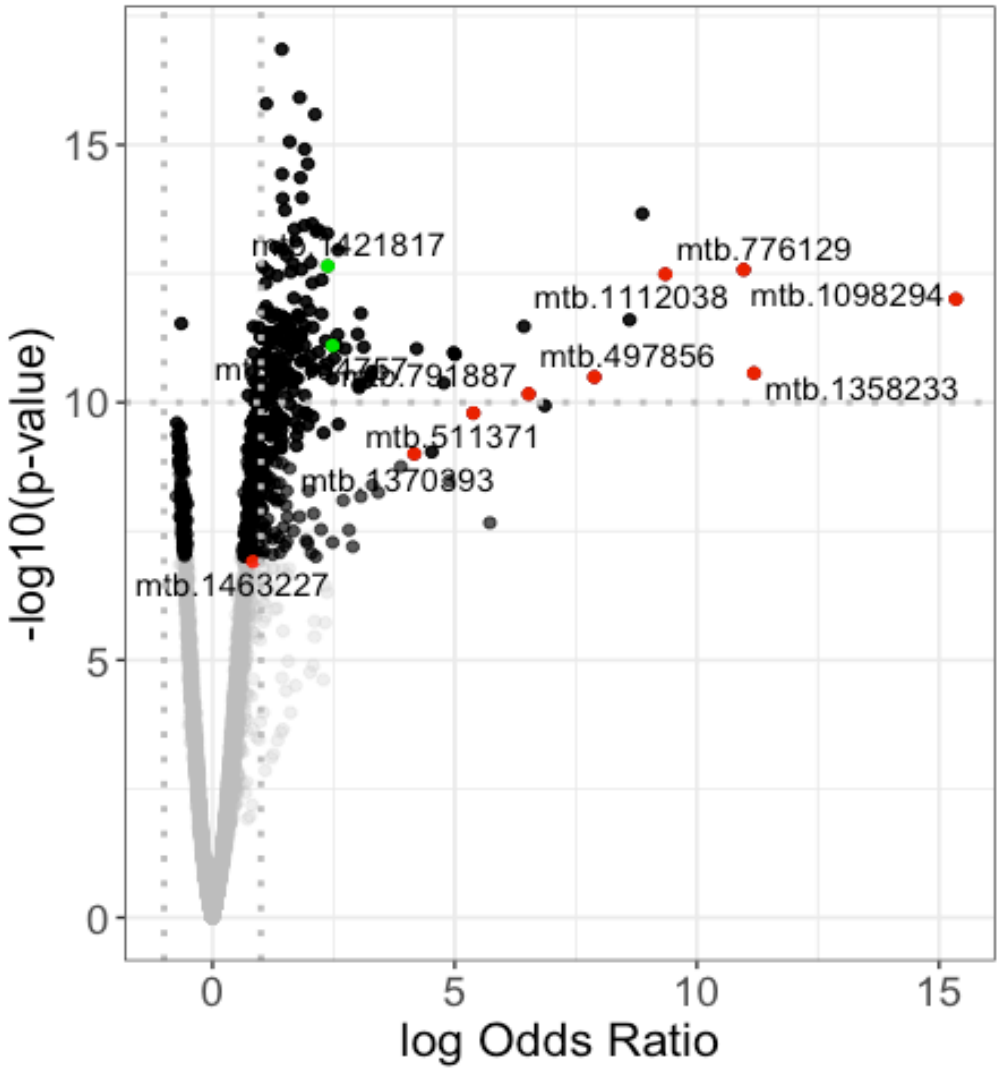

Figure 2.7. Volcano plot of p-values resulting from age and gender adjusted logistic regression model of non-LHON cohort. Negative log of p-value is y axis and log odd ratio is x axis. Some key metabolites are labeled with increased likelihood of associating with non-LHON mitochondrial diseases than healthy. Red points represent 3,5-DiOH fatty acids and green points represent 3-OH fatty acids. mtb. = metabolite

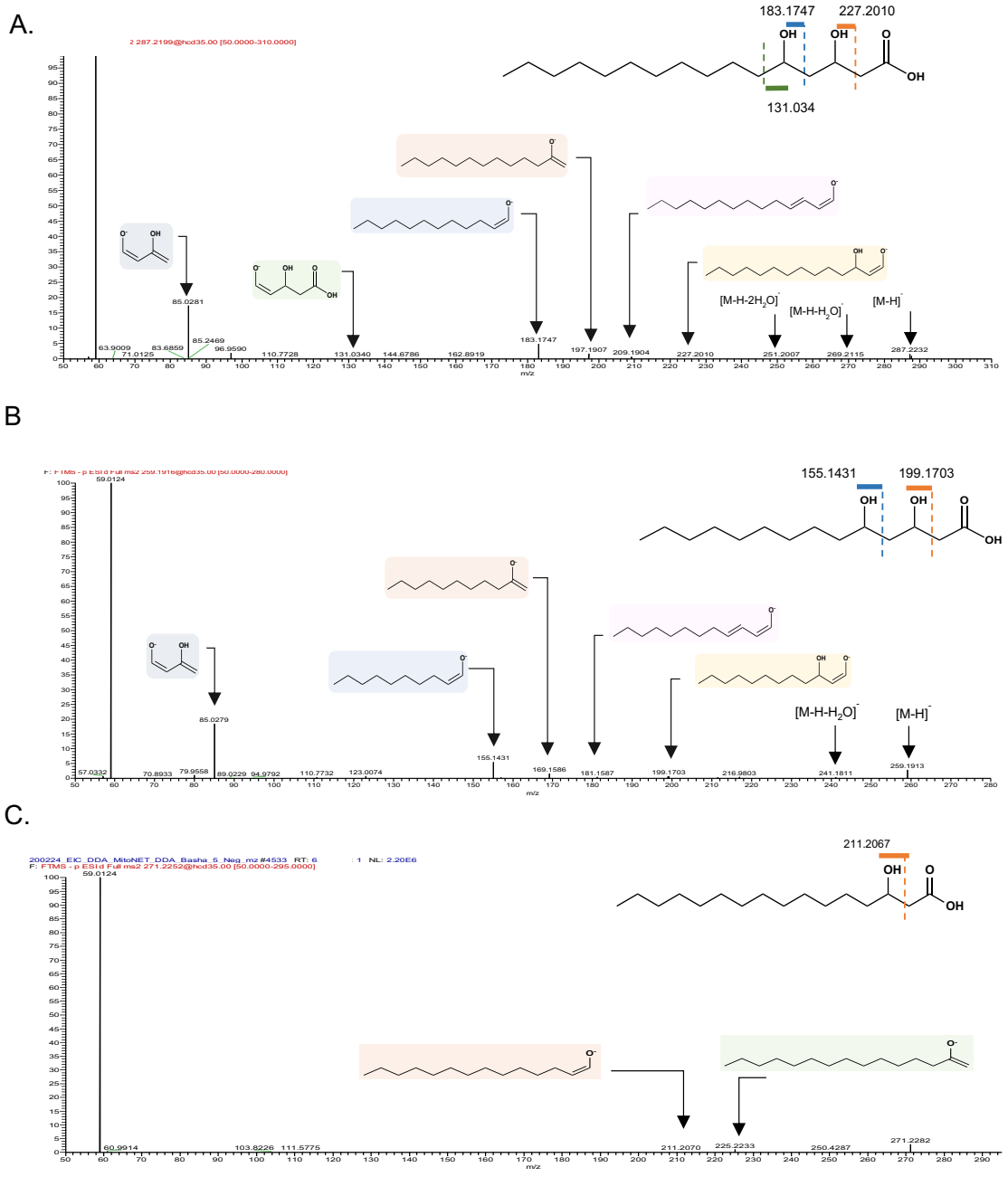

Figure 2.8. MS/MS scans of 3,5-DiOH hexadecanoic acid (3,5-DiOH-C16) (A), 3,5-DiOH tetradecanoic acid (3,5-DiOH-C14) (B), 3-hydroxyhexadecanoic acid (C). $[M-H]^-$ = molecular ion, two peaks for losing water: $[M-H-H_2O]^-$ and $[M-H-2H_2O]^-$.

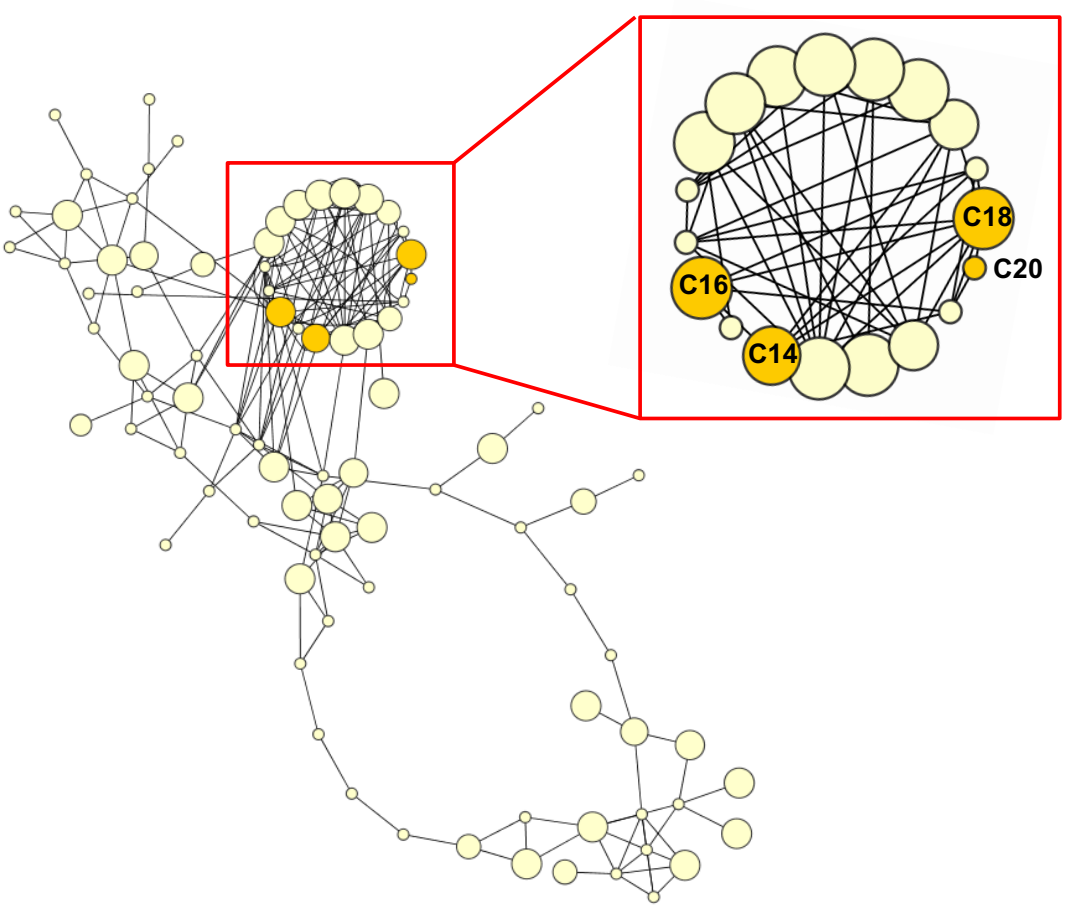

Figure 2.9. Molecular network of top 200 key metabolites in non-LHON cohort. The largest cluster contains 3,5-DiOH FA family in orange circles and labeled with their chain length. The size of cycle reflects p-value (the bigger circle the more significant is)

2.3.3 Association of 3-OH FAs and 3,5-DiOH FAs families with mitochondrial diseases

The subsequent question in this study is how the 3,5-DiOH FA family accumulates and what is the main biochemical pathway responsible for that. The Different classes of long chain FAs are subjected to accumulate in mitochondrial diseases.[173] For example, 3-OH FA accumulate in the diseases of beta oxidation insufficiency, which is a general hallmark of ETC malfunction or genetic defect. It has also been reported that often the level of 3-OH FA increases in long-chain 3-hydroxyacyl-CoA dehydrogenase (LCHAD) deficiency.[174, 175] More biochemical findings have suggested that 3-OH FAs had disturbed mitochondrial calcium retention capacity.[176] They also induce mitochondrial permeability transition pore, reduce mitochondrial $\Delta\Psi_m$, increase apoptosis. In this study, we've seen a significant increase in 3-hydroxytetradecanoic acid and 3-hydroxyhexadecanoic acid. Thus, this finding indicates involvement of FAO insufficiency, although there was no direct mutation for any FAO enzymes. Most likely this insufficiency is secondary for mutations in proteins of ETC process. This might reflect the complexity of pathways and their cross-interactions within mitochondria components.[176-179] Additionally, some 3-OH FAs were found to be formulated by mitochondrial de novo fatty acid synthesis pathway (mtFAS), which is independent of the cytoplasmic FA synthesis.[180]

In general, the substrates of fatty acid synthesis (FAS), malonic acid and acyl group (fatty acid), must be first transferred to a carrier, known as acyl carrier protein (ACP). Briefly, the FAS has universal steps starting with condensation of malonate-ACP and acyl-ACP resulting in 3-ketoacyl-ACP intermediate. The later undergoes reduction to 3-hydroxyl counterpart, followed by dehydration to form enoyl derivative, and the reduction of enoyl to furnish new elongated FA chain with two carbons more.[181-184]

The diseases of MitoNet cohort were classified according to the corresponding affected pathways, to find out which pathway is associated with the novel family, 3,5-DiOH FA. Heat maps were generated to examine levels of the 3,5-DiOH FA members across MitoNet cohort when it was divided according to the affected clinical diagnosis (figure **2.10**) and biochemical pathways (figure **2.11**). For each 3,5-DiOH FA, there are two isomers except for 3,5-dihydroxyicosanoic acid, which is detected as one isomer. Normally, isomers of each member are separated by 30-40 seconds. Moreover, most of 3,5-DiOH have accumulated in systematic disorders more than diseases with single organ involvement. They have accumulated in MERRF, MELAS, CPEO plus, and mitochondrial myopathy as shown in figure **2.10**. Altogether, these diseases have muscles defect as part of their phenotypic characteristics. Similarly, it's been observed in figure **2.11** that they have accumulated more in diseases with defects in tRNA related pathways, such as a mutation in mitochondrially-encoded tRNA genes or proteins involved in tRNA processing enzymes, e.g. mitochondrial tRNA -specific 2-thiouridylase 1, which catalyzes the 2-thiolation of uridine of mitochondrial tRNA of lysine, glutamine and glutamic acid. Unexpectedly, 3,5-dihydroxyicosanoic acid, mtb. 1463227, was not found to be similarly concentrated in diseases or defective pathways as the other 3,5-DiOH FAs.

Remarkably, tRNA biogenesis and mtFAS has an ancient genetic linkage. Ribonuclease P (RNase P) is a nuclease that catalyzes the cleavage of the leader sequence of precursor tRNAs yielding mature 5' end tRNAs. Ribonucleases P protein 14 (RPP14), which is a protein subunit of RNase P, is translated from a bicistronic transcript along with 3-hydroxyacyl-thioester dehydratase (HTD2), which is an enzyme in mtFAS catalyzing the dehydration of 3-hydroxyacyl-ACP to yield enoyl counterpart.[185]

We hypothesized that the primary pathway for the formation of 3,5-DiOH FAs is mtFAS supported by a cellular model from a collaborator indicating the mitochondrial formation of 3,5-DiOH FAs. Additionally, 3-OH FAs could enter mtFAS as substrates leading to the generation and accumulation of 3,5-DiOH FAs when HTD2 enzyme activity is deteriorated. Figure **2.12** elucidates possible the path for the formation of 3,5-DiOH FAs from 3-OH FAs. It was surprising to observe 3,5-DiOH FAs are associated with defects in tRNA biogenesis, which could also mirror the defect in HTD2 activity leading to their accumulation in the body.[186] These findings are supportive to the hypothesis and additional isotopic cellular assays of substrates are required. In addition, these results expand the knowledge about substrate specificity of mtFAS for the production of diverse FAs families.

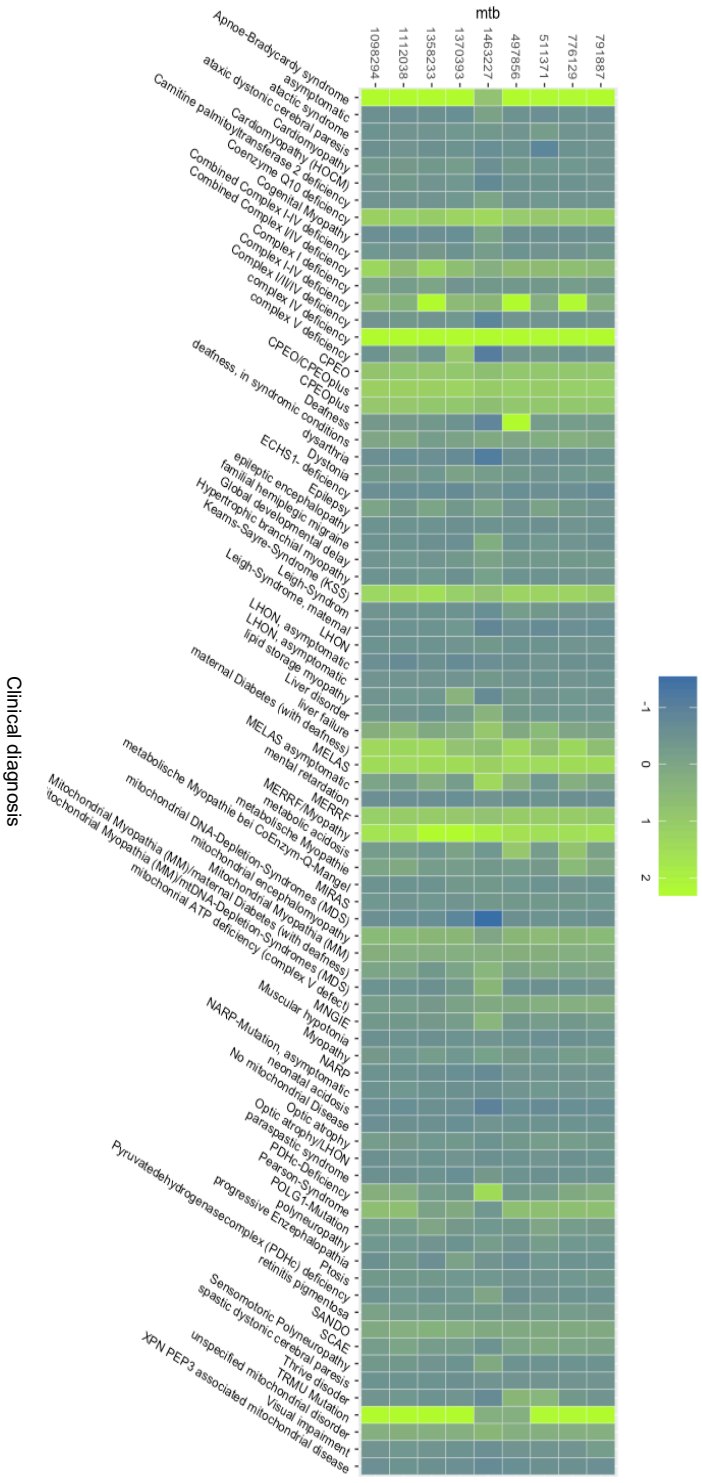

Figure 2.10. Distribution of 3,5-dihydroxyfatty acids among patients with different clinical diagnosis

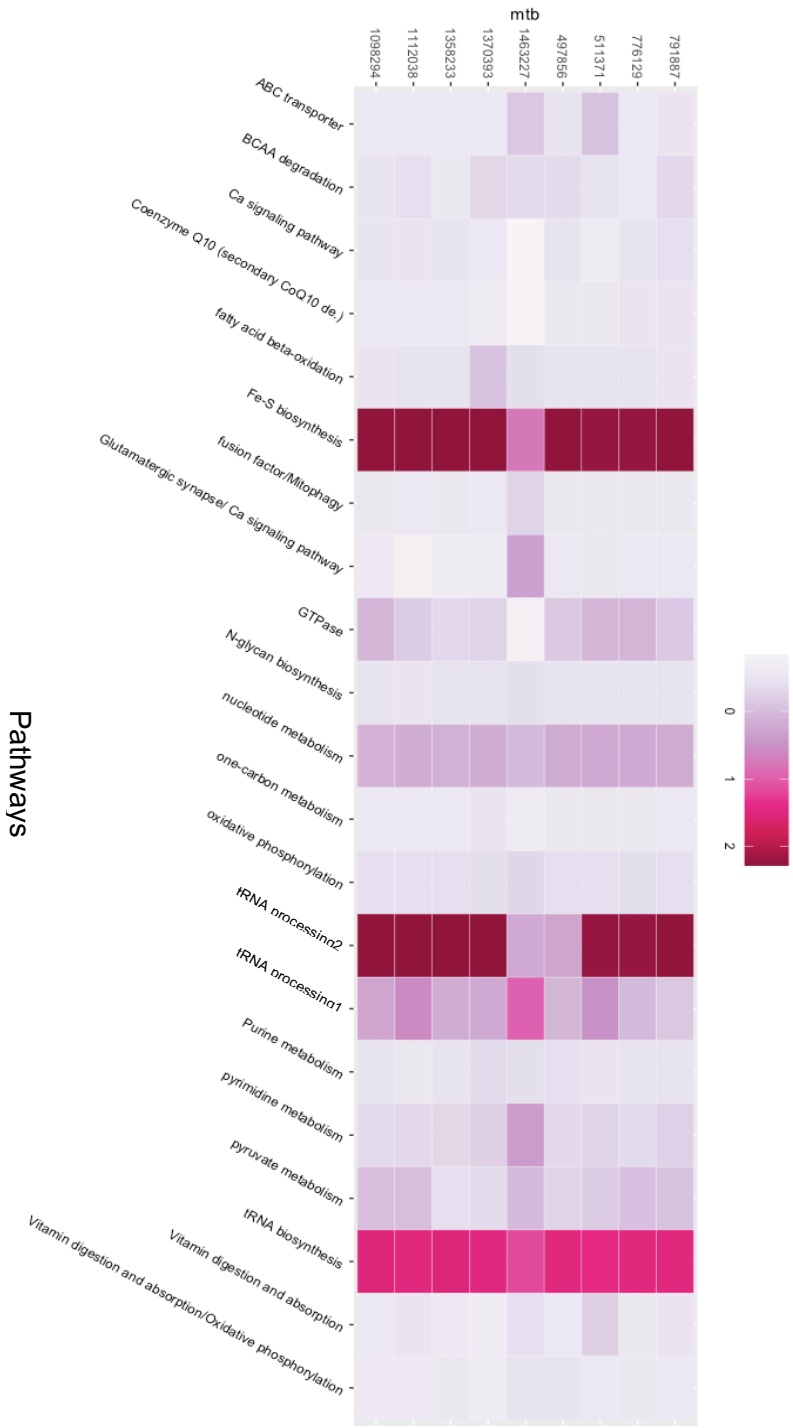

Figure 2.11. Distribution of 3,5-dihydroxyfatty acids among different defects in mitochondrial pathways

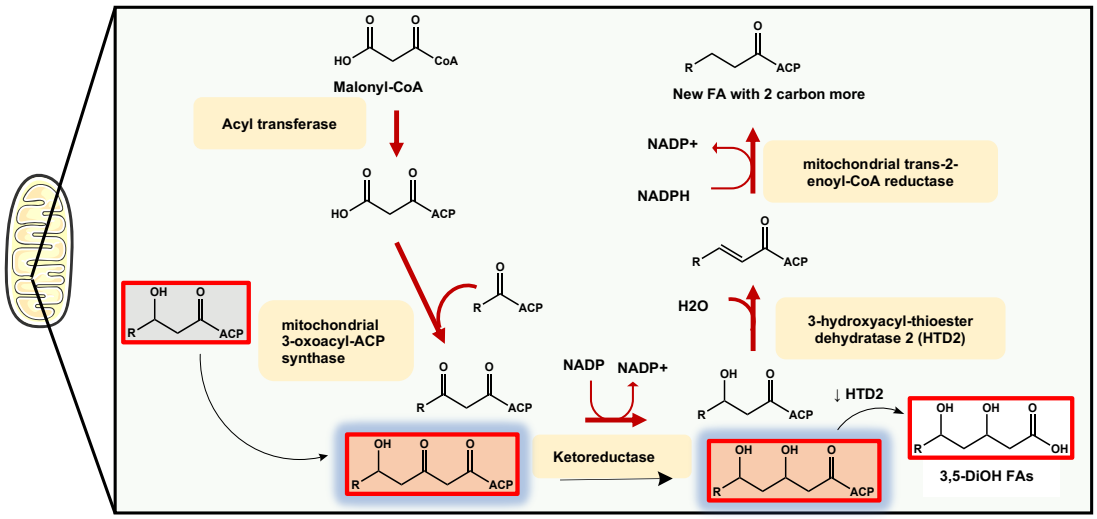

Figure 2.12. Mitochondrial fatty acid synthesis pathway. The grey structure represents 3-OH-ACP that enters mtFAS producing 3-keto-5-hydroxy-ACP (structure in light orange) leading to the production 3,5-DiOH FAs

2.4 Conclusion and future plans

Metabolomics study has revealed some trends of mitochondrial diseases. There are some clinical features manifested in mitochondrial diseases that are reflected at metabolic level in this study. Interestingly, gender bias of some mitochondrial diseases, such as LHON, was reported in the bioactive lipids profile. Furthermore, new FA family was discovered and highly elevated in patients with systematic disorders. The putative biochemical pathway that might be responsible for their synthesis is mtFAS. Finally, multiple cellular models are needed to predict the origin of 3,5-DiOH FAs, and their causality of various pathogenic phenotypes established in the systematic mitochondrial diseases.

Chapter 2, in full, is currently being prepared for a publication, on which I'm a primary author. I discovered new dihydroxyl fatty acid family that is never been reported or published in any scientific journals or patent. Dr. Tao Long and Kysha

Mercader contributed to the project biostatistics aspect. Khoi Dao, Rafael Moranchel, and Mahan Najhawan participated in LC/MS experiments. Dr. Mohit Jain supervised the overall project.

Chapter 3 : Synthesis of Forbesione analogs

3.1 Introduction

The plant of *Garcinia* hanburyi Hook.f. belongs to the family *Guttiferae*. The resin plant contains various caged xanthone family, such as gambogic acid (**3.1**) and forbesione (**3.2**).[105] As summarized in the previous chapter, the vast majority of the research has centered around gambogic acid with only few publications presenting the potential of forbesione in anticancer research.[187-191]

Forbesione has exhibited its predominant antitumor effect more in gastrointestinal tract tumors like cholangiocarcinoma, which is a malignant tumor generated from the bile duct epithelial cells.[188] A combination of forbesione and doxorubicin or 5-fluoroyracil exhibited a significant synergistic effect on preventing growth of cholangiocarcinoma cell lines, such as KKU-100.[187, 191] Similar to **3.1**, forbesione exhibits it antitumor effect by targeting Bcl-2 which play vital role in mitochondrial apoptotic pathway.[188]

Recent SAR studies have shown that cluvenone (**3.3**) is the main pharmacophore responsible for the antitumor activity of **3.1**. In addition, both **3.1** and **3.3** localize intrinsically in the mitochondria, the site of action.[99] The C-ring is an essential structural feature for antitumor activity since Michael acceptor site at C9-C10 acts as conjugate electrophile that is presumably been attached by nucleophile on target proteins, such as side chain amine of lysine or sulfide of cysteine.[101]

Chemical modifications take place on A-ring, such as hydroxylation on C18, (**3.4**) or C6 (**3.5**). Hydroxylation on C6 increases potency by threefold than hydroxy

counterpart on C18.[99] Additionally, chemical modification can be applied in different site, carboxyl group on gambogic acid, to generate analogs through amide bond.[133, 135, 143, 154]

To further advance these SAR profile, we studied forbesione in order to generate a new site of derivatization on C18 via ether linkage which turned out a new natural product, cyclo-forbesione (**3.6**) (figure **3.1**). Furthermore, we studied the installation of couple of amine fragments to help mitochondrial delivery and localization as well as evaluate chemical and biological properties.

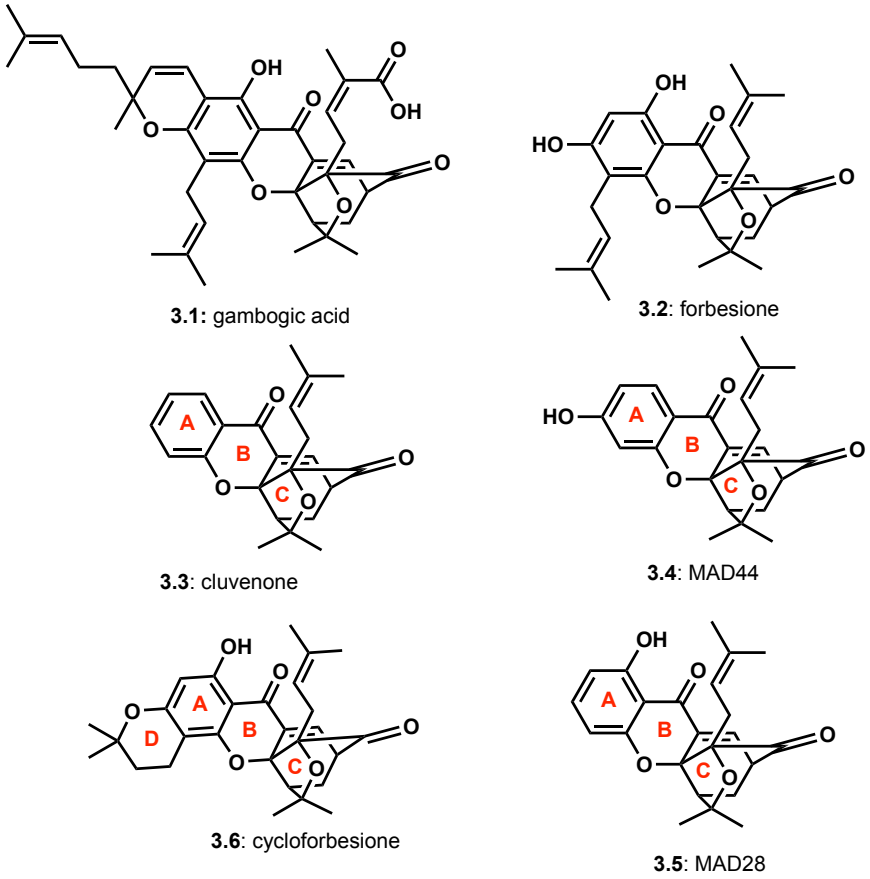

3.1: gambogic acid

3.2: forbesione

3.3: cluvenone

3.4: MAD44

3.6: cycloforbesione

3.5: MAD28

Figure 3.1. Structure of caged Garcinia xanthones.

3.2 Result and discussion

The synthesis of **3.2** started with the formation of the first intermediate tetrahydroxy xanthone (**3.9**), which is highlighted in scheme **3.1**. The xanthone was formed by the reaction of 2,4,6-trihydroxybenzoic acid (**3.7**) and pyrogallol (**3.8**) under $ZnCl_2$ (yield is 40%). The following step is the formation of triallylated compound (**3.10**), which is catalyzed by Pd(0) reverse prenylation using carbonate (**3.11**) in 70% yield. The carbonate reagent is formed over two steps: the first step produces intermediate (**3.12**), which is used for next step to make **3.11** in total yield of 95% as in scheme **3.2**.[97] The hydroxy on C6 is not allylated because of intramolecular hydrogen bond with oxygen of the carbonyl group. Before forming caged structure, it's important to protect hydroxyl group on C6 by acetylation to ultimately enhance forbesione yield. Therefore, O-acetyl-triallylated xanthone (**3.13**) is produced using acetic anhydride (Ac_2O) and catalyzed by 4-(N,N-dimethylamino)pyridine (DMAP) in 51% yield. Next, tandem Claisen/Diels-Alder reaction cascade proceeded to form **3.14** by heating **3.13** in DMF at 130 °C for 3 hrs (45% yield). It is worth noting that other caged structure of forbesione analogs, such as isoforbesione, and neo-forbesione, were formed, but it is not my interest to collect or proceed with these compounds.[95]

In order to obtain **3.2**, compound **3.14** was treated with base to deprotect acetate group. Out of curiosity, acidic deprotection conditions, such as hydrochloride (HCl) or trifluoroacetic acid (TFA), were used to yield a new cyclized compound (**3.6**). Furthermore, **3.6** is mechanistically possible to be formed as pendant alkene of prenyl installed on C17 gets protonated under acidic condition forming most stable carbocation on tertiary carbon. As result, nearby hydroxyl group on C18 acts as nucleophile to attack carbocation forming tetrahydropyran (D-ring) fused to xanthone

scaffold through C17 and C18, which is different than the usual fused tetrahydropyran through C5 and C18 of xanthone backbone found in some analogs of CGXs family.

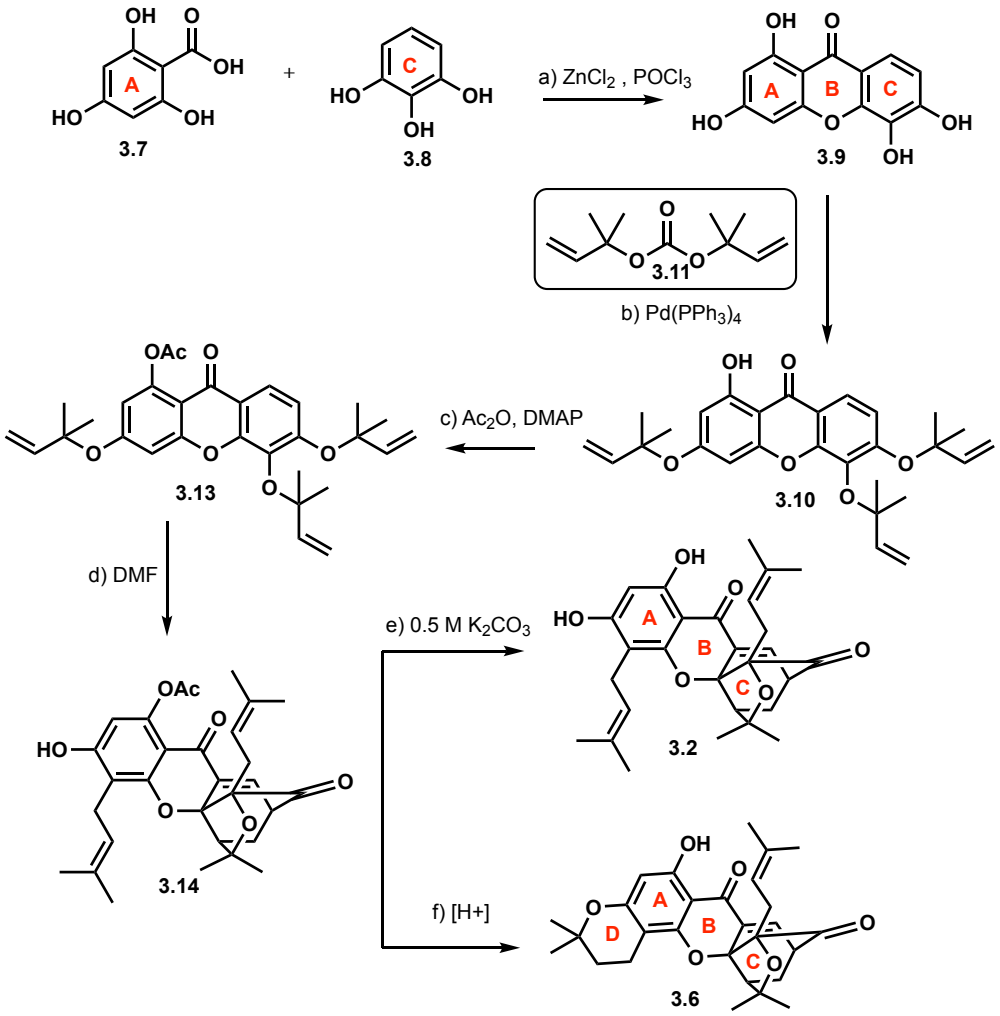

Scheme 3.1. a) $ZnCl_2$ (5 equiv.), $POCl_3$ (15 equiv.), 60 °C, 6 hr; b) $Pd(PPh_3)_4$ (0.1 equiv.), carbonate agent (10 equiv.), **3.11** (10 equiv.) 0 °C, 0.3 hr; c) Ac_2O (25 equiv.), DMAP (0.1 equiv.) rt, 24 hrs; d) DMF, 130 °C, 6 hrs; e) 0.5 M K_2CO_3, rt, 6 hrs; f) TFA (2.2 equiv.), rt, 24 hrs.

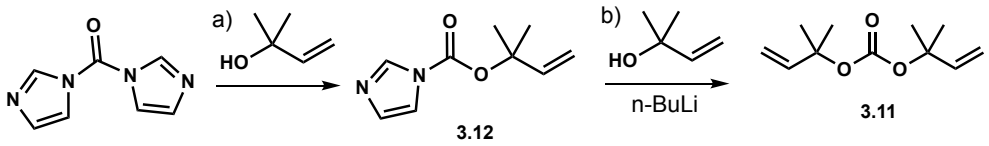

Scheme 3.2. a) carbonyl diimidazole (1.3 equiv.), DCM, rt, 3 hrs; b) 2-methyl-3-buten-2-ol (1 equiv.), n-BuLi (1.1 equiv.), THF, -78 °C for 0.5 hrs and then 3hrs at rt.

A similar A-ring cyclization has been reported in the bractatin series (compounds **3.15** and **3.16**).[192] The main difference here is the oxygen of the hydroxyl group cyclizes with nearby prenyl on the most substituted carbon to form tetrahydrofuran ring fused to A-ring of xanthone nucleus. However, these compounds are found in nature and extracted from *Garcinia bracteata.* Thus, there is high probability that compound **3.6** could be produced in nature but not yet been described. Collectively, these cyclized analogs of CGXs could represent a new sub-class of CGXs. Furthermore, both **3.15** and **3.16** have potent antitumor activity against human lung adenocarcinoma epithelial cell line A549, yet their antitumor activities are comparable with IC_{50} values of 1.45 uM and 1.5 uM, respectively.[193] Both **3.2** and **3.6** were sent for an evaluation of their antitumor activity, and they are likely to be similar in their potency, accordingly.

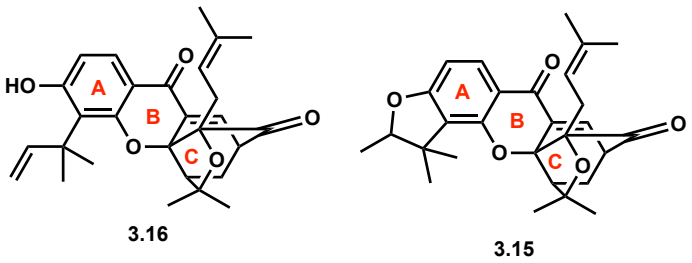

Figure 3.2. Structures of neobractatin (**3.15**) and isobractatin (**3.16**).

In an attempt to generate a library of forbesione analogs, the hydroxyl group on C18 is great site to link various fragments as it is more chemically flexible and novel to be explored. The linkage chemistry of fragment with the main xanthone scaffold of **3.2** is through the substitution of bromide on alkyl bromide fragments with the oxygen of the hydroxyl group forming ether linkage. The preparation of fragment **3.17** was done over two steps as shown in scheme **3.5**.[194] First, phenylbiguanide (**3.18**) is formed under acidic condition from aniline and dicyandiamide at 90 °C. Then, the compound **3.18** was treated with base to free it from its HCl salt counterpart. Finally, condensation of **3.18** free base with ethyl bromo-acetate was occurred to furnish fragment **3.17**. The yield over the two steps is 50%. The other fragment was formed by simple amide coupling reaction of bromo-acetic acid and N-Boc-ethylene diamine using N,N'-dicyclohexylcarbodiimide (DCC) in %90 yield.

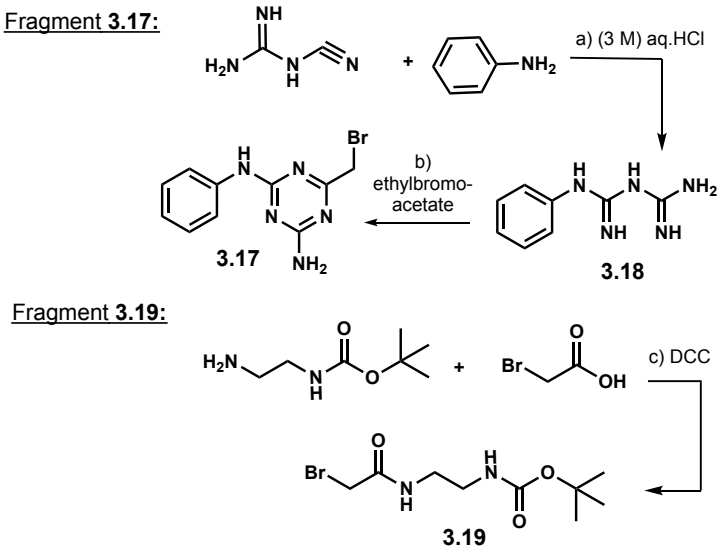

Scheme 3.3. a) 3M aq. HCl, 90 °C, 20 hrs; b) ethylbromo-acetate (2 equiv.), MeOH, 60 °C, 24 hrs; c) DCC (1.13 equiv.), rt, 18 hr.

Subsequently, the substitution reaction was performed under Huning's base (N,N-Diisopropylethylamine (DIPEA)) at room temperature for 24 hrs using fragments

3.17 and **3.19** to afford **3.20** and **3.21**, respectively. It should be mentioned that alkyl chloride counterpart of **3.19** fragment didn't proceed well with substitution reaction. It has been found that alkylation of hydroxyl group on C18 increase potency by twofold than **3.4** or **3.5**.[99] Certain amine containing fragments, such as **3.21**, have been found to be good mitochondria localizing agents because of mitochondrial ($\Delta\Psi_m$).

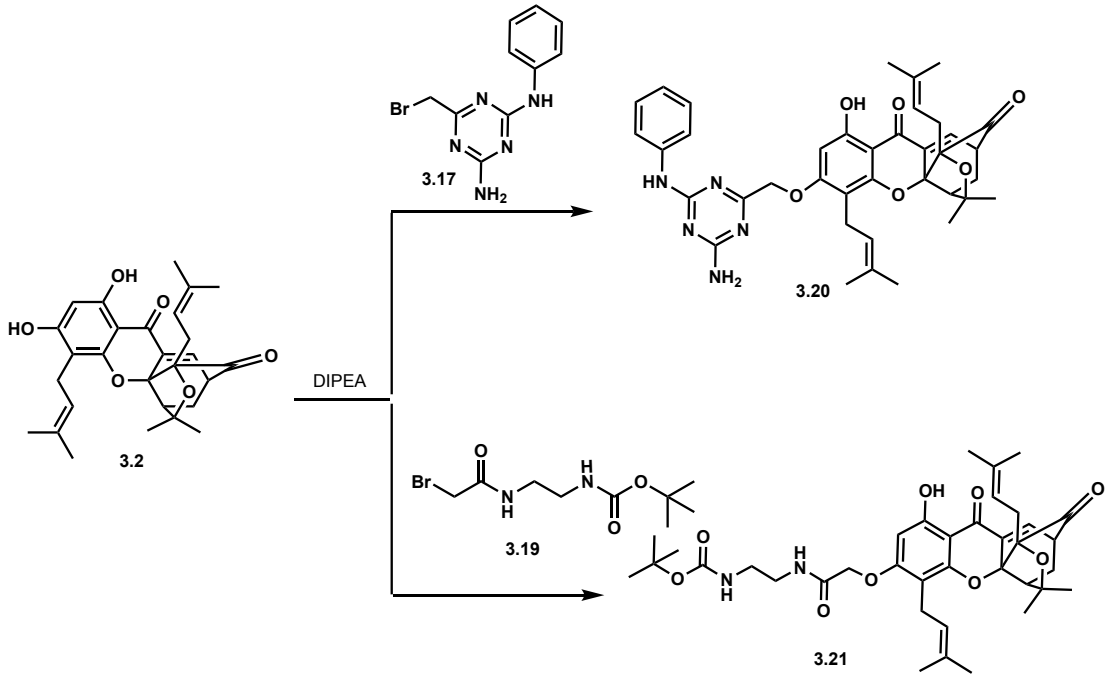

Scheme 3.4. Reaction condition: DIPEA (5 equiv.), rt, 24 hrs**.**

3.3 Conclusion and future plans

A new derivatization site has been utilized on forbesione, and this also can be applied almost to all CGXs in order to generate a library of interest aiming to target certain organelle or acting as probes. New cyclized analog has been detected and isolated from the reaction, which might represent undiscovered new sub-class of CGXs. Evaluation of forbesione analogs is the main factor currently to prove usefulness of this derivatization.

Chapter 3, in full, is currently being prepared for a publication, on which I'm a primary author. I contributed to the project novelty and the entire chemical experiments. I generated for first time a new chemical derivatization, that could also be applied to other caged garcinia xanthones, to produce unique library of forbesione analogs. The compounds were sent to Dr. Mary Alphaugh to perform cytotoxicity assays on breast cancer cell lines. Emmanuel Theodorakis is the advisor.

3.4 Experimental procedure

Compound **3.9**:

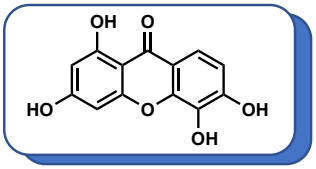

To a round-bottom flask, 2,4,6-trihydroxybezoic acid (2 g, 11.76 mmol, 1 equiv)) and pyrogallol (2.2 g, 17 mmol, 1.4 equiv) were added and followed by $ZnCl_2$ (8 g, 58.75 mmol, 5equiv) and $POCl_3$ (17 mL, 176.4 mmol, 15 equiv). The reaction was heated to 65 °C for 6 hrs. To quench the reaction, it was cooled down to room temperature and added slowly to crushed ice in Erlenmeyer flask placed in ice bath. The product was precipitated as white precipitate and then filtered. The crude material was purified through flash column chromatography (silica 20-80% EtOAc-hexane) to yield the desired product **3.9** (1 g, 40%). **3.9**: light brownish residues.

1H NMR (300 MHz, acetone) δ 13.17 (s, 1H), 9.71 (s, 1H), 9.15 (s, 1H), 8.73 (s, 1H), 7.63 (d, J = 8.7 Hz, 1H), 6.99 (d, J = 8.7 Hz, 1H), 6.43 (s, 1H), 6.24 (s, 1H). 13C NMR (126 MHz, cdcl3) δ 181.10, 165.84, 164.79, 158.71, 152.12, 146.89, 133.22, 117.45, 114.79, 113.68, 103.09, 98.79, 94.76. HRMS calc. for $[C_{28}H_{33}O_6]^-$ is 259.0248, found 259.0247.

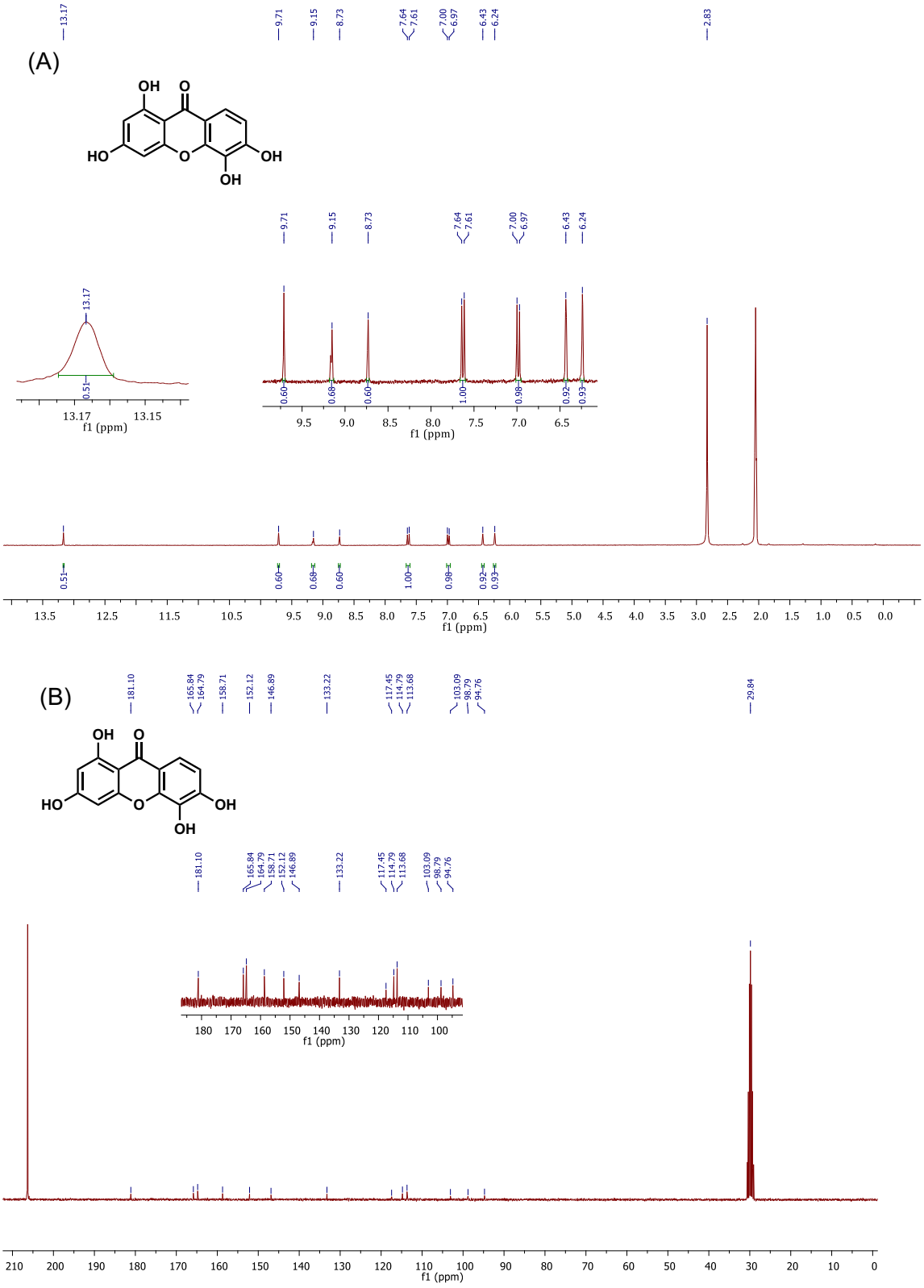

Figure 3.3. NMR spectra of **3.9**. (A) 1H NMR (B) 13C NMR

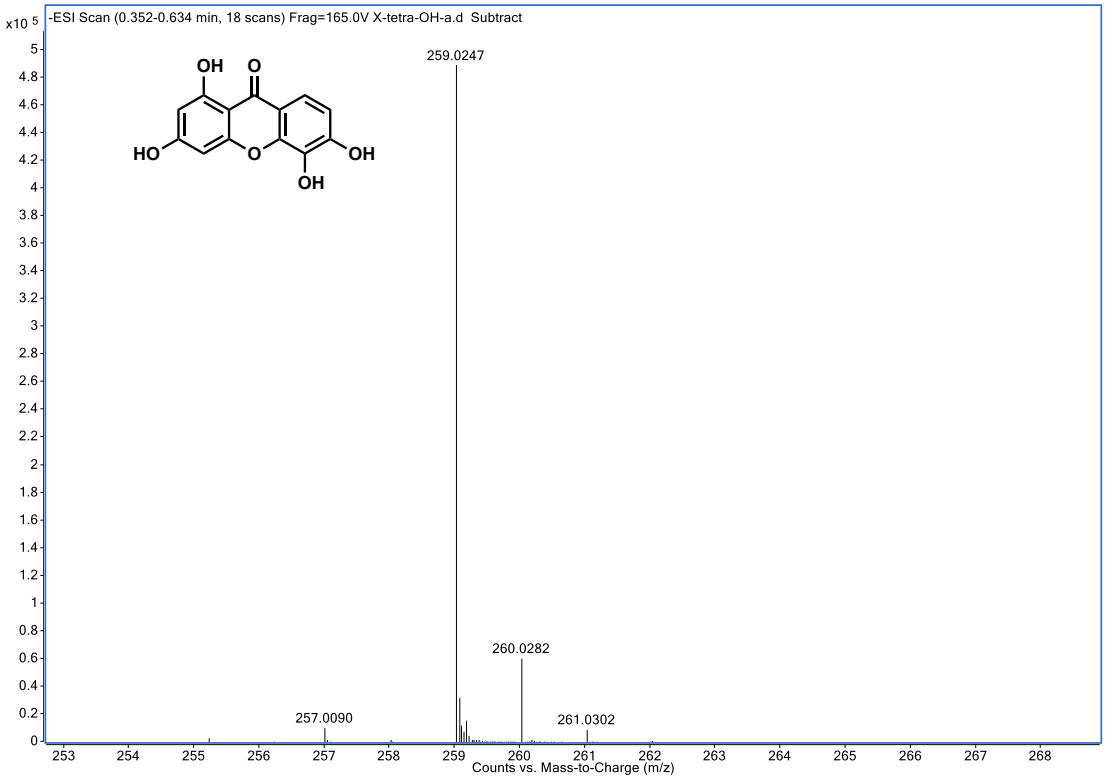

Figure 3.4. MS1 spectrum of **3.9**

Compound **3.10**:

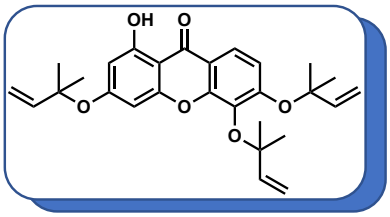

To a 25 mL round-bottomed flask was added tetrahydroxy-xanthone **3.9** (30 mg, 0.45 mmol) followed by THF (0.3 mL). The flask was degassed by argon and placed in an ice bath. To the solution was added bis(1,1-dimethylpropenyl) carbonate **3.11** (0.24 mL, 4.50 mmol), followed by $Pd(PPh_3)_4$ (14 mg, 45.0 µmol). The reaction vessel was stirred under argon at 0 °C for 20 min. The onset of a greenish suspension indicated the formation of triallyl-xanthone **3.10**. The solvent was removed by rotary evaporation and the crude material was purified through flash column chromatography (silica 0-20% EtOAc-hexane) to yield **3.10** (21 mg, 70%). **3.10**: colorless oil. ^{1}H NMR (500 MHz, Chloroform-*d*) δ 12.80 (s, 1H), 7.80 (d, *J* = 9.0 Hz, 1H), 7.09 (d, *J* = 9.0, Hz, 1H), 6.53 (d, *J* = 2.1 Hz, 1H), 6.42 (d, *J* = 2.1Hz, 1H), 6.27 – 6.11 (m, 3H), 5.33 – 5.14 (m, 5H), 5.02 (dd, *J* = 10.8, 0.8 Hz, 1H), 1.57 (s, 12H), 1.55 (s, 6H). 13C NMR (126 MHz, cdcl3) δ 180.66, 163.96, 162.76, 157.19, 156.90, 152.38, 143.74, 143.62, 143.43, 135.60, 120.26, 116.66, 115.75, 114.34, 114.28, 113.23, 103.43, 101.36, 97.55, 83.69, 82.38, 81.30, 27.38, 27.29, 26.99. HRMS calc. for $[C_{28}H_{33}O_6]^+$ is 465.2272, found 465.2273.

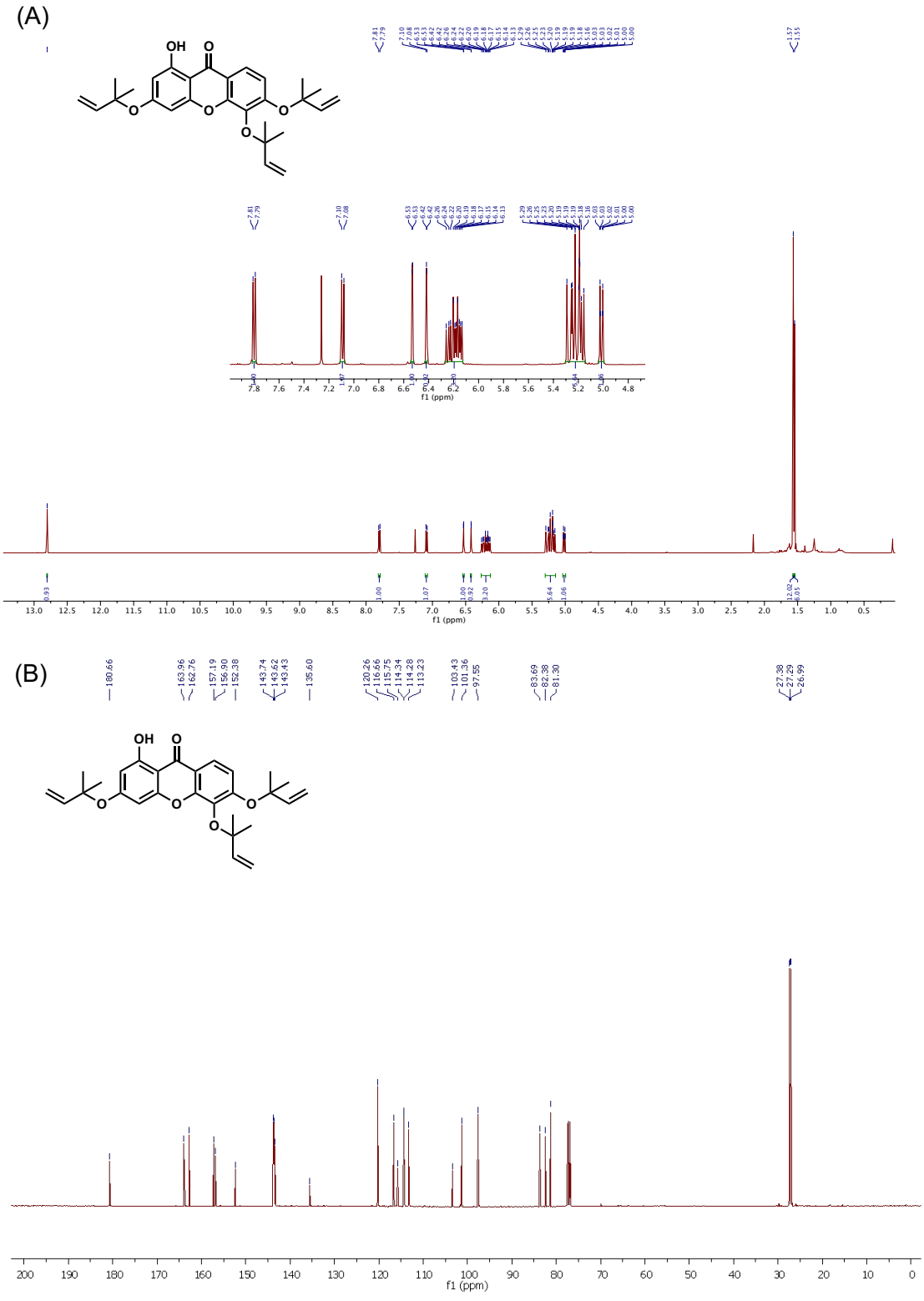

Figure 3.5. NMR spectra of **3.10**. (A) 1H NMR (B) 13C NMR

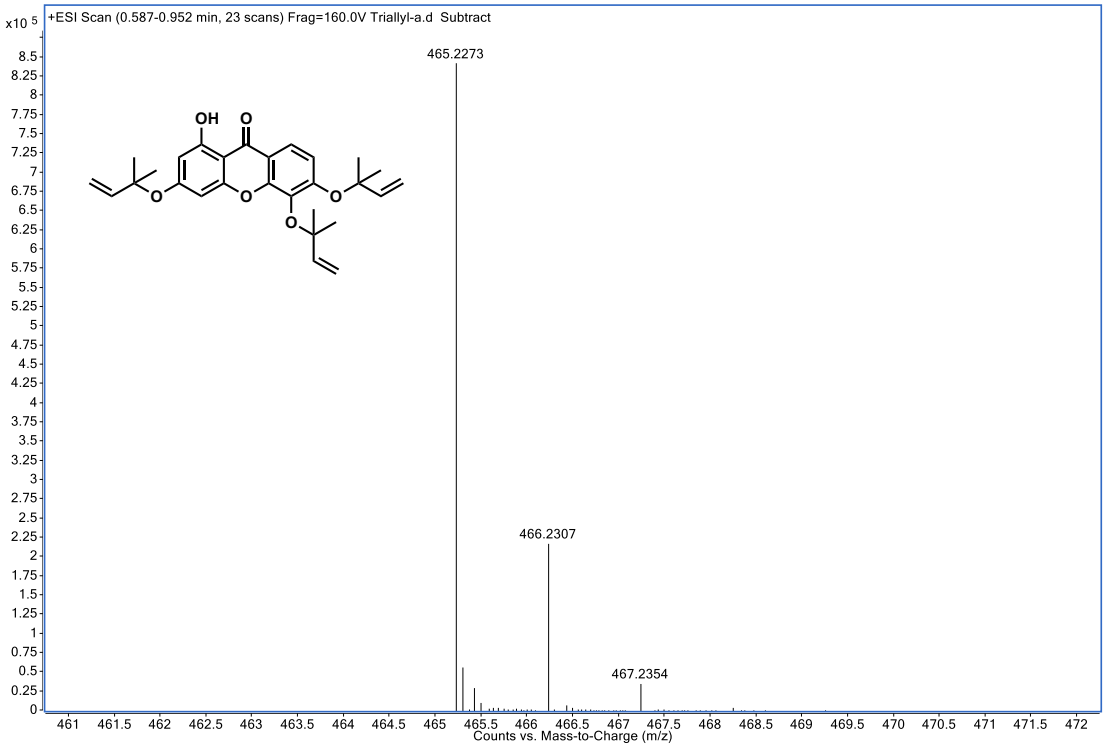

Figure 3.6. MS1 spectrum of **3.10**

Compound **3.13**:

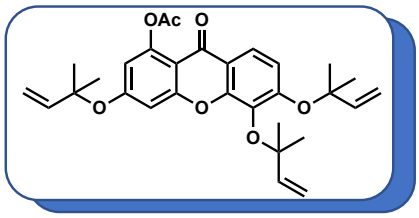

To round-bottom flask containing compound **3.10** (173 mg, 0.37 mmol) dissolved in 1 mL of DCM was added DMAP (4.5 mg, 0.037 mmol), pyridine (0.75 ml, 9.25 mmol), and acetic anhydride (0.87 mL, 9.25 mmol). The reaction mixture was stirred for 24 h at 45 C. The product formation was monitored by TLC. The reaction was quenched by $NaHCO_3$ and extracted with DCM. The organic layer was dried over MgSO4 and solvent was removed by rotary evaporation and purified through flash column chromatography (silica 10-60% Et_2O-hexane) to yield **3.13** (96 mg, 51%). ^1H NMR (300 MHz, Chloroform-*d*) δ 7.78 (d, *J* = 9.0 Hz, 1H), 7.04 (d, *J* = 9.0 Hz, 1H), 6.95 (d, J= 2.4 Hz, 1H), 6.58 (d, J=2.4 Hz, 1H), 6.30 – 6.10 (m, 3H), 5.34 – 5.14 (m, 5H), 5.02 (dd, *J* = 10.8, 1.1 Hz, 1H), 2.45 (s, 3H), 1.57 (s, 7H), 1.54 (s, 12H). ^{13}C NMR (126 MHz, c_6d_6) δ 174.94, 169.94, 161.57, 158.06, 156.50, 151.70, 150.85, 143.72, 143.64, 143.54, 135.63, 120.91, 117.73, 117.10, 114.61, 114.23, 113.06, 110.82, 108.79, 104.21, 83.63, 82.28, 81.58, 27.29, 27.27, 26.99, 21.43. HRMS calc. for $[C_{30}H_{35}O_7]^+$ is 507.2377, found 507.2374.

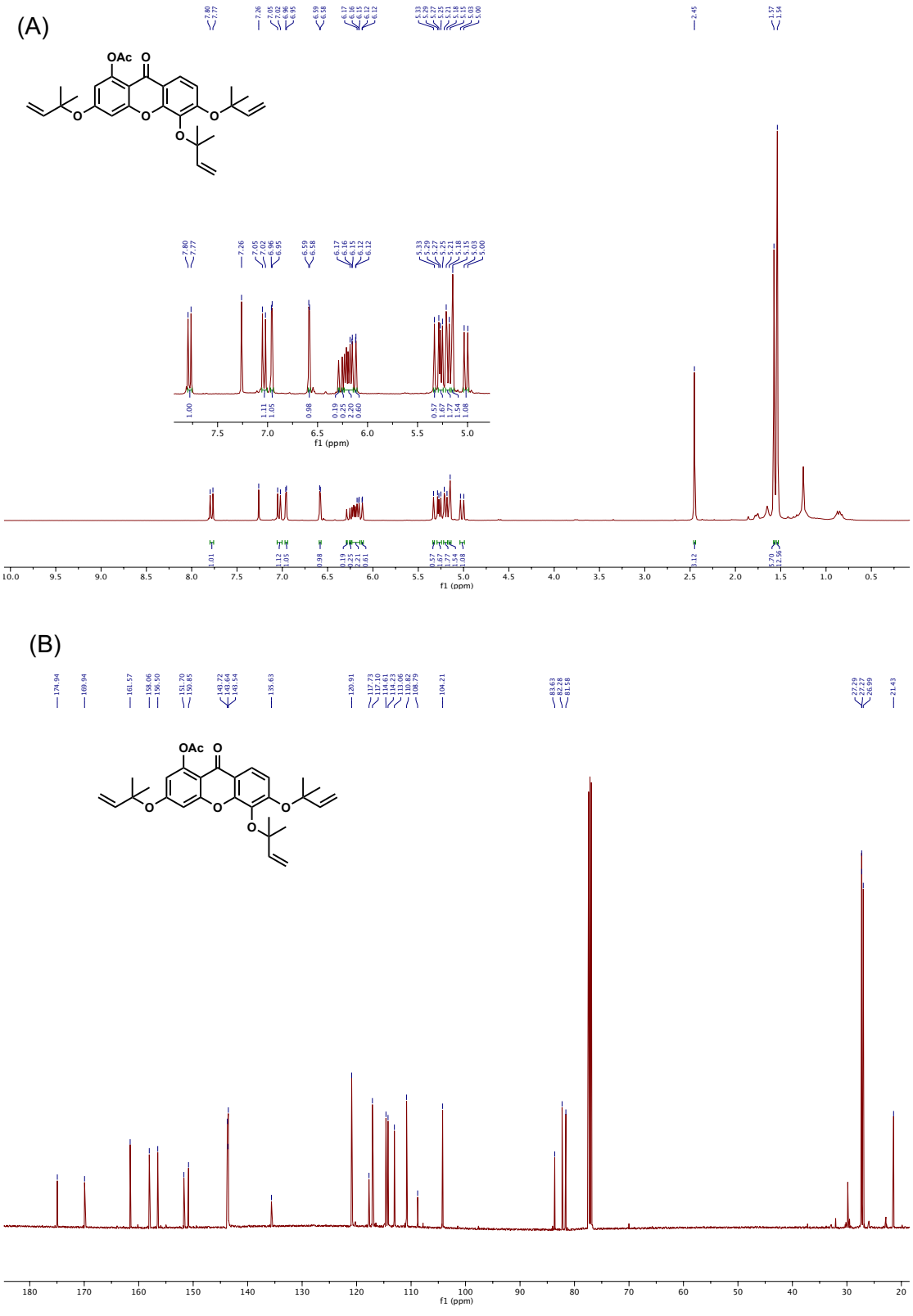

Figure 3.7. NMR spectra of **3.13**. (A) 1H NMR (B) 13C NMR

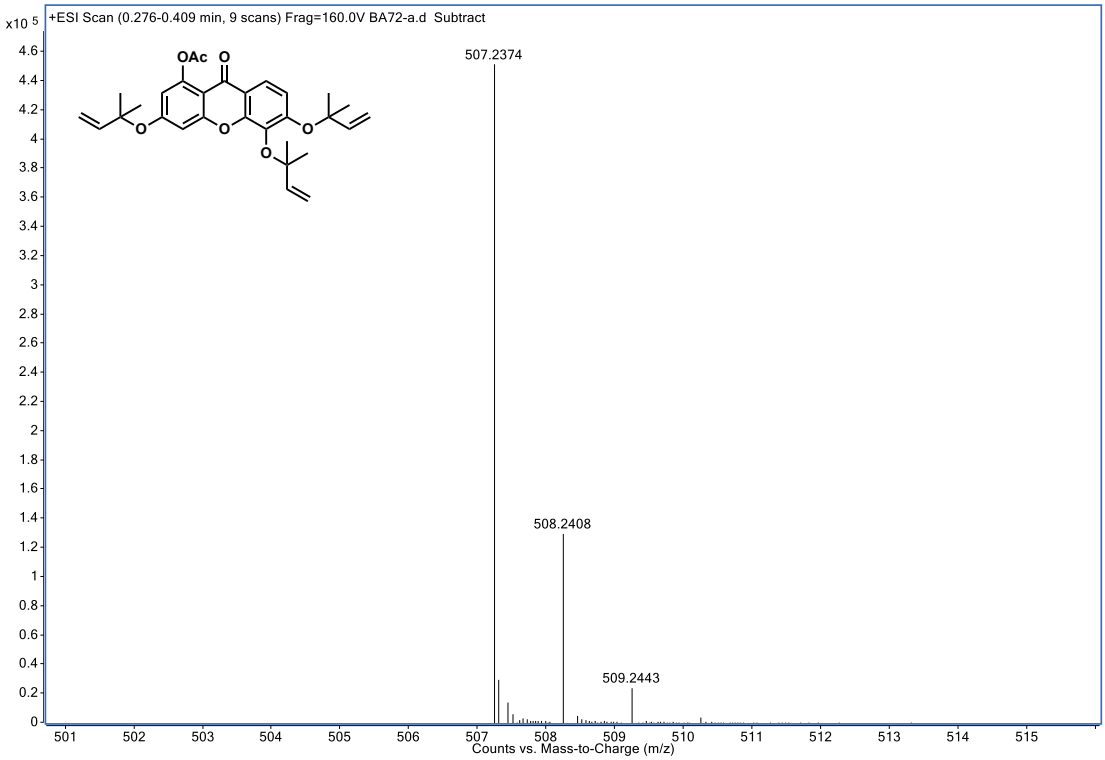

Figure 3.8. MS1 spectrum of **3.13**

Compound **3.14**:

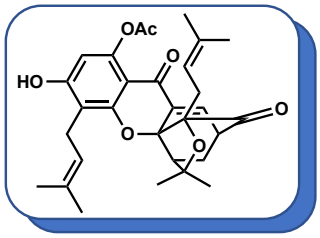

In microwave reaction vial was added compound **3.13** (280 mg, 55.3 mmol) dissolved in 5 mL of DMF and the vial was sealed. Then, the reaction was stirred for 3 h at 130 C. The product formation was monitored by TLC (30% ether:hexane). The reaction was cooled down to room temperature and DMF was removed by azeotropic mixture with several addition of toluene using rotary evaporator at 60 C. The crude material was purified through flash column chromatography (silica 10-60% ether-hexane) to yield **3.14** (125 mg, 45%). ^{1}H NMR (500 MHz,) δ 7.34 (d, *J* = 6.9 Hz, 1H), 6.31 (s, 1H), 6.25 (s, 1H), 5.32 – 5.19 (m, 1H), 4.50 – 4.37 (m, 1H), 3.63 – 3.38 (m, 3H), 2.60-2.56 (m, 1H), 2.53 (d, *J* = 9.7 Hz, 1H), 2.47 (d, *J* = 9.4 Hz, 1H), 2.38 (s, 3H), 2.30 (dd, *J* = 13.4, 4.8 Hz, 1H), 1.82 (s, 3H), 1.78 (s, 3H), 1.67 (s, 3H), 1.39 (s, 3H), 1.31 – 1.30 (m, 1H), 1.27 (s, 3H), 1.06 (s, 3H).13C NMR (126 MHz, cdcl3) δ 203.78, 174.32, 169.86, 161.27, 159.78, 150.37, 136.45, 134.98, 134.52, 133.36, 120.44, 117.76, 112.45, 106.24, 106.02, 90.87, 84.50, 83.10, 49.05, 46.86, 30.15, 29.10, 28.84, 25.85, 25.72, 25.47, 22.78, 21.20, 18.13, 16.84. HRMS calc. for $[C_{30}H_{33}O_7]^-$ is 505.2232, found 505.2227.

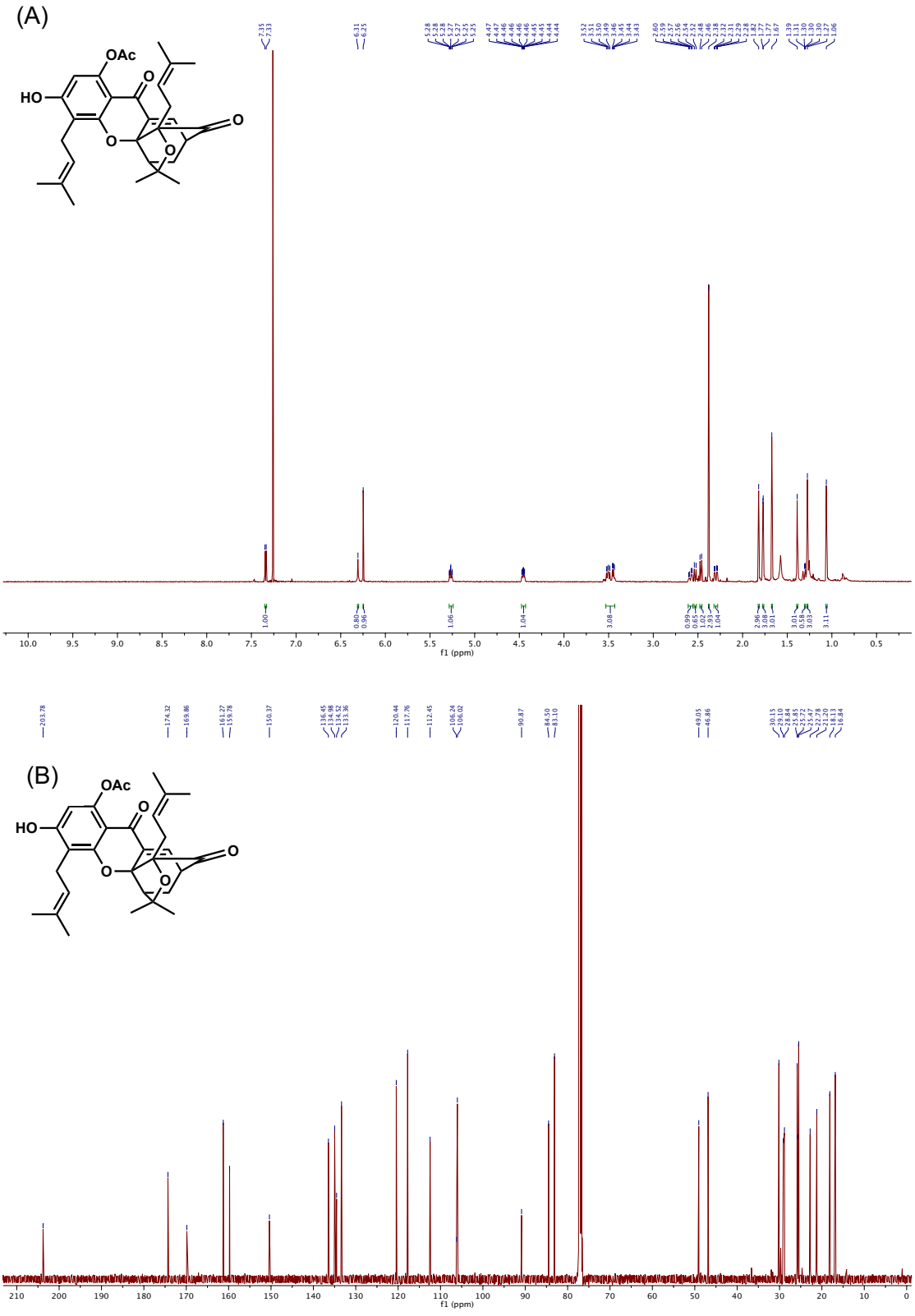

Figure 3.9. NMR spectra of **3.14**. (A) 1H NMR (B) 13C NMR

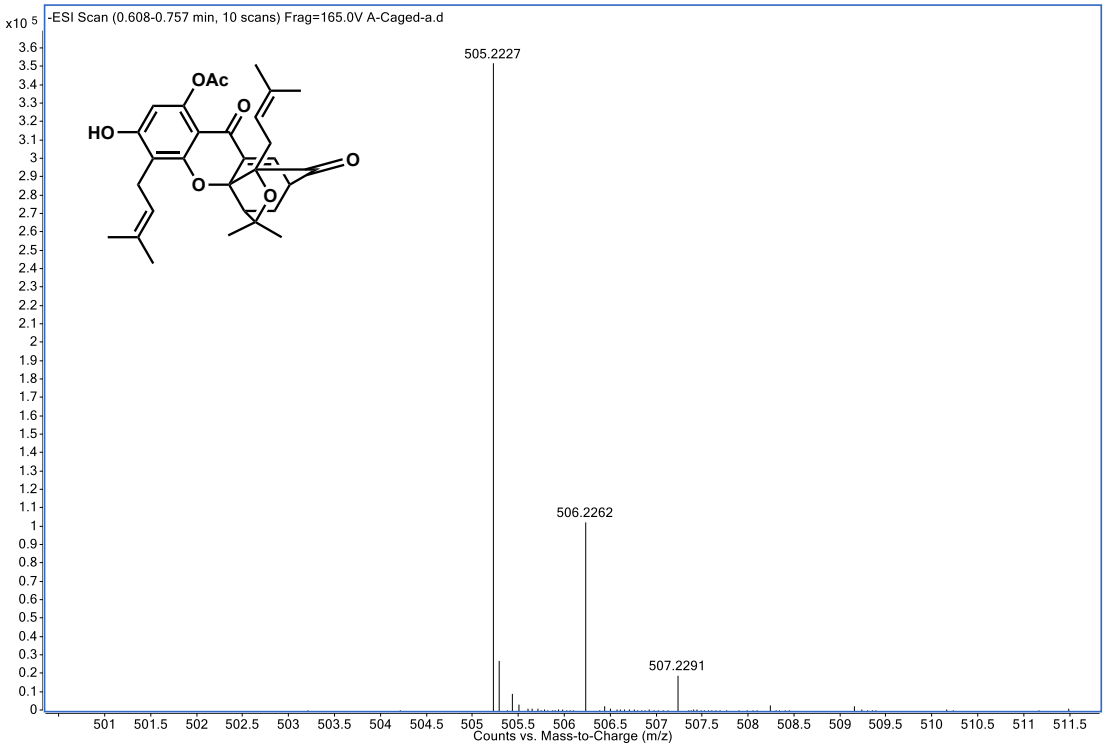

Figure 3.10. MS1 spectrum of **3.14**

Compound **3.2**:

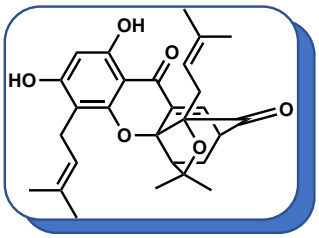

To a solution of compound **3.14** (30 mg, 0.06 mmol) in Methanol (2.5 mL) and 0.6 mL of 0.5 M aq. K_2CO_3 was added at room temperature. The reaction was monitored on TLC (70% Et_2O/hexane) till completion after 5 hrs. The reaction mixture was quenched by addition of 3 M HCl till cloudy yellow solution formed. Then, the product was allowed to precipitate as yellow residues. The yellow residues were filtered and purified further by column chromatography (10-40% Et_2O/hexane) to yield forbesione **3.2** (25 mg, 90%). ^{1}H NMR (500 MHz,) δ 12.60 (s, 1H), 7.46 (d, *J* = 7.1 Hz, 1H), 6.17 (s, 1H), 6.02 (s, 1H), 5.26 – 5.21 (m, 1H), 4.43 – 4.39 (m, 1H), 3.50 (dd, *J* = 6.9, 2.2 Hz, 1H), 3.47 – 3.40 (m, 2H), 2.58-2.54 (m, 2H), 2.48 (d, *J* = 9.4 Hz, 1H), 2.34 (dd, *J* = 13.5, 4.7 Hz, 1H), 1.81 (s, 3H), 1.75 (d, *J* = 1.2 Hz, 3H), 1.68 (s, 3H), 1.37 (s, 3H), 1.35 (dd, *J* = 4.0 Hz, 0.9 Hz, 1H), 1.28 (s, 3H), 1.04 (s, 3H).^{13}C NMR (126 MHz, cdcl$_3$) δ 203.61, 179.85, 164.35, 163.40, 158.32, 135.77, 135.30, 134.28, 133.66, 121.40, 117.96, 105.89, 101.25, 97.18, 90.75, 84.72, 83.37, 49.29, 47.11, 30.33, 29.28, 29.10, 26.01, 25.73, 25.67, 22.31, 18.23, 16.90. HRMS calc. for $[C_{28}H_{33}O_6]^+$ is 464.2272, found 465.2266.

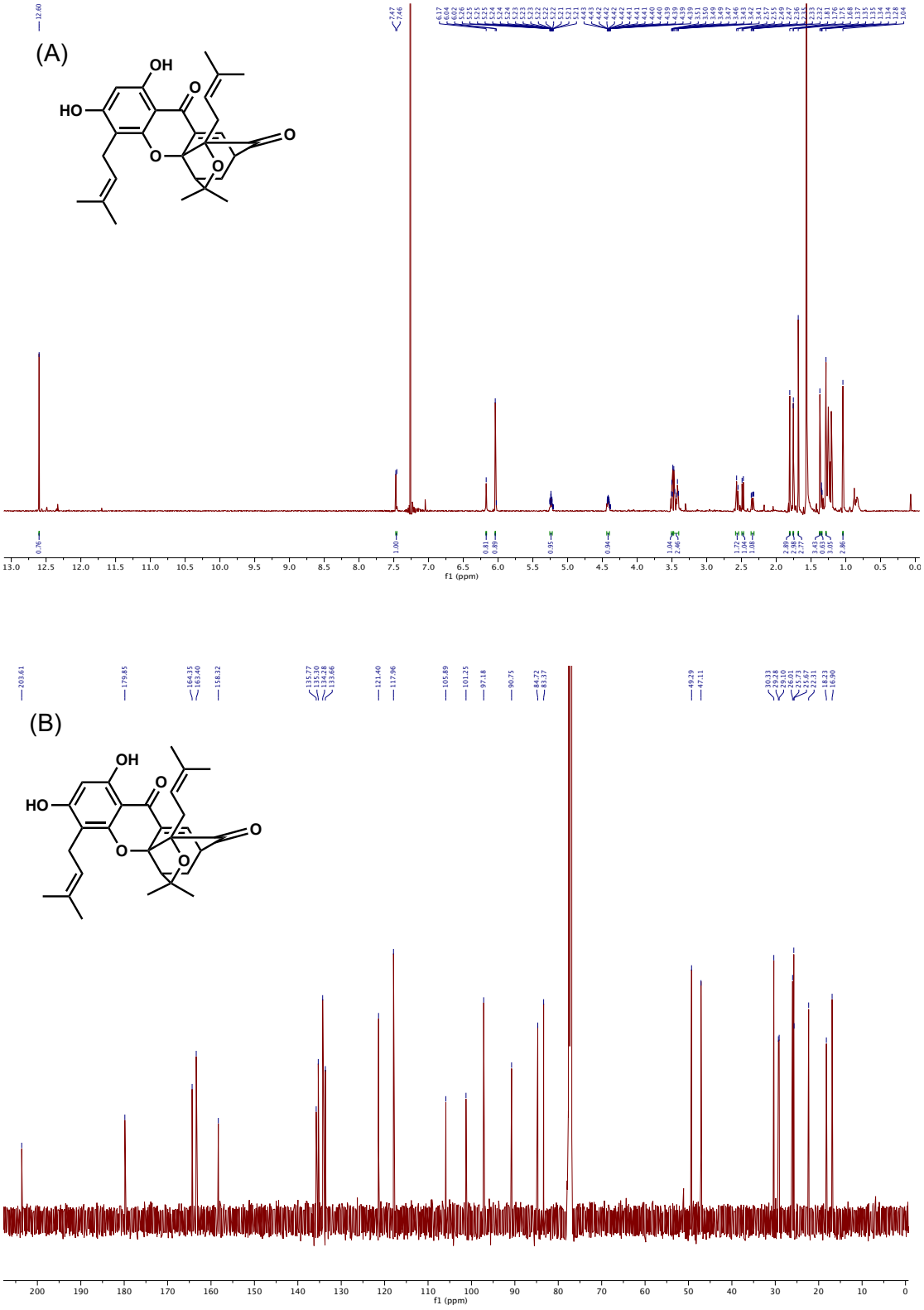

Figure 3.11. NMR spectra of **3.2**. (A) 1H NMR (B) 13C NMR

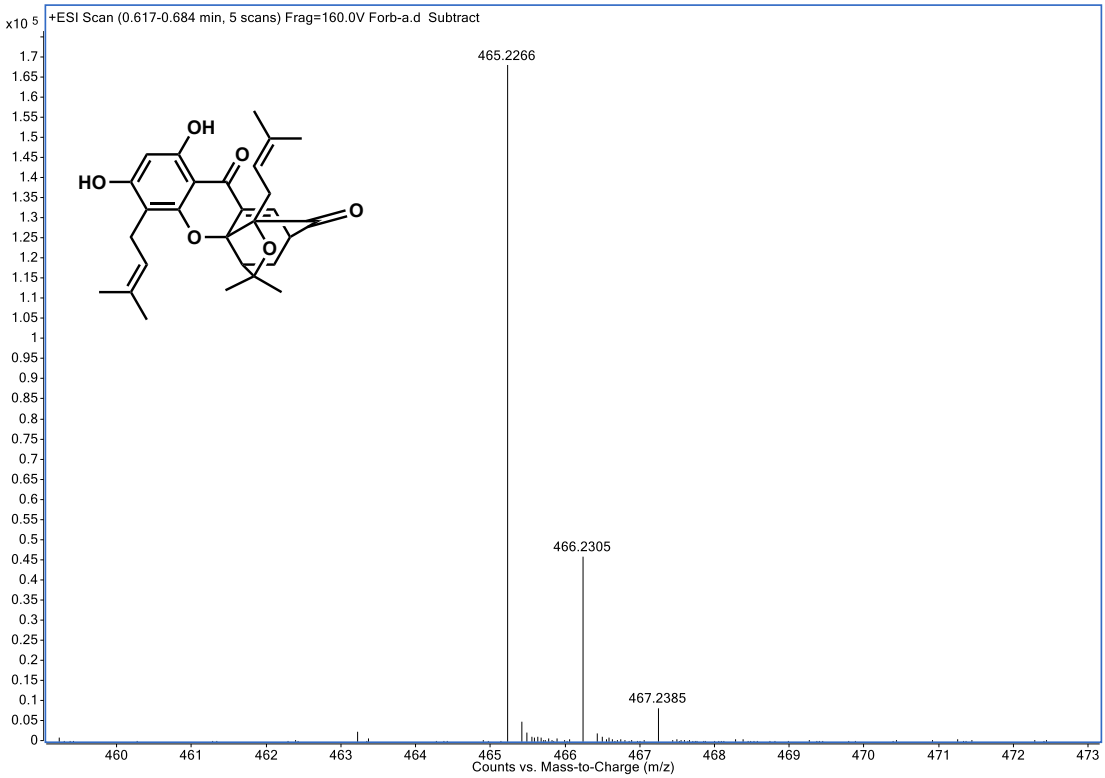

Figure 3.12. MS1 spectrum of **3.2**

Compound **3.6**:

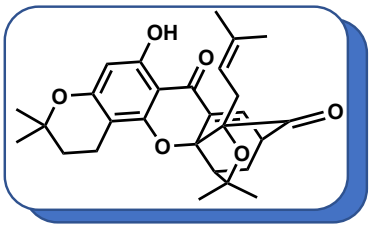

To a 10 ml round-bottom flask, compound **3.14** (3 mg, 0.006 mmol) was dissolved in DCM (1 ml) and TFA (1 ml, 0.013 mmol) was added and reaction left stirring for 36 hr. Then, was quenched by NaHCO3 and extracted with DCM. The organic layer was dried over MgSO4 and solvent was removed by rotary evaporation and purified by preparative TLC (50% Et_2O-hexane) to yield cycled forbesione (1.6 mg, 50%) ^1H NMR (500 MHz, Chloroform-*d*) δ 12.30 (s, 1H), 7.45 (d, *J* = 6.4 Hz, 1H), 5.99 (s, 1H), 4.43 (m, 1H), 3.50 (m, 1H), 2.88 – 2.73 (m, 1H), 2.66 – 2.53 (m, 3H), 2.49 (d, *J* = 9.4 Hz, 1H), 2.34 (dd, *J* = 13.5, 4.7 Hz, 1H), 1.90 – 1.76 (m, 2H), 1.71 (s, 3H), 1.37 (s, 6H), 1.33 (s, 3H), 1.30 (s, 3H), 1.02 (s, 3H). ^{13}C NMR (126 MHz, $cdcl_3$) δ 16.69, 17.53, 25.36, 25.66, 26.11, 27.53, 29.13, 29.22, 30.32, 32.10, 46.93, 49.24, 83.40, 84.70, 90.76, 97.96, 100.46, 100.77, 117.68, 133.88, 135.22, 158.53, 162.48, 163.71, 179.34, 203.31. HRMS calc. for $[C_{28}\ H_{33}\ O_6]^+$ is 464.2272, found 465.226.

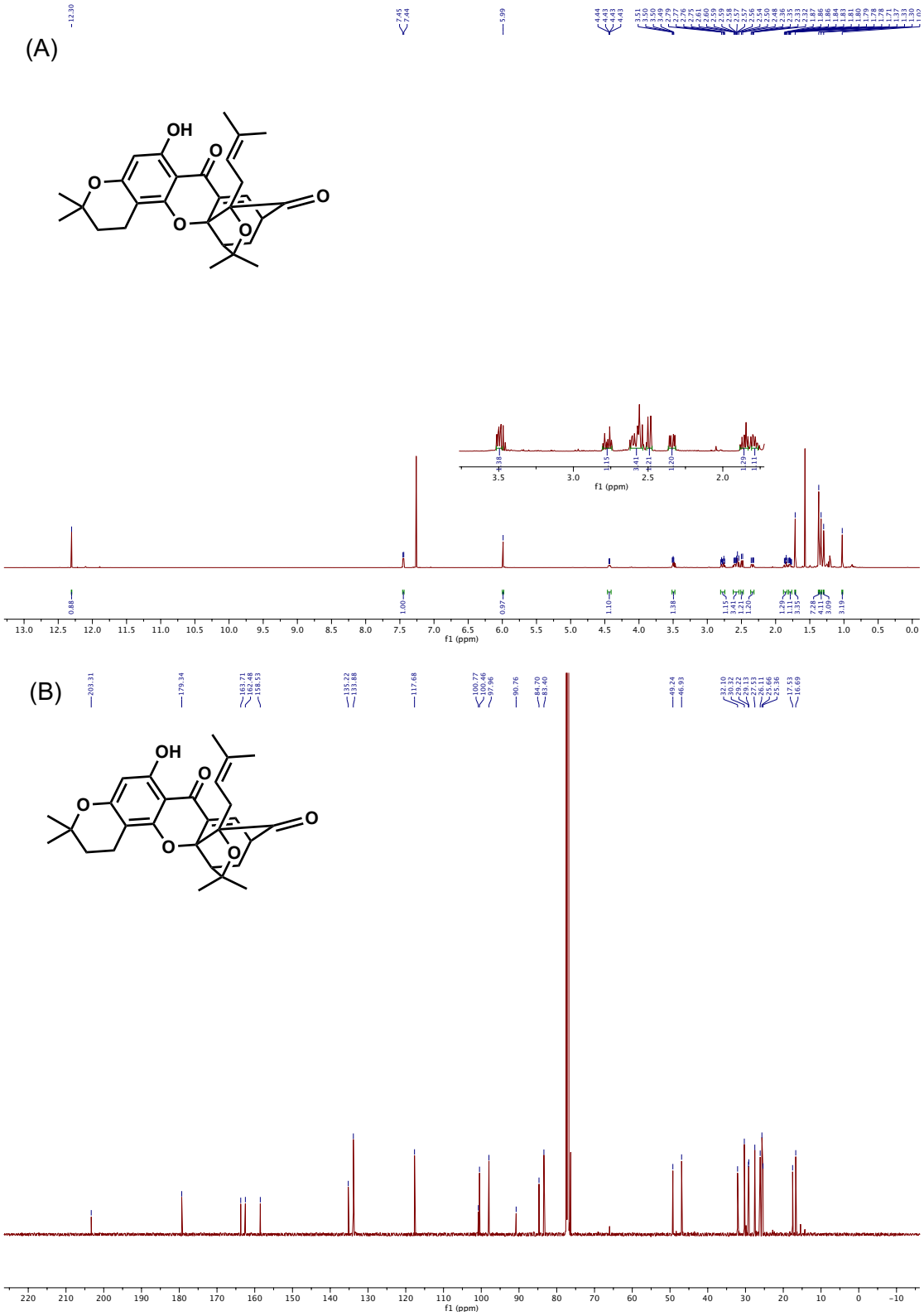

Figure 3.13. NMR spectra of **3.6**. (A) 1H NMR (B) 13C NMR

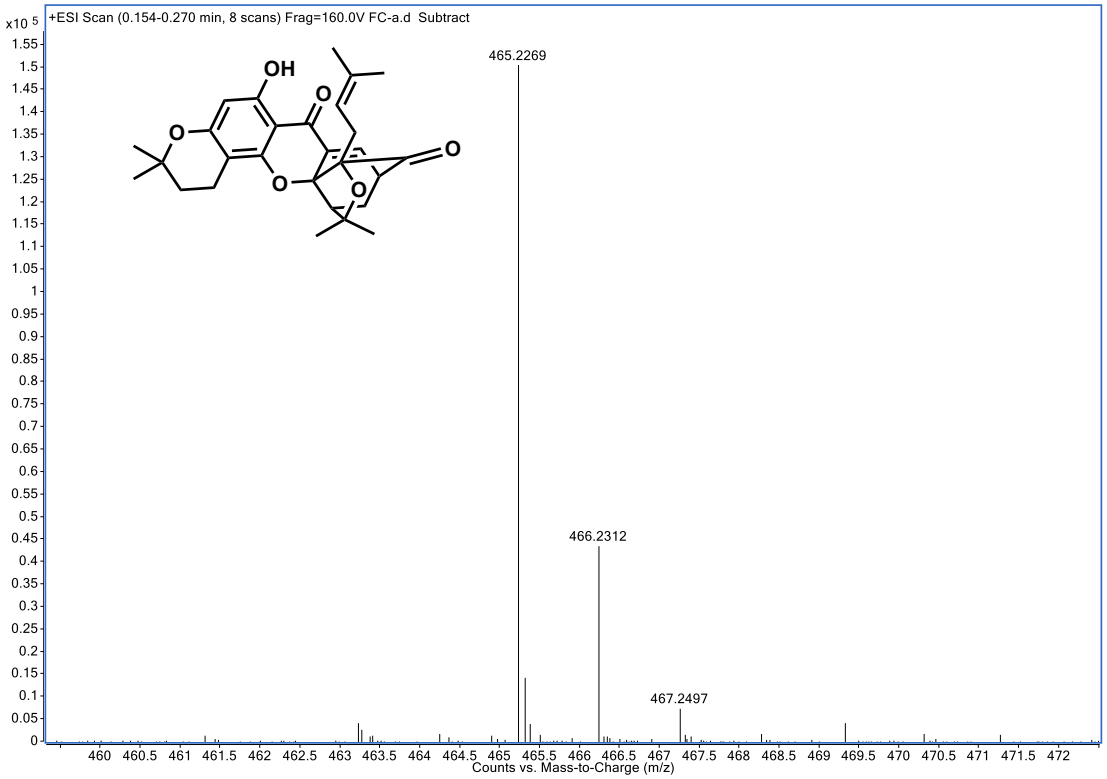

Figure 3.14. MS1 spectrum of **3.6**

Compound **3.17**:

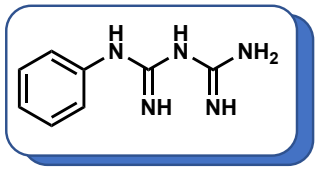

To a round bottom flask, dicyandiamide (1.5 g, 18 mmol, 1 equiv) dissolved in 3 M aq. HCl (11.22 mL, 18 mmol) was added aniline (1.64 mL, 18 mmol). The mixture was heated at 90 C for 20 h. Afterward, the reaction mixture was allowed to cool down and precipitate, phenylbiguanide hydrochloride salt, was formed, which then was filtered and washed with ~ 40 ml of cold water. Then, phenylbiguanide hydrochloride salt residues was neutralized with methanolic sodium methoxide (0.5 M, 36 mL) for 2 h at room temperature. Following filtration, the filtrate was dried by vacuum evaporation. To the residues was added hot ethanol (50 ml) and precipitate was removed. The ethanol layer was evaporated in vacuo to yield phenylbiguanide free base (**3.18**) (2 g, 63 % yield), white residues.

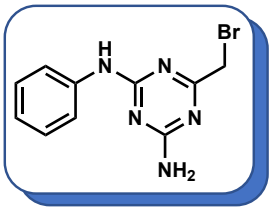

To a microwave vial, was added phenylbiguanide (1 g, 5.64 mmol) in methanol (2 mL) and the vial was sealed under argon. Then, 1.25 mL of ethylbromoacetate (11.29 mmol) was added and the mixture was stirred for 24 h under 60 °C. Afterward, the reaction was allowed to cool down to room temperature. The solvent was removed by rotary evaporation and the crude material was purified through flash column chromatography (silica 20-90% EtOAc-hexane) to yield 6-(Bromomethyl)-N2-phenyl-

1,3,5-triazine-2,4-diamine (**3.17**) (1.26 g, 80%), milky-white gummy residues, R_f= 0.4 (EtOAc:hexane (4:6)). ^{1}H NMR (400 MHz, Chloroform-*d*) δ 7.56 (d, *J* = 8.0 Hz, 2H), 7.34 (t, *J* = 7.8 Hz, 2H), 7.11 (t, *J* = 7.4 Hz, 1H), 5.52 (s, 2H), 4.14 (s, 2H).^{13}C NMR (126 MHz, cdcl$_3$) δ 174.20, 167.35, 164.82, 137.87, 129.11, 124.15, 120.84, 32.71. HRMS calc. for $[C_{10}\ H_{11}\ N_5\ Br]^+$ is 280.0192, found 280.0188.

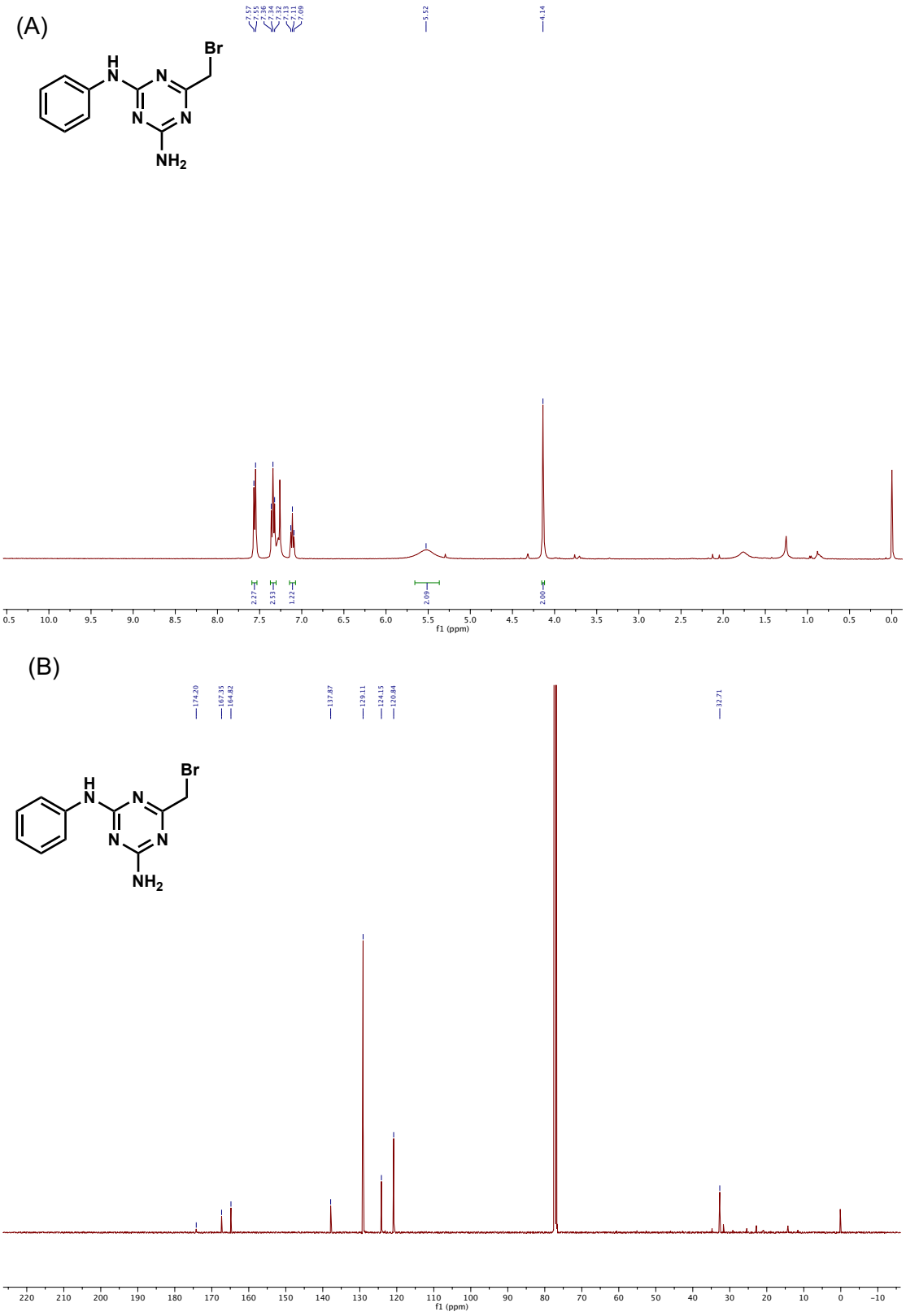

Figure 3.15. NMR spectra of **3.17**. (A) 1H NMR (B) 13C NMR

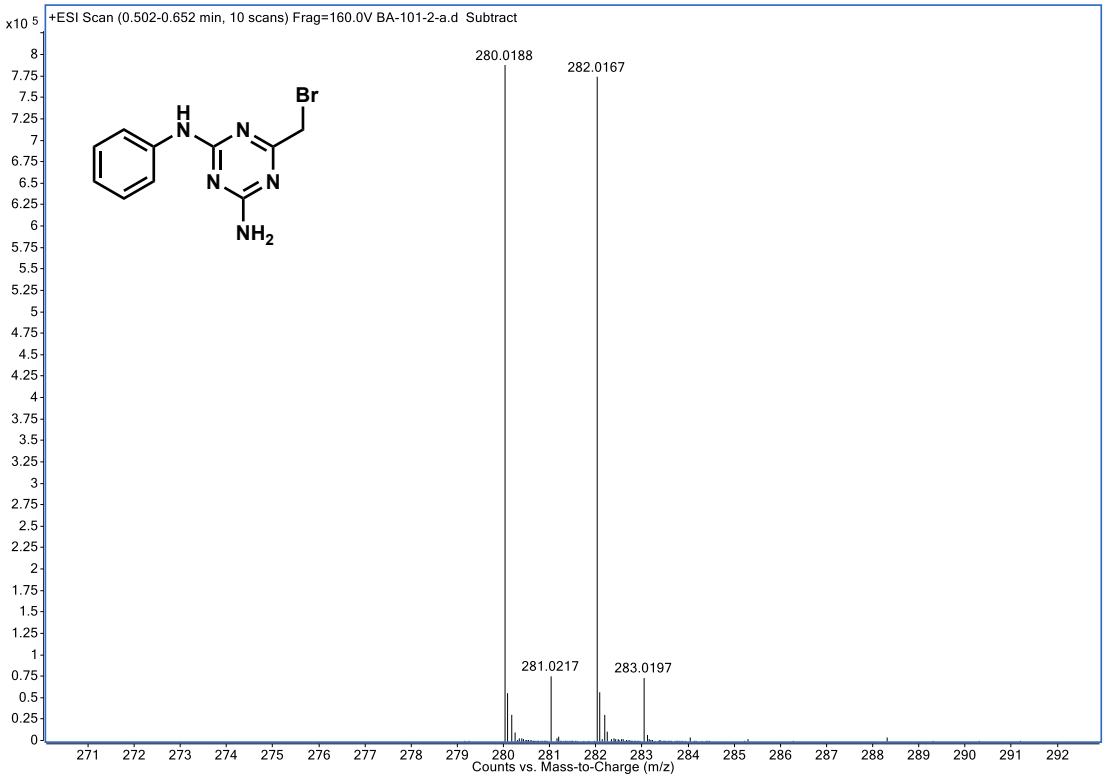

Figure 3.16. MS1 spectrum of **3.17**

Compound **3.19**:

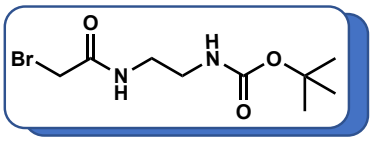

To a stirred solution of bromoacetic acid (0.96 g, 6.9 mmol) and DCC (0.57 g, 3.5 mmol) in DCM (15 mL) was stirred for 40 min at room temperature. Then, N-Boc-ethylenediamine (0.5 mL, 3.1 mmol) in DCM (15 mL) was added to the reaction mixture. After 24 h, the mixture was filtered, and filtrate was dried by rotary evaporation. The crude residues were washed with conc. H_2O and extracted with 3 X DCM (30 ml). The organic layer was dried over MgSO4 and solvent was removed by rotary evaporation and purified through flash column chromatography (silica 10-70% EtOAc-hexane) to yield *tert*-butyl (2-(2-bromoacetamido)ethyl)carbamate (**3.19**) (90% yield). ^{1}H NMR (500 MHz, Chloroform-*d*) δ 7.14 (s, 1H), 4.90 (s, 1H), 3.86 (s, 2H), 3.39 (q, *J* = 5.5 Hz, 3H), 3.32 (t, *J* = 5.9 Hz, 3H), 1.44 (s, 12H).^{13}C NMR (126 MHz, $cdcl_3$) δ 169.68, 166.57, 157.00, 80.13, 41.71, 39.80, 29.02, 28.48. HRMS calc. for $[C_9 H_{17} Br N_2 O_3 Na]^+$ is 303.0315, found 303.0312.

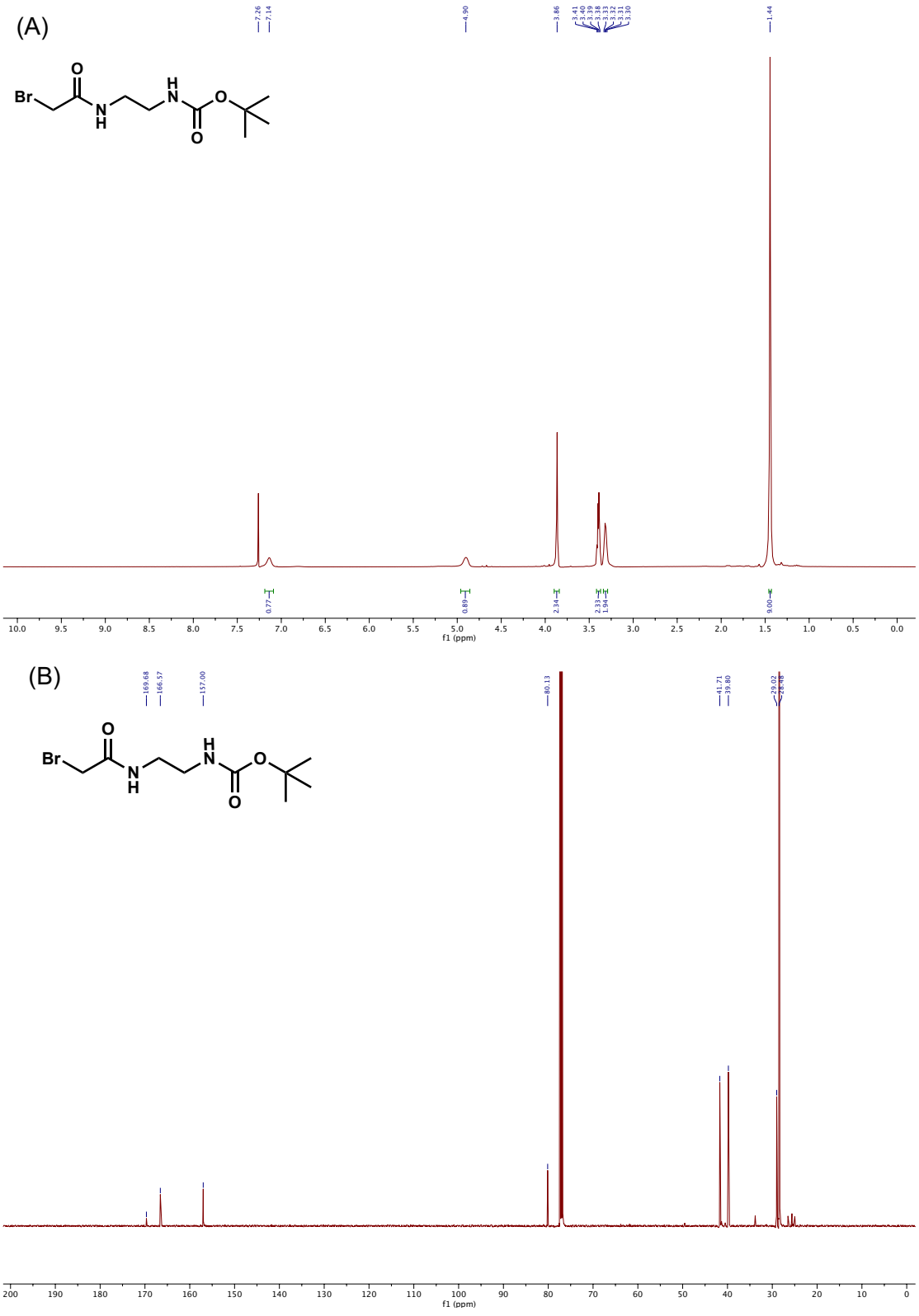

Figure 3.17. NMR spectra of **3.19**. (A) 1H NMR (B) 13C NMR

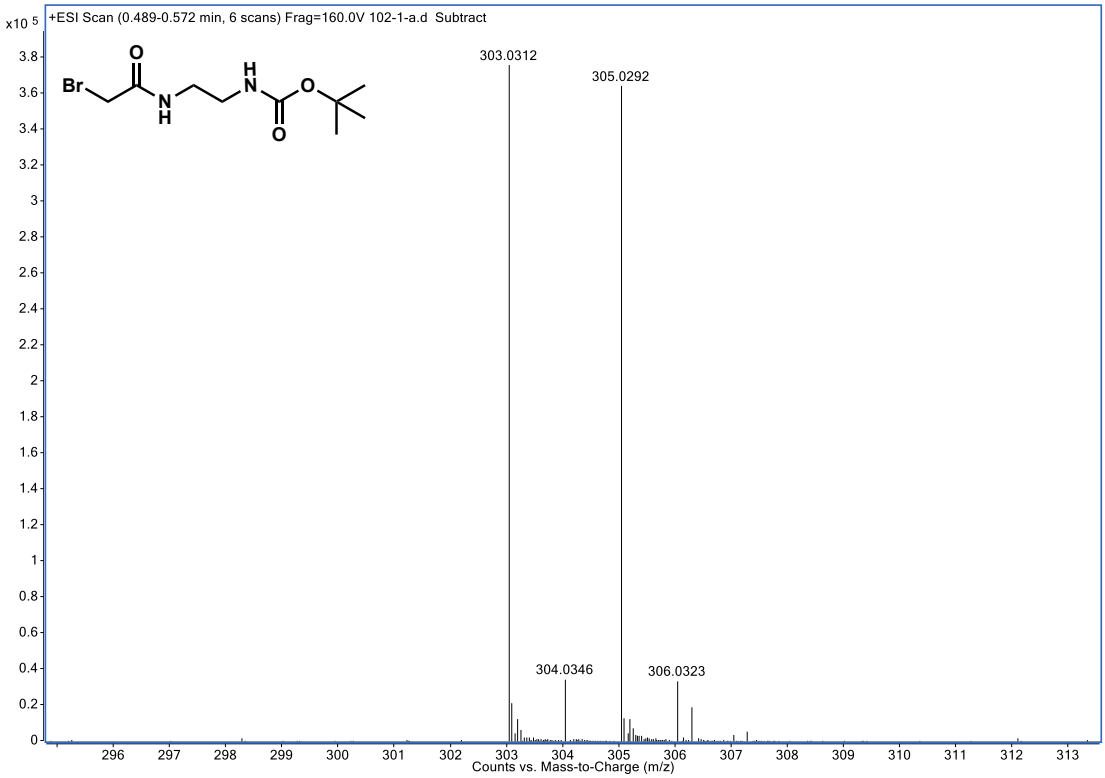

Figure 3.18. MS1 spectrum of **3.19**

Forbesione library: **3.20** and **3.21**

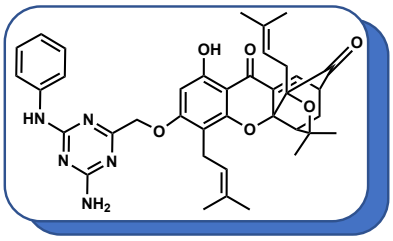

To a 25 ml round bottom flask, was added compound **3.2** (12 mg, 0.026 mmol) in DCM (1 mL) and the flask was sealed under argon. Then, 22.5 uL of DIPEA (0.129 mmol) was added and the mixture was stirred for 20 min. Then, amine fragment was added (0.052 mmol) and the reaction left stirring for 24 hr. Afterward, the solvent was removed by rotary evaporation and the crude material was purified through flash column chromatography (silica 20-50% Et_2O-hexane) to yield forbesione analogs (52% yield for (**3.20**) and 40% yield for (**3.21**)):

a) Compound (**3.20**): ^{1}H NMR (400 MHz, Chloroform-*d*) δ 12.71 (s, 1H), 7.54 (d, *J* = 8.1 Hz, 2H), 7.46 (d, *J* = 6.9 Hz, 1H), 7.32 (t, *J* = 7.7 Hz, 2H), 7.22 – 7.04 (m, 1H), 6.08 (s, 1H), 5.30 (dd, *J* = 13.9, 7.7 Hz, 3H), 4.97 (s, 2H), 4.39 (t, *J* = 7.9 Hz, 1H), 3.56 – 3.39 (m, 3H), 2.59 (d, *J* = 7.6 Hz, 2H), 2.50 (d, *J* = 9.4 Hz, 1H), 2.38 – 2.23 (m, 1H), 1.73 (s, 6H), 1.67 (s, 3H), 1.44 (d, *J* = 6.8 Hz, 1H), 1.35 (s, 3H), 1.29 (s, 3H), 0.98 (s, 3H). ^{13}C NMR (126 MHz, $cdcl_3$) δ 203.74, 179.89, 166.86, 165.13, 164.43, 163.45, 157.71, 137.93, 135.25, 134.23, 133.76, 132.26, 129.05, 123.96, 122.41, 120.63, 118.14, 109.16, 101.26, 93.94, 90.53, 84.86, 83.38, 69.69, 49.29, 47.11, 30.22, 29.85, 29.25, 28.95, 25.97, 25.73, 25.62, 22.09, 18.28, 16.80. HRMS calc. for $[C_{38}H_{42}N_5O_6]^+$ is 664.3130, found 664.3122.

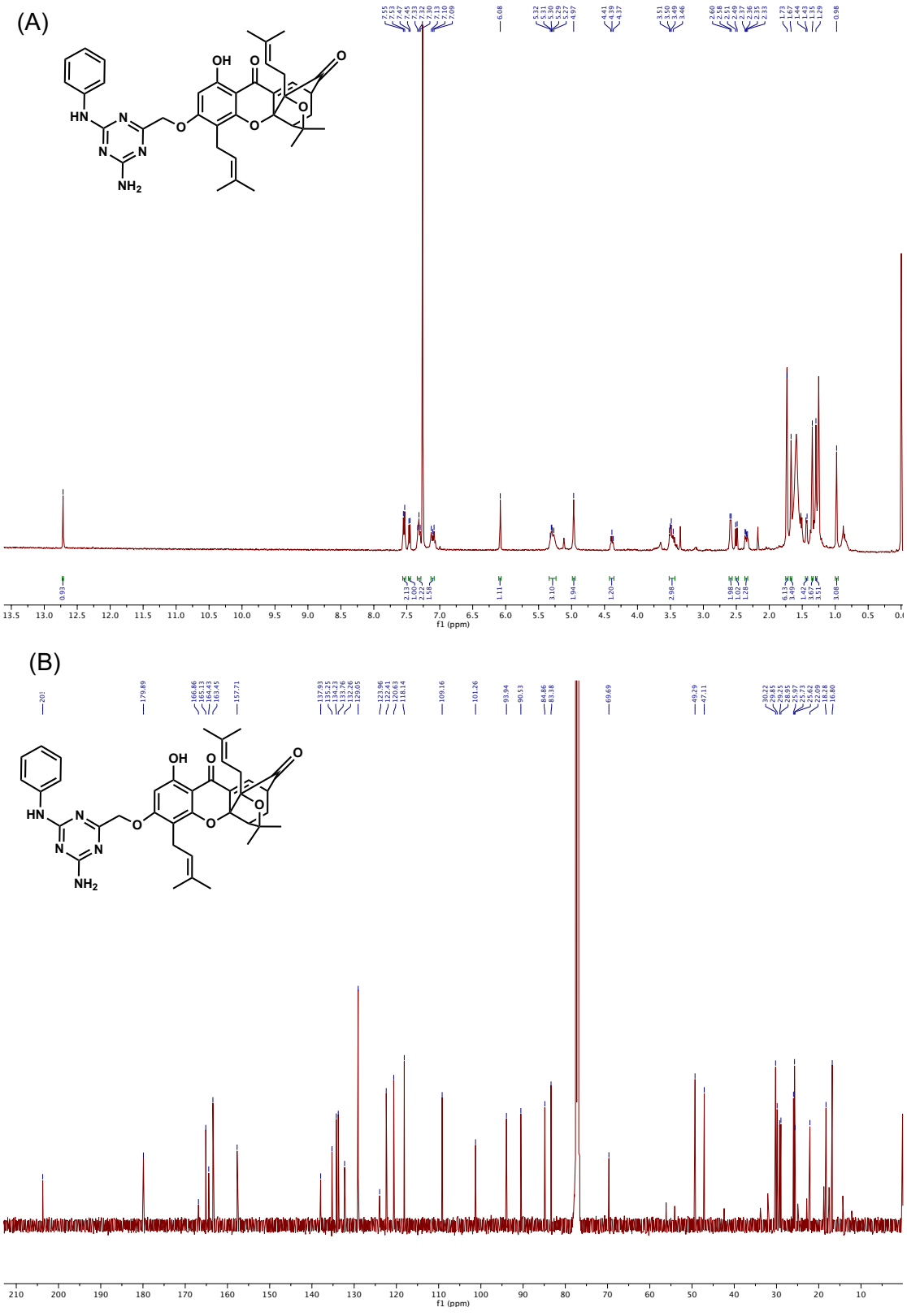

Figure 3.19. NMR spectra of **3.20**. (A) 1H NMR (B) 13C NMR

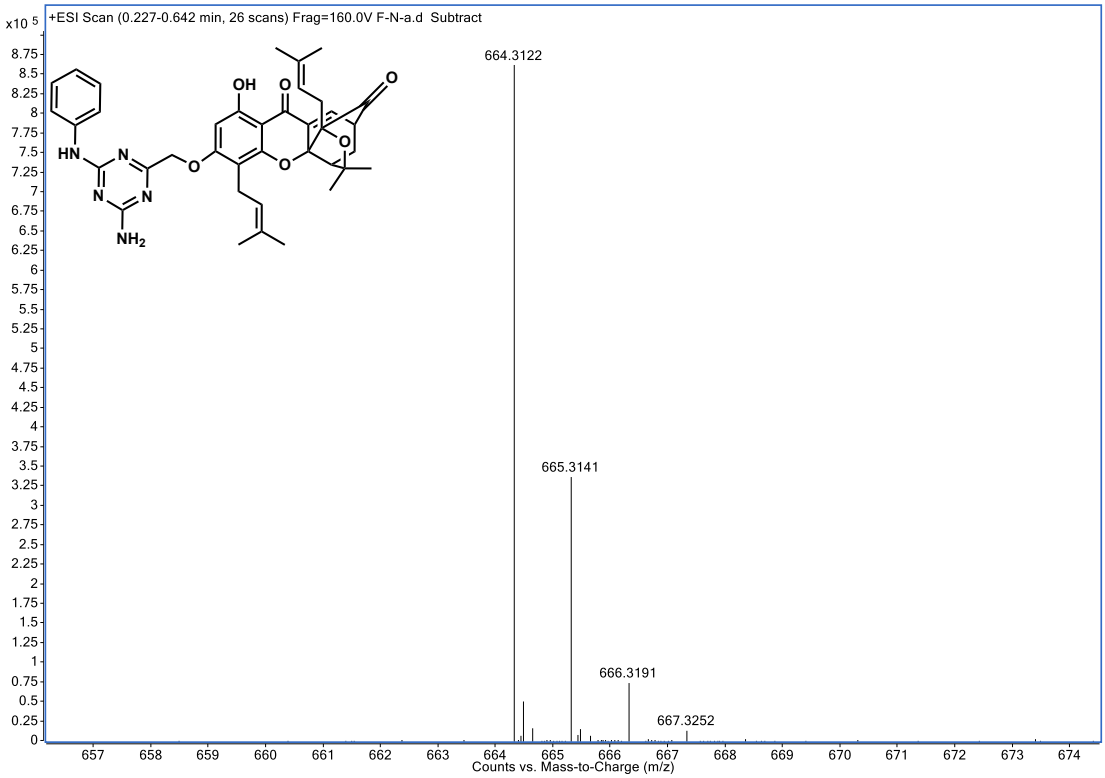

Figure 3.20. MS1 spectrum of **3.20**

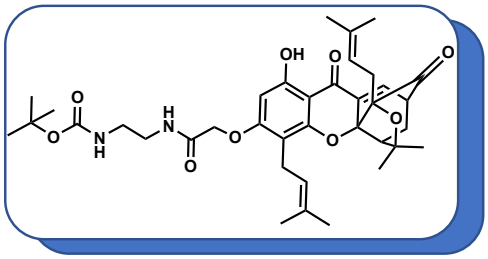

b) Compound (**3.21**):^{1}H NMR (500 MHz, Chloroform-*d*) δ 12.72 (s, 1H), 7.49 (d, *J* = 6.9 Hz, 1H), 6.87 (s, 1H), 6.06 (s, 1H), 5.18 – 5.12 (m, 1H), 4.85 (m, 1H), 4.54 (s, 2H), 4.41 – 4.35 (m, 1H), 3.52 (dd, *J* = 7.0, 4.5 Hz, 1H), 3.43 (d, *J* = 6.1 Hz, 4H), 3.27 (d, *J* = 5.8 Hz, 2H), 2.64 – 2.43 (m, 3H), 2.35 (dd, *J* = 13.3, 4.9 Hz, 1H), 1.77 (s, 3H), 1.71 (s, 3H), 1.69 (s, 3H), 1.41 (s, 12H), 1.35 (s, 3H), 1.29 (s, 3H), 0.98 (s, 3H).^{13}C NMR (126 MHz, cdcl$_3$) δ 203.41, 180.12, 168.03, 163.82, 163.39, 157.71, 156.46, 154.16, 135.23, 134.77, 133.49, 132.95, 122.70, 118.17, 108.55, 101.62, 93.40, 90.69, 84.70, 83.37, 67.32, 49.25, 47.12, 40.54, 40.12, 30.17, 29.85, 29.24, 29.03, 28.46, 25.82, 25.69, 25.61, 22.12, 18.31, 16.86. HRMS calc. for $[C_{37}H_{49}N_2O_9]^+$ is 665.3433, found 665.3428.

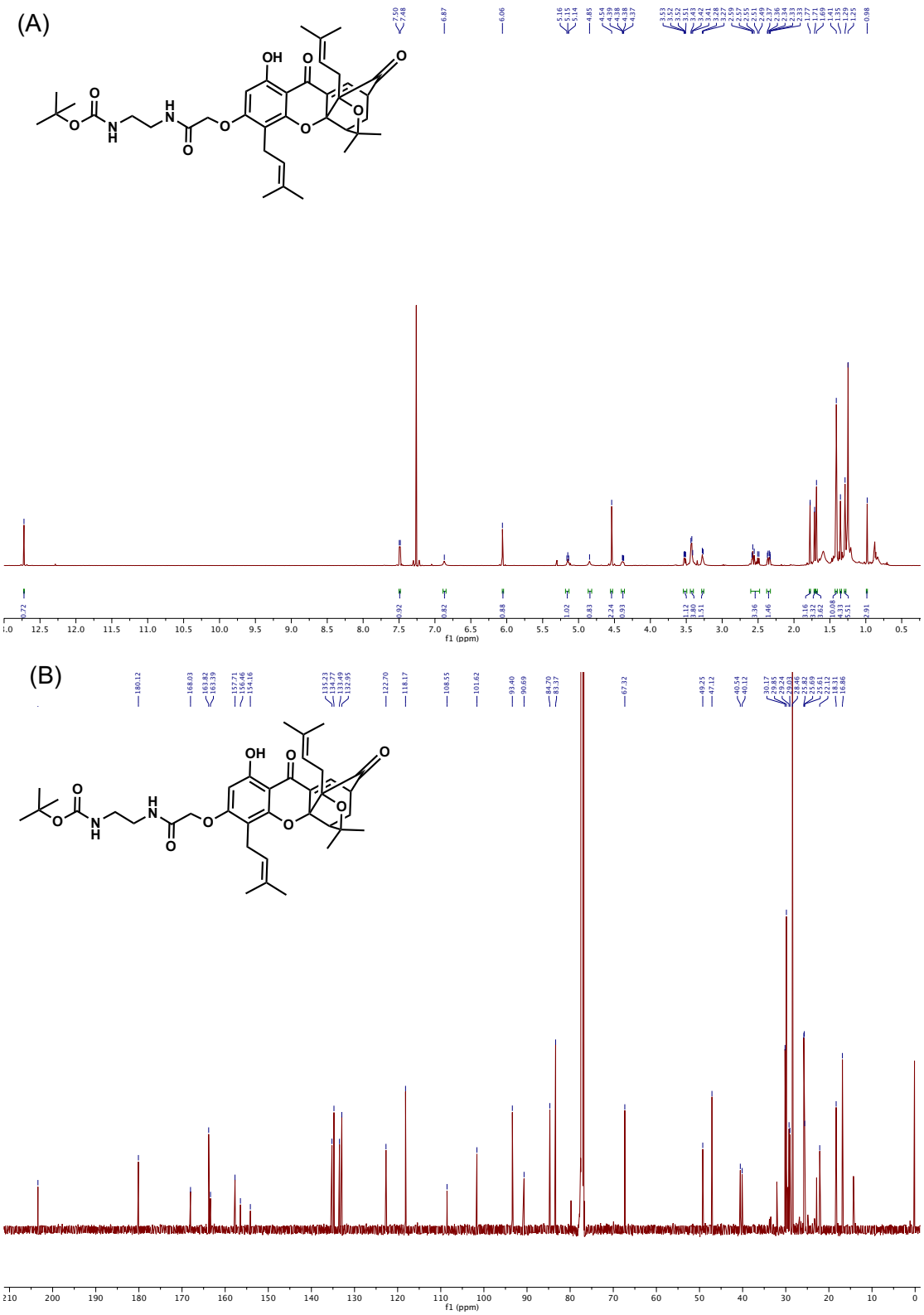

Figure 3.21. NMR spectra of **3.21**. (A) 1H NMR (B) 13C NMR

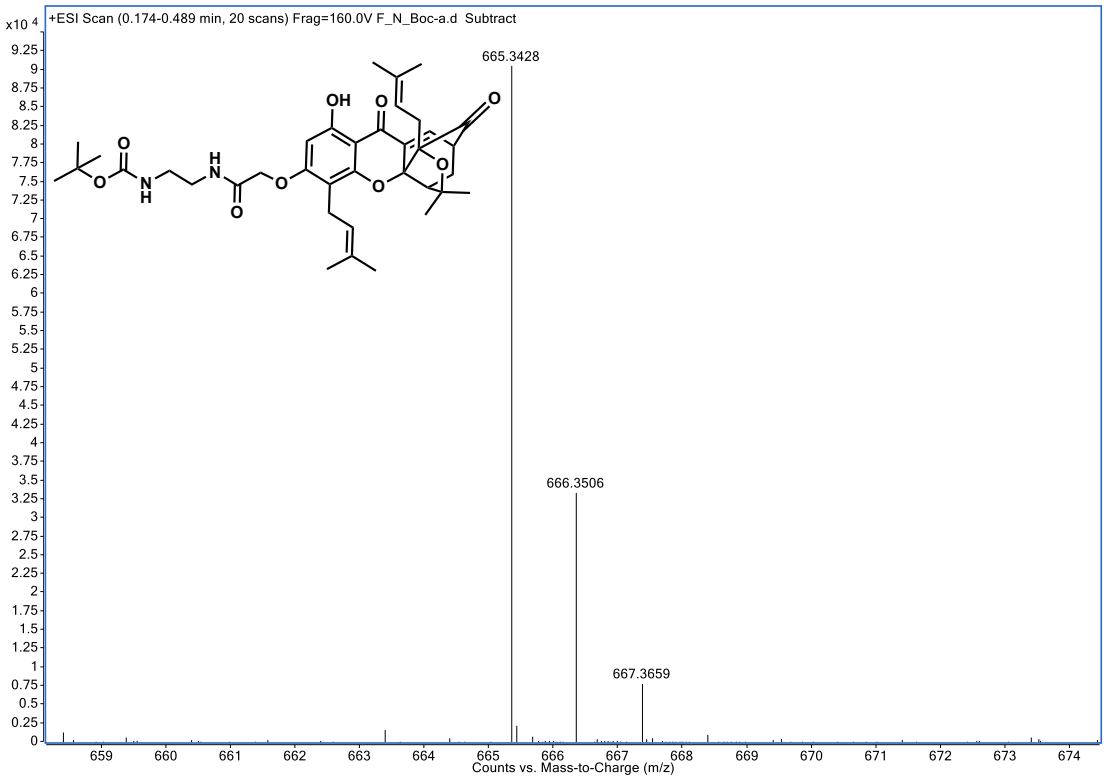

Figure 3.22. MS1 spectrum of **3.21**

Compound **3.12**:

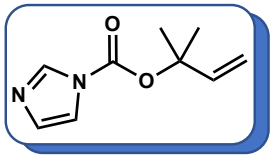

To round-bottomed flask, 2-methyl-3-buten-2-ol (5.1 mL, 48.79 mmol) was dissolved in dry DCM (20 mL) the stirring solution was added carbonyl diimidazole (10 g, 61.7 mmol) at room temperature. After 3 hrs, the reaction mixture was washed with water (2 x 35 mL) and extracted with DCM (45 mL). The organic layer was dried over $MgSO_4$, filtered, and concentrated by rotary evaporation to yield 2-methylbut-3-en-2-yl 1*H*-imidazole-1-carboxylate (**3.12**) (8.34 g, 95%) which was used in the next step without further purification: colorless liquid; *Rf* = 0.48 (25% EtOAc-hexane); ^{1}H NMR (500 MHz, Chloroform-*d*) δ 8.08 (s, 1H), 7.37 (s, 1H), 7.03 (s, 1H), 6.16 (dd, *J* = 17.4, 10.9 Hz, 1H), 5.32 (d, *J* = 17.4 Hz, 1H), 5.23 (d, *J* = 10.9 Hz, 1H), 1.69 (s, 6H).; ^{13}C NMR (126 MHz, $cdcl_3$) δ 146.97, 140.52, 137.16, 130.41, 117.23, 114.97, 85.60, 26.30.

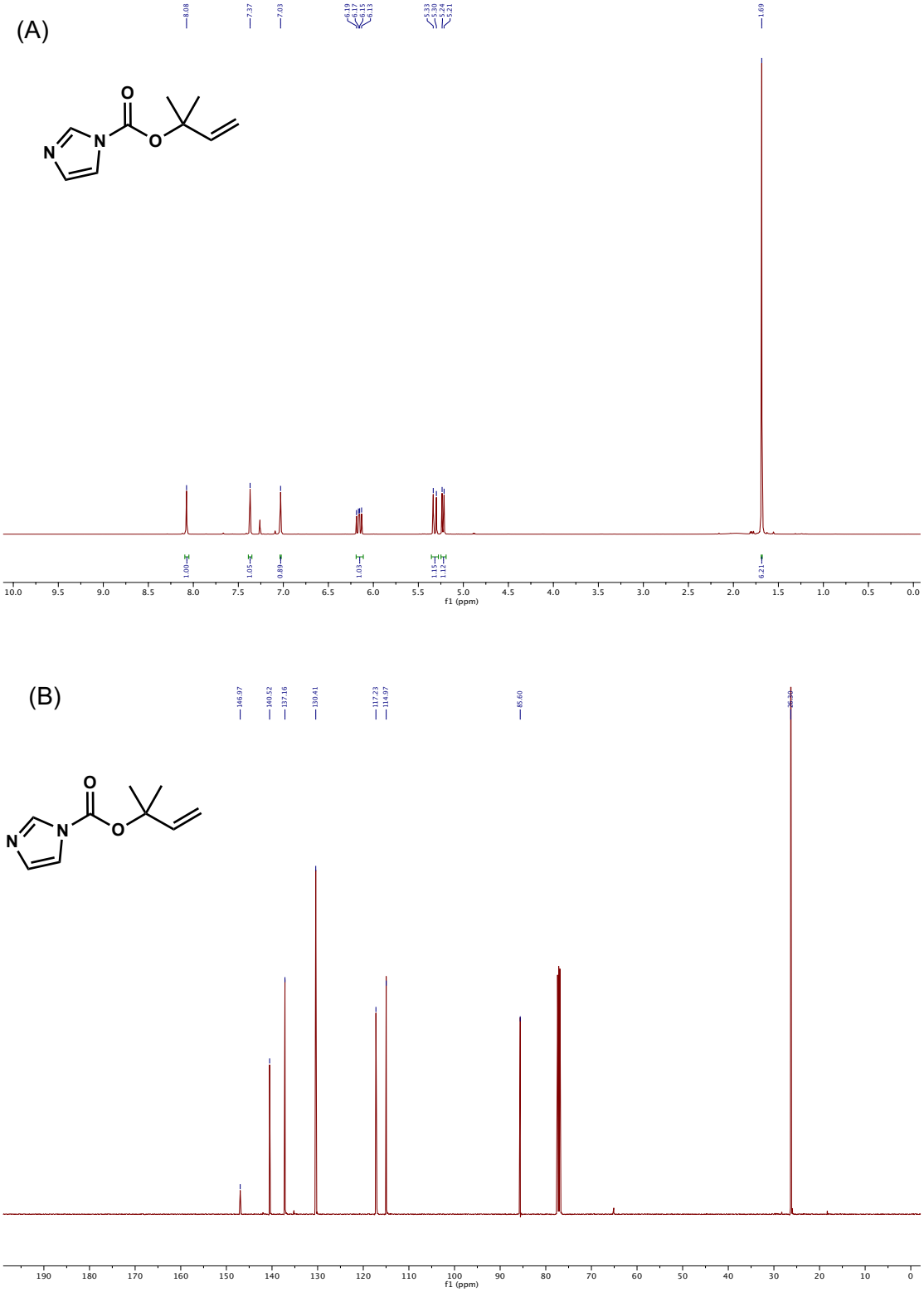

Figure 3.23. NMR spectra of **3.12**. (A) 1H NMR (B) 13C NMR

compound **3.11**:

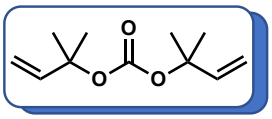

To a solution of 2-methyl-3-buten-2-ol (4.1 mL, 39 mmol) in dry THF (80 mL) under argon at -78 °C was added 1.6 M *n*-BuLi in hexane (26.7 mL, 42.7 mmol) dropwise via syringe. After stirring for 30 min at -78 °C, 2-methylbut-3-en-2-yl 1*H*-imidazole-1-carboxylate (6.7 mL, 38.8 mmol) was added. The reaction mixture was allowed to warm to room temperature and stirred for another 3 hrs. The reaction mixture was then quenched with saturated aqueous NH_4Cl (20 mL) and extracted with diethyl ether (2 x 25 mL). The combined organic layers were washed with water (2 x 20 mL) and brine (20 mL), dried over $MgSO_4$, and concentrated in vacuo. Purification by flash column chromatography (silica, 100% hexane) gave bis(2-methylbut-3-en-2-yl) carbonate **3.11** (6.92 g, 90%). **10c:** colorless liquid; *Rf* = 0.60 (25% EtOAc-hexane); ^{1}H NMR (500 MHz, Chloroform-*d*) δ 6.09 (dd, *J* = 17.5, 11.0 Hz, 2H), 5.18 (d, *J* = 17.5 Hz, 2H), 5.10 (d, *J* = 10.9 Hz, 2H), 1.52 (s, 12H); ^{113}C NMR (126 MHz, $cdcl_3$) δ 151.79, 142.16, 113.42, 81.88, 26.48.

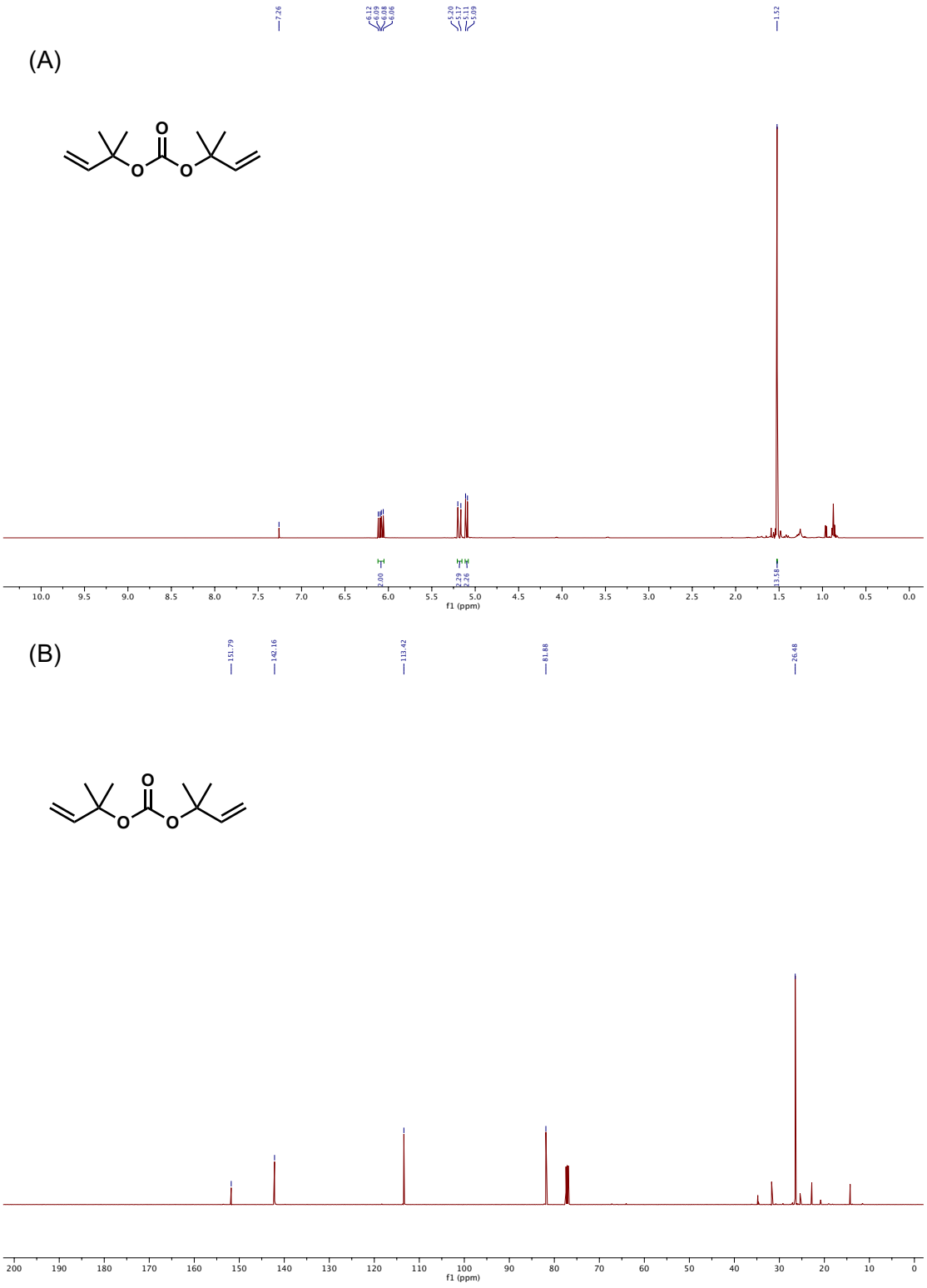

Figure 3.24. NMR spectra of **3.11**. (A) 1H NMR (B) 13C NMR

Reference:

1. Wang, X.; Galli, G.; Campanella, M. Mitochondrial pharmacology: featured mechanisms and approaches for therapy translation. *Br J Pharmacol* **2019,** 176, 4245-4246.

2. Smith, R. A.; Hartley, R. C.; Cocheme, H. M.; Murphy, M. P. Mitochondrial pharmacology. *Trends Pharmacol Sci* **2012,** 33, 341-52.

3. Zampieri, M.; Sekar, K.; Zamboni, N.; Sauer, U. Frontiers of high-throughput metabolomics. *Curr Opin Chem Biol* **2017,** 36, 15-23.

4. Gorman, G. S.; Chinnery, P. F.; DiMauro, S.; Hirano, M.; Koga, Y.; McFarland, R.; Suomalainen, A.; Thorburn, D. R.; Zeviani, M.; Turnbull, D. M. Mitochondrial diseases. *Nature Reviews Disease Primers* **2016,** 2, 1-22.

5. Cogliati, S.; Enriquez, J. A.; Scorrano, L. Mitochondrial Cristae: Where Beauty Meets Functionality. *Trends Biochem Sci* **2016,** 41, 261-273.

6. Kristal, B. S.; Krasnikov, B. F. Structure-(Dys)function relationships in mitochondrial electron transport chain complex II? *Sci Aging Knowledge Environ* **2003,** 2003, PE3.

7. Boggan, R. M.; Lim, A.; Taylor, R. W.; McFarland, R.; Pickett, S. J. Resolving complexity in mitochondrial disease: Towards precision medicine. *Mol Genet Metab* **2019,** 128, 19-29.

8. Anderson, S.; Bankier, A. T.; Barrell, B. G.; Debruijn, M. H. L.; Coulson, A. R.; Drouin, J.; Eperon, I. C.; Nierlich, D. P.; Roe, B. A.; Sanger, F.; Schreier, P. H.; Smith, A. J. H.; Staden, R.; Young, I. G. Sequence and Organization of the Human Mitochondrial Genome. *Nature* **1981,** 290, 457-465.

9. St. John, J. C. Chapter 34 - Mitochondrial DNA: Its Transmission from Gametes and Embryos. In *Principles of Cloning (Second Edition)*, Cibelli, J.; Gurdon, J.; Wilmut, I.; Jaenisch, R.; Lanza, R.; West, M. D.; Campbell, K. H. S., Eds. Academic Press: San Diego, 2014; pp 429-439.

10. Plesofsky, N.; Gardner, N.; Videira, A.; Brambl, R. NADH dehydrogenase in Neurospora crassa contains myristic acid covalently linked to the ND5 subunit peptide. *Biochim Biophys Acta* **2000,** 1495, 223-30.

11. Martinez, J.; Marmisolle, I.; Tarallo, D.; Quijano, C. Mitochondrial Bioenergetics and Dynamics in Secretion Processes. *Front Endocrinol (Lausanne)* **2020,** 11, 319.

12. Nosek, J.; Fukuhara, H. Nadh Dehydrogenase Subunit Genes in the Mitochondrial-DNA of Yeasts. *Journal of Bacteriology* **1994,** 176, 5622-5630.

13. Kalyanaraman, B.; Cheng, G.; Hardy, M.; Ouari, O.; Lopez, M.; Joseph, J.; Zielonka, J.; Dwinell, M. B. A review of the basics of mitochondrial bioenergetics,

metabolism, and related signaling pathways in cancer cells: Therapeutic targeting of tumor mitochondria with lipophilic cationic compounds. *Redox Biol* **2018,** 14, 316-327.

14. Swerdlow, R. H. Mitochondria and Cell Bioenergetics: Increasingly Recognized Components and a Possible Etiologic Cause of Alzheimer's Disease. *Antioxidants & Redox Signaling* **2012,** 16, 1434-U163.

15. Zhang, J.; Kang, Z.; Chen, J.; Du, G. Optimization of the heme biosynthesis pathway for the production of 5-aminolevulinic acid in Escherichia coli. *Sci Rep* **2015,** 5, 8584.

16. Du, C. Y.; Cao, S. Y.; Shi, X. Y.; Nie, X. T.; Zheng, J. S.; Deng, Y.; Ruan, L. F.; Peng, D. H.; Sun, M. Genetic and Biochemical Characterization of a Gene Operon for trans-Aconitic Acid, a Novel Nematicide from Bacillus thuringiensis. *Journal of Biological Chemistry* **2017,** 292, 3517-3530.

17. Chun, H. L.; Lee, S. Y.; Lee, S. H.; Lee, C. S.; Park, H. H. Enzymatic reaction mechanism of cis-aconitate decarboxylase based on the crystal structure of IRG1 from Bacillus subtilis. *Scientific Reports* **2020,** 10.

18. Carling, D.; Mayer, F. V.; Sanders, M. J.; Gamblin, S. J. AMP-activated protein kinase: nature's energy sensor. *Nature Chemical Biology* **2011,** 7, 512-518.

19. Hardie, D. G. AMP-activated protein kinase-an energy sensor that regulates all aspects of cell function. *Genes & Development* **2011,** 25, 1895-1908.

20. Rahman, J.; Rahman, S. Mitochondrial medicine in the omics era. *Lancet* **2018,** 391, 2560-2574.

21. Schon, K. R.; Ratnaike, T.; van den Ameele, J.; Horvath, R.; Chinnery, P. F. Mitochondrial Diseases: A Diagnostic Revolution. *Trends in Genetics* **2020,** 36, 702-717.

22. Niyazov, D. M.; Kahler, S. G.; Frye, R. E. Primary Mitochondrial Disease and Secondary Mitochondrial Dysfunction: Importance of Distinction for Diagnosis and Treatment. *Molecular Syndromology* **2016,** 7, 122-137.

23. Taanman, J. W. The mitochondrial genome: structure, transcription, translation and replication. *Biochimica Et Biophysica Acta-Bioenergetics* **1999,** 1410, 103-123.

24. Stewart, J. B.; Chinnery, P. F. The dynamics of mitochondrial DNA heteroplasmy: implications for human health and disease. *Nature Reviews Genetics* **2015,** 16, 530-542.

25. Chinnery, P. F.; Thorburn, D. R.; Samuels, D. C.; White, S. L.; Dahl, H. H. M.; Turnbull, D. M.; Lightowlers, R. N.; Howell, N. The inheritance of mitochondrial DNA heteroplasmy: random drift, selection or both? *Trends in Genetics* **2000,** 16, 500-505.

26. Mak, C. M.; Lee, H. C.; Chan, A. Y.; Lam, C. W. Inborn errors of metabolism and expanded newborn screening: review and update. *Crit Rev Clin Lab Sci* **2013,** 50, 142-62.

27. Lee, H. C.; Mak, C. M.; Lam, C. W.; Yuen, Y. P.; Chan, A. O.; Shek, C. C.; Siu, T. S.; Lai, C. K.; Ching, C. K.; Siu, W. K.; Chen, S. P.; Law, C. Y.; Tai, H. L.; Tam, S.; Chan, A. Y. Analysis of inborn errors of metabolism: disease spectrum for expanded newborn screening in Hong Kong. *Chin Med J (Engl)* **2011,** 124, 983-9.

28. Marigliano, M.; Anton, G.; Sabbion, A.; Morandi, A.; Morandi, G.; Degani, D.; Maffeis, C. Difficult management of glucose homeostasis in a 21-month-old child with type 1 diabetes and unknown glutaric aciduria type I: a case report. *Diabetes Care* **2013,** 36, e135-6.

29. Mak, C. M.; Law, E. C.; Lee, H. H.; Siu, W. K.; Chow, K. M.; Au Yeung, S. K.; Ngan, H. Y.; Tse, N. K.; Kwong, N. S.; Chan, G. C.; Lee, K. W.; Chan, W. P.; Wong, S. F.; Tang, M. H.; Kan, A. S.; Hui, A. P.; So, P. L.; Shek, C. C.; Lee, R. S.; Wong, K. Y.; Yau, E. K.; Poon, K. H.; Siu, S.; Poon, G. W.; Kwok, A. M.; Ng, J. W.; Yim, V. C.; Ma, G. G.; Chu, C. H.; Tong, T. Y.; Chong, Y. K.; Chen, S. P.; Ching, C. K.; Chan, A. O.; Tam, S.; Lau, R. L.; Ng, W. F.; Lee, K. C.; Chan, A. Y.; Lam, C. W. The first pilot study of expanded newborn screening for inborn errors of metabolism and survey of related knowledge and opinions of health care professionals in Hong Kong. *Hong Kong Med J* **2018,** 24, 226-237.

30. Mordaunt, D.; Cox, D.; Fuller, M. Metabolomics to Improve the Diagnostic Efficiency of Inborn Errors of Metabolism. *Int J Mol Sci* **2020,** 21.

31. Brown, C. S.; Lichter-Konecki, U. Phenylketonuria (PKU): A problem solved? *Mol Genet Metab Rep* **2016,** 6, 8-12.

32. Bruinenberg, V. M.; van Vliet, D.; van der Goot, E.; Counotte, D. S.; Kuhn, M.; van Spronsen, F. J.; van der Zee, E. A. Long-term dietary intervention with low Phe and/or a specific nutrient combination improve certain aspects of brain functioning in phenylketonuria (PKU). *PLoS One* **2019,** 14, e0213391.

33. Casey, L. Caring for children with phenylketonuria. *Can Fam Physician* **2013,** 59, 837-40.

34. van Wegberg, A. M. J.; MacDonald, A.; Ahring, K.; Belanger-Quintana, A.; Blau, N.; Bosch, A. M.; Burlina, A.; Campistol, J.; Feillet, F.; Gizewska, M.; Huijbregts, S. C.; Kearney, S.; Leuzzi, V.; Maillot, F.; Muntau, A. C.; van Rijn, M.; Trefz, F.; Walter, J. H.; van Spronsen, F. J. The complete European guidelines on phenylketonuria: diagnosis and treatment. *Orphanet J Rare Dis* **2017,** 12, 162.

35. Gorman, G. S.; Taylor, R. W. Mitochondrial DNA abnormalities in ophthalmological disease. *Saudi Journal of Ophthalmology* **2011,** 25, 395-404.

36. Parikh, S.; Goldstein, A.; Koenig, M. K.; Scaglia, F.; Enns, G. M.; Saneto, R.; Anselm, I.; Cohen, B. H.; Falk, M. J.; Greene, C.; Gropman, A. L.; Haas, R.; Hirano, M.; Morgan, P.; Sims, K.; Tarnopolsky, M.; Van Hove, J. L. K.; Wolfe, L.; DiMauro, S.

Diagnosis and management of mitochondrial disease: a consensus statement from the Mitochondrial Medicine Society. *Genetics in Medicine* **2015,** 17, 689-701.

37. Fohner, A. E.; Garrison, N. A.; Austin, M. A.; Burke, W. Patient care standards for primary mitochondrial disease: a consensus statement from the Mitochondrial Medicine Society Respose. *Genetics in Medicine* **2017,** 19.

38. Agana, M.; Frueh, J.; Kamboj, M.; Patel, D. R.; Kanungo, S. Common metabolic disorder (inborn errors of metabolism) concerns in primary care practice. *Annals of Translational Medicine* **2018,** 6.

39. Woidy, M.; Muntau, A. C.; Gersting, S. W. Inborn errors of metabolism and the human interactome: a systems medicine approach. *Journal of Inherited Metabolic Disease* **2018,** 41, 285-296.

40. Fraser, J. A.; Biousse, V.; Newman, N. J. The neuro-ophthalmology of mitochondrial disease. *Surv Ophthalmol* **2010,** 55, 299-334.

41. Kisilevsley, E.; Freund, P.; Margolin, E. Mitochondrial disorders and the eye. *Survey of Ophthalmology* **2020,** 65, 294-311.

42. Finsterer, J.; Zarrouk-Mahjoub, S.; Daruich, A. The Eye on Mitochondrial Disorders. *Journal of Child Neurology* **2016,** 31, 652-662.

43. Schrier, S. A.; Falk, M. J. Mitochondrial disorders and the eye. *Current Opinion in Ophthalmology* **2011,** 22, 325-331.

44. Yu-Wai-Man, P.; Griffiths, P. G.; Chinnery, P. F. Mitochondrial optic neuropathies - disease mechanisms and therapeutic strategies. *Prog Retin Eye Res* **2011,** 30, 81-114.

45. Chinnery, P. F.; Andrews, R. M.; Turnbull, D. M.; Howell, N. Leber hereditary optic neuropathy: Does heteroplasmy influence the inheritance and expression of the G11778A mitochondrial DNA mutation? *American Journal of Medical Genetics* **2001,** 98, 235-243.

46. Yu-Wai-Man, P.; Votruba, M.; Burte, F.; La Morgia, C.; Barboni, P.; Carelli, V. A neurodegenerative perspective on mitochondrial optic neuropathies. *Acta Neuropathologica* **2016,** 132, 789-806.

47. Kumar, M.; Tanwar, M.; Saxena, R.; Sharma, P.; Dada, R. Identification of novel mitochondrial mutations in Leber's hereditary optic neuropathy. *Molecular Vision* **2010,** 16, 782-792.

48. Wu, Y.; Kang, L.; Wu, H. L.; Hou, Y.; Wang, Z. X. Optical coherence tomography findings in chronic progressive external ophthalmoplegia. *Chin Med J (Engl)* **2019,** 132, 1202-1207.

49. Lee, S. J.; Na, J. H.; Han, J.; Lee, Y. M. Ophthalmoplegia in Mitochondrial Disease. *Yonsei Medical Journal* **2018,** 59, 1190-1196.

50. Filosto, M.; Lanzi, G.; Nesti, C.; Vielmi, V.; Marchina, E.; Galvagni, A.; Giliani, S.; Santorelli, F. M.; Padovani, A. A novel mitochondrial tRNA(Ala) gene variant causes chronic progressive external ophthalmoplegia in a patient with Huntington disease. *Molecular Genetics and Metabolism Reports* **2016,** 6, 70-73.

51. Zhao, D. H.; Wang, Z. X.; Hong, D. J.; Zhang, W.; Yuan, Y. Chronic progressive external ophthalmoplegia coexistent with motor neuron disease in a patient with a novel large-scale mitochondrial DNA deletion. *Clinical Neurology and Neurosurgery* **2013,** 115, 1490-1492.

52. Whittaker, R. G.; Schaefer, A. M.; Taylor, R. W.; Turnbull, D. M. Differential diagnosis in ptosis and ophthalmoplegia: mitochondrial disease or myasthenia? *Journal of Neurology* **2007,** 254, 1138-1139.

53. Carta, A.; Carelli, V.; D'Adda, T.; Ross-Cisneros, F. N.; Sadun, A. A. Human extraocular muscles in mitochondrial diseases: comparing chronic progressive external ophthalmoplegia with Leber's hereditary optic neuropathy. *British Journal of Ophthalmology* **2005,** 89, 825-827.

54. Maresca, A.; la Morgia, C.; Caporali, L.; Valentino, M. L.; Carelli, V. The optic nerve: a "mito-window" on mitochondrial neurodegeneration. *Mol Cell Neurosci* **2013,** 55, 62-76.

55. Reskenielsen, E.; Lou, H. C.; Lowes, M. Progressive External Ophthalmoplegia - Evidence for a Generalized Mitochondrial Disease with a Defect in Pyruvate Metabolism. *Acta Ophthalmologica* **1976,** 54, 553-573.

56. Klopstock, T.; Schlamp, V.; Schmidt, F.; Gekeler, F.; Hartard, M.; Pongratz, D.; Walter, M.; Gasser, T.; Straube, A.; Dieterich, M.; Muller-Felber, W. Creatine monohydrate in mitochondrial diseases: A double-blind, placebo-controlled, cross-over-study in 16 patients with chronic progressive external ophthalmoplegia or mitochondrial myopathy. *Neurology* **1999,** 52, A543-A544.

57. Frazier, A. E.; Thorburn, D. R.; Compton, A. G. Mitochondrial energy generation disorders: genes, mechanisms, and clues to pathology. *Journal of Biological Chemistry* **2019,** 294, 5386-5395.

58. Schrimpe-Rutledge, A. C.; Codreanu, S. G.; Sherrod, S. D.; McLean, J. A. Untargeted Metabolomics Strategies-Challenges and Emerging Directions. *J Am Soc Mass Spectrom* **2016,** 27, 1897-1905.

59. Wishart, D. S. Metabolomics for Investigating Physiological and Pathophysiological Processes. *Physiol Rev* **2019,** 99, 1819-1875.

60. Johnson, C. H.; Ivanisevic, J.; Siuzdak, G. Metabolomics: beyond biomarkers and towards mechanisms. *Nature Reviews Molecular Cell Biology* **2016,** 17, 451-459.

61. Wishart, D. S. Metabolomics for Investigating Physiological and Pathophysiological Processes. *Physiological Reviews* **2019,** 99, 1819-1875.

62. Goldansaz, S. A.; Guo, A. C.; Sajed, T.; Steele, M. A.; Plastow, G. S.; Wishart, D. S. Livestock metabolomics and the livestock metabolome: A systematic review. *Plos One* **2017,** 12.

63. Bowling, F. G.; Thomas, M. Analyzing the Metabolome. *Clinical Bioinformatics, 2nd Edition* **2014,** 1168, 31-45.

64. Southam, A. D.; Lange, A.; Al-Salhi, R.; Hill, E. M.; Tyler, C. R.; Viant, M. R. Distinguishing between the metabolome and xenobiotic exposome in environmental field samples analysed by direct-infusion mass spectrometry based metabolomics and lipidomics. *Metabolomics* **2014,** 10, 1050-1058.

65. Oliver, S. G.; Winson, M. K.; Kell, D. B.; Baganz, F. Systematic functional analysis of the yeast genome. *Trends Biotechnol* **1998,** 16, 373-8.

66. Nicholson, J. K.; Lindon, J. C.; Holmes, E. 'Metabonomics': understanding the metabolic responses of living systems to pathophysiological stimuli via multivariate statistical analysis of biological NMR spectroscopic data. *Xenobiotica* **1999,** 29, 1181-9.

67. Wang, S. Y.; Blair, I. A.; Mesaros, C. Analytical Methods for Mass Spectrometry-Based Metabolomics Studies. *Advancements of Mass Spectrometry in Biomedical Research, 2nd Edition* **2019,** 1140, 635-647.

68. Jacyna, J.; Kordalewska, M.; Markuszewski, M. J. Design of Experiments in metabolomics-related studies: An overview. *Journal of Pharmaceutical and Biomedical Analysis* **2019,** 164, 598-606.

69. Zhou, B.; Xiao, J. F.; Tuli, L.; Ressom, H. W. LC-MS-based metabolomics. *Molecular bioSystems* **2012,** 8, 470-481.

70. Khamis, M. M.; Adamko, D. J.; El-Aneed, A. Mass spectrometric based approaches in urine metabolomics and biomarker discovery. *Mass Spectrometry Reviews* **2017,** 36, 115-134.

71. Yan, M.; Xu, G. W. Current and future perspectives of functional metabolomics in disease studies-A review. *Analytica Chimica Acta* **2018,** 1037, 41-54.

72. Watrous, J. D.; Henglin, M.; Claggett, B.; Lehmann, K. A.; Larson, M. G.; Cheng, S.; Jain, M. Visualization, Quantification, and Alignment of Spectral Drift in Population Scale Untargeted Metabolomics Data. *Anal Chem* **2017,** 89, 1399-1404.

73. Kohler, I.; Verhoeven, A.; Derks, R. J.; Giera, M. Analytical pitfalls and challenges in clinical metabolomics. *Bioanalysis* **2016,** 8, 1509-32.

74. Misra, B. B. New tools and resources in metabolomics: 2016-2017. *Electrophoresis* **2018,** 39, 909-923.

75. Navarro-Reig, M.; Bedia, C.; Tauler, R.; Jaumot, J. Chemometric Strategies for Peak Detection and Profiling from Multidimensional Chromatography. *Proteomics* **2018,** 18, e1700327.

76. Karaman, I. Preprocessing and Pretreatment of Metabolomics Data for Statistical Analysis. *Adv Exp Med Biol* **2017,** 965, 145-161.

77. Gross, T.; Mapstone, M.; Miramontes, R.; Padilla, R.; Cheema, A. K.; Macciardi, F.; Federoff, H. J.; Fiandaca, M. S. Toward Reproducible Results from Targeted Metabolomic Studies: Perspectives for Data Pre-processing and a Basis for Analytic Pipeline Development. *Curr Top Med Chem* **2018,** 18, 883-895.

78. Fan, T. W.; Lorkiewicz, P. K.; Sellers, K.; Moseley, H. N.; Higashi, R. M.; Lane, A. N. Stable isotope-resolved metabolomics and applications for drug development. *Pharmacol Ther* **2012,** 133, 366-91.

79. Mahieu, N. G.; Genenbacher, J. L.; Patti, G. J. A roadmap for the XCMS family of software solutions in metabolomics. *Curr Opin Chem Biol* **2016,** 30, 87-93.

80. Gertsman, I.; Barshop, B. A. Promises and pitfalls of untargeted metabolomics. *Journal of Inherited Metabolic Disease* **2018,** 41, 355-366.

81. Wang, M.; Carver, J. J.; Phelan, V. V.; Sanchez, L. M.; Garg, N.; Peng, Y.; Nguyen, D. D.; Watrous, J.; Kapono, C. A.; Luzzatto-Knaan, T.; Porto, C.; Bouslimani, A.; Melnik, A. V.; Meehan, M. J.; Liu, W. T.; Crusemann, M.; Boudreau, P. D.; Esquenazi, E.; Sandoval-Calderon, M.; Kersten, R. D.; Pace, L. A.; Quinn, R. A.; Duncan, K. R.; Hsu, C. C.; Floros, D. J.; Gavilan, R. G.; Kleigrewe, K.; Northen, T.; Dutton, R. J.; Parrot, D.; Carlson, E. E.; Aigle, B.; Michelsen, C. F.; Jelsbak, L.; Sohlenkamp, C.; Pevzner, P.; Edlund, A.; McLean, J.; Piel, J.; Murphy, B. T.; Gerwick, L.; Liaw, C. C.; Yang, Y. L.; Humpf, H. U.; Maansson, M.; Keyzers, R. A.; Sims, A. C.; Johnson, A. R.; Sidebottom, A. M.; Sedio, B. E.; Klitgaard, A.; Larson, C. B.; P, C. A. B.; Torres-Mendoza, D.; Gonzalez, D. J.; Silva, D. B.; Marques, L. M.; Demarque, D. P.; Pociute, E.; O'Neill, E. C.; Briand, E.; Helfrich, E. J. N.; Granatosky, E. A.; Glukhov, E.; Ryffel, F.; Houson, H.; Mohimani, H.; Kharbush, J. J.; Zeng, Y.; Vorholt, J. A.; Kurita, K. L.; Charusanti, P.; McPhail, K. L.; Nielsen, K. F.; Vuong, L.; Elfeki, M.; Traxler, M. F.; Engene, N.; Koyama, N.; Vining, O. B.; Baric, R.; Silva, R. R.; Mascuch, S. J.; Tomasi, S.; Jenkins, S.; Macherla, V.; Hoffman, T.; Agarwal, V.; Williams, P. G.; Dai, J.; Neupane, R.; Gurr, J.; Rodriguez, A. M. C.; Lamsa, A.; Zhang, C.; Dorrestein, K.; Duggan, B. M.; Almaliti, J.; Allard, P. M.; Phapale, P.; Nothias, L. F.; Alexandrov, T.; Litaudon, M.; Wolfender, J. L.; Kyle, J. E.; Metz, T. O.; Peryea, T.; Nguyen, D. T.; VanLeer, D.; Shinn, P.; Jadhav, A.; Muller, R.; Waters, K. M.; Shi, W.; Liu, X.; Zhang, L.; Knight, R.; Jensen, P. R.; Palsson, B. O.; Pogliano, K.; Linington, R. G.; Gutierrez, M.; Lopes, N. P.; Gerwick, W. H.; Moore, B. S.; Dorrestein, P. C.; Bandeira, N. Sharing and community curation of mass spectrometry data with Global Natural Products Social Molecular Networking. *Nat Biotechnol* **2016,** 34, 828-837.

82. Vargas, F.; Weldon, K. C.; Sikora, N.; Wang, M.; Zhang, Z.; Gentry, E. C.; Panitchpakdi, M. W.; Caraballo-Rodriguez, A. M.; Dorrestein, P. C.; Jarmusch, A. K. Protocol for community-created public MS/MS reference spectra within the Global

Natural Products Social Molecular Networking infrastructure. *Rapid Commun Mass Spectrom* **2020,** 34, e8725.

83. Porporato, P. E.; Filigheddu, N.; Pedro, J. M. B.; Kroemer, G.; Galluzzi, L. Mitochondrial metabolism and cancer. *Cell Res* **2018,** 28, 265-280.

84. Nagrath, D.; Caneba, C.; Karedath, T.; Bellance, N. Metabolomics for mitochondrial and cancer studies. *Biochim Biophys Acta* **2011,** 1807, 650-63.

85. Brand, R. A. Biographical sketch: Otto Heinrich Warburg, PhD, MD. *Clin Orthop Relat Res* **2010,** 468, 2831-2.

86. Luo, S. T.; Zhang, D. M.; Qin, Q.; Lu, L.; Luo, M.; Guo, F. C.; Shi, H. S.; Jiang, L.; Shao, B.; Li, M.; Yang, H. S.; Wei, Y. Q. The Promotion of Erythropoiesis via the Regulation of Reactive Oxygen Species by Lactic Acid. *Sci Rep* **2017,** 7, 38105.

87. Martinez, J.; Marmisolle, I.; Tarallo, D.; Quijano, C. Mitochondrial Bioenergetics and Dynamics in Secretion Processes. *Frontiers in Endocrinology* **2020,** 11.

88. Assi, M. The differential role of reactive oxygen species in early and late stages of cancer. *Am J Physiol Regul Integr Comp Physiol* **2017,** 313, R646-R653.

89. Sullivan, L. B.; Chandel, N. S. Mitochondrial reactive oxygen species and cancer. *Cancer Metab* **2014,** 2, 17.

90. Giorgi, C.; Marchi, S.; Pinton, P. The machineries, regulation and cellular functions of mitochondrial calcium. *Nat Rev Mol Cell Biol* **2018,** 19, 713-730.

91. Horobin, R. W.; Trapp, S.; Weissig, V. Mitochondriotropics: a review of their mode of action, and their applications for drug and DNA delivery to mammalian mitochondria. *J Control Release* **2007,** 121, 125-36.

92. Guzman-Villanueva, D.; Weissig, V. Mitochondria-Targeted Agents: Mitochondriotropics, Mitochondriotoxics, and Mitocans. *Handb Exp Pharmacol* **2017,** 240, 423-438.

93. Laws, K.; Eskandari, A.; Lu, C.; Suntharalingam, K. Highly Charged, Cytotoxic, Cyclometalated Iridium(III) Complexes as Cancer Stem Cell Mitochondriotropics. *Chemistry* **2018,** 24, 15205-15210.

94. Tisdale, E. J.; Slobodov, I.; Theodorakis, E. A. Biomimetic total synthesis of forbesione and desoxymorellin utilizing a tandem Claisen/Diels--Alder/Claisen rearrangement. *Org Biomol Chem* **2003,** 1, 4418-22.

95. Tisdale, E. J.; Slobodov, I.; Theodorakis, E. A. Unified synthesis of caged Garcinia natural products based on a site-selective Claisen/Diels-Alder/Claisen rearrangement. *Proc Natl Acad Sci U S A* **2004,** 101, 12030-5.

96. Batova, A.; Lam, T.; Waschol owski, V.; Yu, A. L.; Giannis, A.; Theodorakis, E. A. Synthesis and evaluation of caged Garcinia xanthones. *Org Biomol Chem* **2007,** 5, 494-500.

97. Chantarasriwong, O.; Cho, W. C.; Batova, A.; Chavasiri, W.; Moore, C.; Rheingold, A. L.; Theodorakis, E. A. Evaluation of the pharmacophoric motif of the caged Garcinia xanthones. *Org Biomol Chem* **2009,** 7, 4886-94.

98. Guizzunti, G.; Batova, A.; Chantarasriwong, O.; Dakanali, M.; Theodorakis, E. A. Subcellular Localization and Activity of Gambogic Acid. *Chembiochem* **2012,** 13, 1191-1198.

99. Elbel, K. M.; Guizzunti, G.; Theodoraki, M. A.; Xu, J.; Batova, A.; Dakanali, M.; Theodorakis, E. A. A-ring oxygenation modulates the chemistry and bioactivity of caged Garcinia xanthones. *Org Biomol Chem* **2013,** 11, 3341-8.

100. Yim, K. H.; Prince, T. L.; Qu, S.; Bai, F.; Jennings, P. A.; Onuchic, J. N.; Theodorakis, E. A.; Neckers, L. Gambogic acid identifies an isoform-specific druggable pocket in the middle domain of Hsp90beta. *Proc Natl Acad Sci U S A* **2016,** 113, E4801-9.

101. Chantarasriwong, O.; Althufairi, B. D.; Checchia, N. J.; Theodorakis, E. A. Chapter 4 - Caged Garcinia Xanthones: Synthetic Studies and Pharmacophore Evaluation. In *Studies in Natural Products Chemistry*, Atta ur, R., Ed. Elsevier: 2018; Vol. 58, pp 93-131.

102. Ovalle-Magallanes, B.; Eugenio-Perez, D.; Pedraza-Chaverri, J. Medicinal properties of mangosteen (Garcinia mangostana L.): A comprehensive update. *Food Chem Toxicol* **2017,** 109, 102-122.

103. Xu, Y. J.; Yip, S. C.; Kosela, S.; Fitri, E.; Hana, M.; Goh, S. H.; Sim, K. Y. Novel cytotoxic, polyprenylated heptacyclic xanthonoids from Indonesian Garcinia gaudichaudii (Guttiferae). *Org Lett* **2000,** 2, 3945-8.

104. Kartha, G.; Ramachandran, G. N.; Bhat, H. B.; Nair, P. M.; Raghavan, V. K. V.; Venkataraman, K. The Constitution of Morellin. *Tetrahedron Letters* **1963**, 459-472.

105. Peter Yates: S. S. Karmarkar, D. R., G. H. Stout and V. F. Stou. Acetyl-α-gambogic acid. *Tetrahedron Letters* **1963,** 4, 1623-1629.

106. Mehta, G.; Maity, P. Construction of the 3-prenyl-4-oxa-tricyclo[4.3.1.03,7]dec-8-en-2-one core of caged xanthonoid natural products via tandem Wessely oxidation–intramolecular [4+2] cycloaddition. *Tetrahedron Letters* **2008,** 49, 318-322.

107. Liesenklas, W.; Auterhoff, H. [The constitution of gambogic acid and its isomerization. 4. Chemistry of gum-resin]. *Arch Pharm Ber Dtsch Pharm Ges* **1966,** 299, 797-8.

108. Nicolaou, K. C.; Sasmal, P. K.; Xu, H. Biomimetically inspired total synthesis and structure activity relationships of 1-O-methyllateriflorone. 6 pi electrocyclizations in organic synthesis. *J Am Chem Soc* **2004,** 126, 5493-501.

109. Yi, J.; Li, K.; Draths, K. M.; Frost, J. W. Modulation of phosphoenolpyruvate synthase expression increases shikimate pathway product yields in E. coli. *Biotechnol Prog* **2002,** 18, 1141-8.

110. McConkey, G. A. Targeting the shikimate pathway in the malaria parasite Plasmodium falciparum. *Antimicrob Agents Chemother* **1999,** 43, 175-7.

111. Keeling, P. J.; Palmer, J. D.; Donald, R. G.; Roos, D. S.; Waller, R. F.; McFadden, G. I. Shikimate pathway in apicomplexan parasites. *Nature* **1999,** 397, 219-20.

112. Herrmann, K. M.; Weaver, L. M. The Shikimate Pathway. *Annu Rev Plant Physiol Plant Mol Biol* **1999,** 50, 473-503.

113. Le Marechal, P.; Azerad, R. The shikimate pathway. III. 3-dehydroquinate synthetase of E. coli. Mechanistic studies by kinetic isotope effect. *Biochimie* **1976,** 58, 1123-8.

114. Le Marechal, P.; Azerad, R. The shikimate pathway. IV. 3-dehydroquinate synthetase of E. coli. Substrate analogs and inhibitors. *Biochimie* **1976,** 58, 1145-8.

115. Bentley, R. The shikimate pathway--a metabolic tree with many branches. *Crit Rev Biochem Mol Biol* **1990,** 25, 307-84.

116. Bennett, G. J.; Lee, H. H. The Biosynthesis of Mangostin - the Origin of the Xanthone Skeleton. *Journal of the Chemical Society-Chemical Communications* **1988**, 619-620.

117. Bennett, G. J.; Lee, H. H.; Das, N. P. Biosynthesis of Mangostin .1. The Origin of the Xanthone Skeleton. *Journal of the Chemical Society-Perkin Transactions 1* **1990**, 2671-2676.

118. Beerhues, L.; Liu, B. Biosynthesis of biphenyls and benzophenones--evolution of benzoic acid-specific type III polyketide synthases in plants. *Phytochemistry* **2009,** 70, 1719-27.

119. Carpenter, I.; Locksley, H. D.; Scheinmann, F. Xanthones in Higher Plants - Biogenetic Proposals and a Chemotaxonomic Survey. *Phytochemistry* **1969,** 8, 2013-+.

120. Locksley, H. D.; Moore, I.; Scheinmann, F. Extractives from guttiferae—VI: The significance of maclurin in xanthone biosynthesis. *Tetrahedron* **1967,** 23, 2229-2234.

121. Grover, P. K.; Shah, G. D.; Shah, R. C. Xanthones. Part IV. A new synthesis of hydroxyxanthones and hydroxybenzophenones. *Journal of the Chemical Society (Resumed)* **1955**, 3982-3985.

122. Genoux-Bastide, E.; Lorendeau, D.; Nicolle, E.; Yahiaoui, S.; Magnard, S.; Di Pietro, A.; Baubichon-Cortay, H.; Boumendjel, A. Identification of xanthones as selective killers of cancer cells overexpressing the ABC transporter MRP1. *ChemMedChem* **2011,** 6, 1478-84.

123. Cardona, L.; Garcia, B.; Pedro, J. R.; Perez, J. 6-Prenyloxy-7-Methoxycoumarin, a Coumarin-Hemiterpene Ether from Carduus-Tenuiflorus. *Phytochemistry* **1992,** 31, 3989-3991.

124. Yang, L.; Pu, X.; Niu, D.; Fu, Z.; Zhang, X. Copper-Catalyzed Asymmetric Propargylation of Indolizines. *Org Lett* **2019,** 21, 8553-8557.

125. Nicolaou, K. C.; Li, J. "Biomimetic" cascade reactions in organic synthesis: Construction of 4-oxatricyclo[4.3.1.0]decan-2-one systems and total synthesis of 1-O-methylforbesione via tandem claisen rearrangement/Diels-Alder reactions. *Angewandte Chemie-International Edition* **2001,** 40, 4264-4268.

126. Wang, X.; Chen, Y.; Han, Q. B.; Chan, C. Y.; Wang, H.; Liu, Z.; Cheng, C. H.; Yew, D. T.; Lin, M. C.; He, M. L.; Xu, H. X.; Sung, J. J.; Kung, H. F. Proteomic identification of molecular targets of gambogic acid: role of stathmin in hepatocellular carcinoma. *Proteomics* **2009,** 9, 242-53.

127. Zhou, Y.; Li, W.; Zhang, X.; Zhang, H.; Xiao, Y. Global profiling of cellular targets of gambogic acid by quantitative chemical proteomics. *Chem Commun (Camb)* **2016,** 52, 14035-14038.

128. Yue, Q.; Feng, L.; Cao, B.; Liu, M.; Zhang, D.; Wu, W.; Jiang, B.; Yang, M.; Liu, X.; Guo, D. Proteomic Analysis Revealed the Important Role of Vimentin in Human Cervical Carcinoma HeLa Cells Treated With Gambogic Acid. *Mol Cell Proteomics* **2016,** 15, 26-44.

129. Danial, N. N. BCL-2 family proteins: critical checkpoints of apoptotic cell death. *Clin Cancer Res* **2007,** 13, 7254-63.

130. Xu, X.; Liu, Y.; Wang, L.; He, J.; Zhang, H.; Chen, X.; Li, Y.; Yang, J.; Tao, J. Gambogic acid induces apoptosis by regulating the expression of Bax and Bcl-2 and enhancing caspase-3 activity in human malignant melanoma A375 cells. *Int J Dermatol* **2009,** 48, 186-92.

131. Davenport, J.; Manjarrez, J. R.; Peterson, L.; Krumm, B.; Blagg, B. S.; Matts, R. L. Gambogic acid, a natural product inhibitor of Hsp90. *J Nat Prod* **2011,** 74, 1085-92.

132. Miyata, Y. Hsp90 inhibitor geldanamycin and its derivatives as novel cancer chemotherapeutic agents. *Current Pharmaceutical Design* **2005,** 11, 1131-1138.

133. Zhang, L. R.; Yi, Y. T.; Chen, J. J.; Sun, Y. F.; Guo, Q. J.; Zheng, Z. H.; Song, S. Y. Gambogic acid inhibits Hsp90 and deregulates TNF-alpha/NF-kappa B in HeLa cells. *Biochemical and Biophysical Research Communications* **2010,** 403, 282-287.

134. Powers, M. V.; Workman, P. Targeting of multiple signalling pathways by heat shock protein 90 molecular chaperone inhibitors. *Endocrine-Related Cancer* **2006,** 13, S125-S135.

135. Huang, H. B.; Chen, D.; Li, S. J.; Li, X. F.; Liu, N. N.; Lu, X. Y.; Liu, S. T.; Zhao, K.; Zhao, C. G.; Guo, H. P.; Yang, C. S.; Zhou, P.; Dong, X. X.; Zhang, C. G.; Guanmei; Dou, Q. P.; Liu, J. B. Gambogic acid enhances proteasome inhibitor-induced anticancer activity. *Cancer Letters* **2011,** 301, 221-228.

136. Kasibhatla, S.; Jessen, K. A.; Maliartchouk, S.; Wang, J. Y.; English, N. M.; Drewe, J.; Qiu, L.; Archer, S. P.; Ponce, A. E.; Sirisoma, N.; Jiang, S. C.; Zhang, H. Z.; Gehlsen, K. R.; Cai, S. X.; Green, D. R.; Tseng, B. A role for transferrin receptor in triggering apoptosis when targeted with gambogic acid. *Proceedings of the National Academy of Sciences of the United States of America* **2005,** 102, 12095-12100.

137. Daniels, T. R.; Bernabeu, E.; Rodriguez, J. A.; Patel, S.; Kozman, M.; Chiappetta, D. A.; Holler, E.; Ljubimova, J. Y.; Helguera, G.; Penichet, M. L. The transferrin receptor and the targeted delivery of therapeutic agents against cancer. *Biochimica Et Biophysica Acta-General Subjects* **2012,** 1820, 291-317.

138. He, H. Y.; Shen, W.; Jiang, Z. G.; Jing, W.; Xiao, W.; Wang, Z. Z.; Guo, Q. M.; Li, J.; Chen, S. H. Michael acceptor in Gambogic acid - its role and application for potent antitumor agents. *Abstracts of Papers of the American Chemical Society* **2015,** 250.

139. Wang, S. P.; Wang, L.; Chen, M. W.; Wang, Y. T. Gambogic acid sensitizes resistant breast cancer cells to doxorubicin through inhibiting P-glycoprotein and suppressing survivin expression. *Chemico-Biological Interactions* **2015,** 235, 76-84.

140. Zhang, H. Z.; Kasibhatla, S.; Wang, Y.; Herich, J.; Guastella, J.; Tseng, B.; Drewe, J.; Cai, S. X. Discovery, characterization and SAR of gambogic acid as a potent apoptosis inducer by a HTS assay. *Bioorganic & Medicinal Chemistry* **2004,** 12, 309-317.

141. Wang, J.; Shen, W.; Yuan, Z. L.; Lan, L. H.; Xu, J. W.; Wang, C.; Ma, G. M.; Shi, W. H.; Han, L. X.; Zhang, Z. X.; Hou, L. J.; Shen, L.; Jiang, Z. G.; He, H. Y.; Xiao, W.; Wang, Z. Z.; Guo, Q. M.; Li, J.; Chen, S. H. Michael acceptor in gambogic acid-Its role and application for potent antitumor agents. *Bioorganic & Medicinal Chemistry Letters* **2015,** 25, 2844-2848.

142. Wang, J. X.; Zhao, L.; Hu, Y.; Guo, Q. L.; Zhang, L.; Wang, X. J.; Li, N. G.; You, Q. D. Studies on chemical structure modification and biology of a natural product, Gambogic acid (I): Synthesis and biological evaluation of oxidized analogues of gambogic acid. *European Journal of Medicinal Chemistry* **2009,** 44, 2611-2620.

143. Wang, J. X.; Zhang, B. H.; Xu, D. D.; Miao, G. Q.; Wang, F.; Guo, Q. L.; You, Q. D. Synthesis and anti-tumor activity of NO-donating derivatives of gambogic acid. *Chinese Journal of Natural Medicines* **2013,** 11, 87-96.

144. Chen, T.; Zhang, R. H.; He, S. C.; Xu, Q. Y.; Ma, L.; Wang, G. C.; Qiu, N.; Peng, F.; Chen, J. Y.; Qiu, J. X.; Peng, A. H.; Chen, L. J. Synthesis and Antiangiogenic Activity of Novel Gambogic Acid Derivatives. *Molecules* **2012,** 17, 6249-6268.

145. Neckers, L. Hsp90 inhibitors as novel cancer chemotherapeutic agents. *Trends in Molecular Medicine* **2002,** 8, S55-S61.

146. Cai, L. L.; Qiu, N.; Xiang, M. L.; Tong, R. S.; Yan, J. F.; He, L.; Shi, J. Y.; Chen, T.; Wen, J. L.; Wang, W. W.; Chen, L. J. Improving aqueous solubility and antitumor effects by nanosized gambogic acid-mPEG(2000) micelles. *International Journal of Nanomedicine* **2014,** 9, 243-255.

147. Tang, X.; Zhang, P.; Ye, H.; Zhang, C.; Shen, W.; Ping, Q. Water-soluble gambogic acid PEGylated prodrugs: synthesis, characterization, physicochemical properties and in vitro hydrolysis. *Pharmazie* **2008,** 63, 711-7.

148. Ding, Y.; Zhang, P.; Tang, X. Y.; Zhang, C.; Ding, S.; Ye, H.; Ding, Q. L.; Shen, W. B.; Ping, Q. N. PEG prodrug of gambogic
acid: Amino acid and dipeptide spacer effects. *Polymer* **2012,** 53, 1694-1702.

149. Zhang, Z. H.; Wang, X. P.; Ayman, W. Y.; Munyendo, W. L. L.; Lv, H. X.; Zhou, J. P. Studies on lactoferrin nanoparticles of gambogic acid for oral delivery. *Drug Delivery* **2013,** 20, 86-93.

150. Qu, G. W.; Zhu, X.; Zhang, C.; Ping, Q. N. Modified chitosan derivative micelle system for natural anti-tumor product gambogic acid delivery. *Drug Delivery* **2009,** 16, 363-370.

151. Fang, L. H.; Chen, B. A.; Liu, S. L.; Wang, R. P.; Hu, S. Y.; Xia, G. H.; Tian, Y. L.; Cai, X. H. Synergistic effect of a combination of nanoparticulate Fe3O4 and gambogic acid on phosphatidylinositol 3-kinase/Akt/Bad pathway of LOVO cells. *International Journal of Nanomedicine* **2012,** 7, 4109-4118.

152. Michalet, X.; Pinaud, F. F.; Bentolila, L. A.; Tsay, J. M.; Doose, S.; Li, J. J.; Sundaresan, G.; Wu, A. M.; Gambhir, S. S.; Weiss, S. Quantum dots for live cells, in vivo imaging, and diagnostics. *Science* **2005,** 307, 538-544.

153. Xu, P. P.; Li, J. Y.; Shi, L. X.; Selke, M.; Chen, B. A.; Wang, X. M. Synergetic effect of functional cadmium-tellurium quantum dots conjugated with gambogic acid for HepG2 cell-labeling and proliferation inhibition. *International Journal of Nanomedicine* **2013,** 8, 3729-3736.

154. Xu, P. P.; Chen, B. A.; Li, J. Y.; Wang, X. M. Gambogic Acid Combined With CdTe QDs For Leukemia Cancer Cells Inhibition and Their Bio-Safety For Rat Brain. *Blood* **2013,** 122.

155. Zhou, Y.; Wang, R. J.; Chen, B.; Sun, D.; Hu, Y.; Xu, P. P. Daunorubicin and gambogic acid coloaded cysteamine-CdTe quantum dots minimizing the multidrug resistance of lymphoma in vitro and in vivo. *International Journal of Nanomedicine* **2016,** 11.

156. Jiao, F. C.; Zhao, L.; Wu, X. F.; Song, Z. B.; Li, Y. P. Metabolome and transcriptome analyses of the molecular mechanisms of flower color mutation in tobacco. *Bmc Genomics* **2020,** 21.

157. Russell, O. M.; Gorman, G. S.; Lightowlers, R. N.; Turnbull, D. M. Mitochondrial Diseases: Hope for the Future. *Cell* **2020,** 181, 168-188.

158. Wirth, C.; Brandt, U.; Hunte, C.; Zickermann, V. Structure and function of mitochondrial complex I. *Biochim Biophys Acta* **2016,** 1857, 902-14.

159. Altmann, J.; Buchner, B.; Nadaj-Pakleza, A.; Schafer, J.; Jackson, S.; Lehmann, D.; Deschauer, M.; Kopajtich, R.; Lautenschlager, R.; Kuhn, K. A.; Karle, K.; Schols, L.; Schulz, J. B.; Weis, J.; Prokisch, H.; Kornblum, C.; Claeys, K. G.; Klopstock, T. Expanded phenotypic spectrum of the m.8344A>G "MERRF" mutation: data from the German mitoNET registry. *J Neurol* **2016,** 263, 961-972.

160. Gempel, K.; Topaloglu, H.; Talim, B.; Schneiderat, P.; Schoser, B. G. H.; Hans, V. H.; Palmafy, B.; Kale, G.; Tokatli, A.; Quinzii, C.; Hirano, M.; Naini, A.; DiMauro, S.; Prokisch, H.; Lochmuller, H.; Horvath, R. The myopathic form of coenzyme Q10 deficiency is caused by mutations in the electron-transferring-flavoprotein dehydrogenase (ETFDH) gene. *Brain* **2007,** 130, 2037-2044.

161. Horvath, R.; Hudson, G.; Ferrari, G.; Futterer, N.; Ahola, S.; Lamantea, E.; Prokisch, H.; Lochmuller, H.; McFarland, R.; Ramesh, V.; Klopstock, T.; Freisinger, P.; Salvi, F.; Mayr, J. A.; Santer, R.; Tesarova, M.; Zeman, J.; Udd, B.; Taylor, R. W.; Turnbull, D.; Hanna, M.; Fialho, D.; Suomalainen, A.; Zeviani, M.; Chinnery, P. F. Phenotypic spectrum associated with mutations of the mitochondrial polymerase gamma gene. *Brain* **2006,** 129, 1674-1684.

162. Lagerborg, K. A.; Watrous, J. D.; Cheng, S.; Jain, M. High-Throughput Measure of Bioactive Lipids Using Non-targeted Mass Spectrometry. *Methods Mol Biol* **2019,** 1862, 17-35.

163. Kantz, E. D.; Tiwari, S.; Watrous, J. D.; Cheng, S.; Jain, M. Deep Neural Networks for Classification of LC-MS Spectral Peaks. *Analytical Chemistry* **2019,** 91, 12407-12413.

164. Nick, T. G.; Campbell, K. M. Logistic regression. *Methods Mol Biol* **2007,** 404, 273-301.

165. Lee, K. M.; Jeon, J. Y.; Lee, B. J.; Lee, H.; Choi, H. K. Application of Metabolomics to Quality Control of Natural Product Derived Medicines. *Biomol Ther (Seoul)* **2017,** 25, 559-568.

166. Caporali, L.; Maresca, A.; Capristo, M.; Del Dotto, V.; Tagliavini, F.; Valentino, M. L.; La Morgia, C.; Carelli, V. Incomplete penetrance in mitochondrial optic neuropathies. *Mitochondrion* **2017,** 36, 130-137.

167. Rohart, F.; Eslami, A.; Matigian, N.; Bougeard, S.; Lê Cao, K.-A. MINT: a multivariate integrative method to identify reproducible molecular signatures across independent experiments and platforms. *BMC Bioinformatics* **2017,** 18, 128.

168. Fantini, M.; Asanad, S.; Karanjia, R.; Sadun, A. Hormone replacement therapy in Leber's hereditary optic neuropathy: Accelerated visual recovery in vivo. *J Curr Ophthalmol* **2019,** 31, 102-105.

169. Pisano, A.; Preziuso, C.; Iommarini, L.; Perli, E.; Grazioli, P.; Campese, A. F.; Maresca, A.; Montopoli, M.; Masuelli, L.; Sadun, A. A.; d'Amati, G.; Carelli, V.; Ghelli, A.; Giordano, C. Targeting estrogen receptor beta as preventive therapeutic strategy for Leber's hereditary optic neuropathy. *Human Molecular Genetics* **2015,** 24, 6921-6931.

170. Yu, D.; Jia, X.; Zhang, A. M.; Guo, X.; Zhang, Y. P.; Zhang, Q.; Yao, Y. G. Molecular characterization of six Chinese families with m.3460G>A and Leber hereditary optic neuropathy. *Neurogenetics* **2010,** 11, 349-56.

171. Guijas, C.; Montenegro-Burke, J. R.; Domingo-Almenara, X.; Palermo, A.; Warth, B.; Hermann, G.; Koellensperger, G.; Huan, T.; Uritboonthai, W.; Aisporna, A. E.; Wolan, D. W.; Spilker, M. E.; Benton, H. P.; Siuzdak, G. METLIN: A Technology Platform for Identifying Knowns and Unknowns. *Analytical chemistry* **2018,** 90, 3156-3164.

172. Otasek, D.; Morris, J. H.; Boucas, J.; Pico, A. R.; Demchak, B. Cytoscape Automation: empowering workflow-based network analysis. *Genome Biol* **2019,** 20, 185.

173. Knottnerus, S. J. G.; Bleeker, J. C.; Wust, R. C. I.; Ferdinandusse, S.; L, I. J.; Wijburg, F. A.; Wanders, R. J. A.; Visser, G.; Houtkooper, R. H. Disorders of mitochondrial long-chain fatty acid oxidation and the carnitine shuttle. *Rev Endocr Metab Disord* **2018,** 19, 93-106.

174. Tamaoki, Y.; Kimura, M.; Hasegawa, Y.; Iga, M.; Inoue, M.; Yamaguchi, S. A survey of Japanese patients with mitochondrial fatty acid beta-oxidation and related disorders as detected from 1985 to 2000. *Brain Dev* **2002,** 24, 675-80.

175. Takusa, Y.; Yamaguchi, S. [Myopathies with miscellaneous disorders related to mitochondrial fatty acid oxidation: defective synthesis of ketone body, long-chain fatty acid transport defect, and muscular coenzyme Q10 deficiency]. *Ryoikibetsu Shokogun Shirizu* **2001**, 90-4.

176. Tonin, A. M.; Amaral, A. U.; Busanello, E. N.; Grings, M.; Castilho, R. F.; Wajner, M. Long-chain 3-hydroxy fatty acids accumulating in long-chain 3-hydroxyacyl-CoA dehydrogenase and mitochondrial trifunctional protein deficiencies uncouple oxidative phosphorylation in heart mitochondria. *J Bioenerg Biomembr* **2013,** 45, 47-57.

177. Hagenbuchner, J.; Scholl-Buergi, S.; Karall, D.; Ausserlechner, M. J. Very long-/and long Chain-3-Hydroxy Acyl CoA Dehydrogenase Deficiency correlates with deregulation of the mitochondrial fusion/fission machinery. *Scientific Reports* **2018,** 8.

178. Tonin, A. M.; Amaral, A. U.; Busanello, E. N.; Gasparotto, J.; Gelain, D. P.; Gregersen, N.; Wajner, M. Mitochondrial bioenergetics deregulation caused by long-chain 3-hydroxy fatty acids accumulating in LCHAD and MTP deficiencies in rat brain: A possible role of mPTP opening as a pathomechanism in these disorders? *Biochimica Et Biophysica Acta-Molecular Basis of Disease* **2014,** 1842, 1658-1667.

179. Jones, P. M.; Butt, Y.; Bennett, M. J. Accumulation of 3-hydroxy-fatty acids in the culture medium of long-chain L-3-hydroxyacyl CoA dehydrogenase (LCHAD) and mitochondrial trifunctional protein-deficient skin fibroblasts: Implications for medium chain triglyceride dietary treatment of LCHAD deficiency. *Pediatric Research* **2003,** 53, 783-787.

180. Mikolajczyk, S.; Brody, S. De novo fatty acid synthesis mediated by acyl-carrier protein in Neurospora crassa mitochondria. *Eur J Biochem* **1990,** 187, 431-7.

181. Hiltunen, J. K.; Schonauer, M. S.; Autio, K. J.; Mittelmeier, T. M.; Kastaniotis, A. J.; Dieckmann, C. L. Mitochondrial fatty acid synthesis type II: more than just fatty acids. *J Biol Chem* **2009,** 284, 9011-5.

182. Nakazawa, M.; Ando, H.; Nishimoto, A.; Ohta, T.; Sakamoto, K.; Ishikawa, T.; Ueda, M.; Sakamoto, T.; Nakano, Y.; Miyatake, K.; Inui, H. Anaerobic respiration coupled with mitochondrial fatty acid synthesis in wax ester fermentation by Euglena gracilis. *FEBS Lett* **2018,** 592, 4020-4027.

183. Hiltunen, J. K.; Autio, K. J.; Schonauer, M. S.; Kursu, V. A.; Dieckmann, C. L.; Kastaniotis, A. J. Mitochondrial fatty acid synthesis and respiration. *Biochim Biophys Acta* **2010,** 1797, 1195-202.

184. Schneider, R.; Brors, B.; Massow, M.; Weiss, H. Mitochondrial fatty acid synthesis: a relic of endosymbiontic origin and a specialized means for respiration. *FEBS Lett* **1997,** 407, 249-52.

185. Autio, K. J.; Kastaniotis, A. J.; Pospiech, H.; Miinalainen, I. J.; Schonauer, M. S.; Dieckmann, C. L.; Hiltunen, J. K. An ancient genetic link between vertebrate mitochondrial fatty acid synthesis and RNA processing. *Faseb j* **2008,** 22, 569-78.

186. Schonauer, M. S.; Kastaniotis, A. J.; Hiltunen, J. K.; Dieckmann, C. L. Intersection of RNA processing and the type II fatty acid synthesis pathway in yeast mitochondria. *Mol Cell Biol* **2008,** 28, 6646-57.

187. Boueroy, P.; Hahnvajanawong, C.; Boonmars, T.; Saensa-ard, S.; Wattanawongdon, W.; Kongsanthia, C.; Salao, K.; Wongwajana, S.; Anantachoke, N.; Reutrakul, V. Synergistic Effect of Forbesione From Garcinia hanburyi in Combination with 5-Fluorouracil on Cholangiocarcinoma. *Asian Pac J Cancer Prev* **2017,** 18, 3343-3351.

188. Boueroy, P.; Hahnvajanawong, C.; Boonmars, T.; Saensa-Ard, S.; Anantachoke, N.; Vaeteewoottacharn, K.; Reutrakul, V. Antitumor effect of forbesione isolated from Garcinia hanburyi on cholangiocarcinoma in vitro and in vivo. *Oncol Lett* **2016,** 12, 4685-4698.

189. Reutrakul, V.; Anantachoke, N.; Pohmakotr, M.; Jaipetch, T.; Sophasan, S.; Yoosook, C.; Kasisit, J.; Napaswat, C.; Santisuk, T.; Tuchinda, P. Cytotoxic and anti-HIV-1 caged xanthones from the resin and fruits of Garcinia hanburyi. *Planta Med* **2007,** 73, 33-40.

190. Hahnvajanawong, C.; Boonyanugomol, W.; Nasomyon, T.; Loilome, W.; Namwat, N.; Anantachoke, N.; Tassaneeyakul, W.; Sripa, B.; Namwat, W.; Reutrakul, V. Apoptotic activity of caged xanthones from Garcinia hanburyi in cholangiocarcinoma cell lines. *World J Gastroenterol* **2010,** 16, 2235-43.

191. Hahnvajanawong, C.; Wattanawongdon, W.; Chomvarin, C.; Anantachoke, N.; Kanthawong, S.; Sripa, B.; Reutrakul, V. Synergistic effects of isomorellin and forbesione with doxorubicin on apoptosis induction in human cholangiocarcinoma cell lines. *Cancer Cell Int* **2014,** 14, 68.

192. Hartati, S.; Triyono, I. K.; Handayani, S. CYTOTOXIC ISOBRACTATIN (PRENYLATED XANTHONE) EPIMER MIXTURE OF Garcinia eugenifolia. *Indonesian Journal of Chemistry* **2014,** 14, 277-282.

193. Shen, T.; Li, W.; Wang, Y.-Y.; Zhong, Q.-Q.; Wang, S.-Q.; Wang, X.-N.; Ren, D.-M.; Lou, H.-X. Antiproliferative activities of Garcinia bracteata extract and its active ingredient, isobractatin, against human tumor cell lines. *Archives of Pharmacal Research* **2014,** 37, 412-420.

194. Kothayer, H.; Morelli, M.; Brahemi, G.; Elshanawani, A. A.; Abu Kull, M. E.; El-Sabbagh, O. I.; Shekhar, M. P. V.; Westwell, A. D. Optimised synthesis of diamino-triazinylmethyl benzoates as inhibitors of Rad6B ubiquitin conjugating enzyme. *Tetrahedron Letters* **2014,** 55, 7015-7018.